

MODELING NATURAL ATTENUATION OF PETROLEUM HYDROCARBONS  
(BTEX) IN HETEROGENEOUS AQUIFERS

A THESIS SUBMITTED TO  
THE GRADUATE SCHOOL OF NATURAL AND APPLIED SCIENCES  
OF  
MIDDLE EAST TECHNICAL UNIVERSITY

BY

TUĞBA UÇANKUS

IN PARTIAL FULFILLMENT OF THE REQUIREMENTS  
FOR  
THE DEGREE OF MASTER OF SCIENCE  
IN  
ENVIRONMENTAL ENGINEERING

DECEMBER 2005

Approval of the Graduate School of Natural and Applied Sciences

---

Prof. Dr. Canan ÖZGEN

Director

I certify that this thesis satisfies all the requirements as a thesis for the degree of Master of Science.

---

Prof. Dr. Filiz B. DİLEK

Head of Department

This is to certify that we have read this thesis and that in our opinion it is fully adequate, in scope and quality, as a thesis for the degree of Master of Science.

---

Prof. Dr. Kahraman ÜNLÜ

Supervisor

**Examining Committee Members**

Prof. Dr. Ülkü YETİŞ

(METU,ENVE)

Prof. Dr. Kahraman ÜNLÜ

(METU,ENVE)

Asst. Prof. Dr. Ayşegül AKSOY

(METU,ENVE)

Prof. Dr. Erdal ÇOKÇA

(METU,CE)

Prof. Dr. Nurkan KARAHANOĞLU

(METU,GEOE)

**I hereby declare that all information in this document has been obtained and presented in accordance with academic rules and ethical conduct. I also declare that, as required by these rules and conduct, I have fully cited and referenced all material and results that are not original to this work.**

**Name, Last name: Tuğba UÇANKUS**

**Signature :**

## **ABSTRACT**

### **MODELING NATURAL ATTENUATION OF PETROLEUM HYDROCARBONS (BTEX) IN HETEROGENEOUS AQUIFERS**

Uçankuş, Tuğba

M.Sc., Department of Environmental Engineering

Supervisor : Prof. Dr. Kahraman Ünlü

December 2005, 127 pages

Natural Attenuation can be an effective cleanup option for remediation of Groundwater contamination by BTEX. One of the important aspects of the methodology that has been recognized recently is that mass removal rates, the most important parameters used to determine effectiveness of the methodology, is controlled by groundwater flow regime, which to a large extent controlled by aquifer heterogeneity. Considering this recognition, the primary objective of this research is to quantitatively describe the relationship between natural attenuation rates of BTEX and aquifer heterogeneity using numerical solution techniques. To represent different levels of aquifer heterogeneity, hydraulic conductivity distributions are simulated using Turning Bands Algorithm, changing statistical parameters Coefficient of Variation (CV) and correlation length (h). Visual MODFLOW is used to model the transport of BTEX contamination, at different hydraulic conductivity fields. Degradation rates are calculated by Buscheck&Alcantar and Conservative Tracer

Methods. The results show that, for a given  $h$ , as  $CV$  increases, the plume slows down and stays longer at the domain, so areal extent of plume decreases. For anisotropic field, plumes are more dispersed along  $x$  and  $y$ -direction, and areal extents of the plumes are greater. During MNA feasibility studies, for the aquifer heterogeneity level of  $CV$  and  $h$  smaller than 100 % and 10 m, respectively, a minimum recommended biodegradation rate constant of  $0.02 \text{ d}^{-1}$  can be used, whereas for the aquifer heterogeneity level of  $CV$  and  $h$  greater than 100 % and 10 m, respectively, using a minimum biodegradation rate constant of  $0.06 \text{ d}^{-1}$  can be recommended.

Keywords: Natural Attenuation, BTEX, Hydraulic Conductivity, Heterogeneity, Numerical Simulations.

# ÖZ

## HETEROJEN AKİFERLERDE PETROL HİDROKARBONLARININ (BTEX) DOĞAL GİDERİMİNİN MODELLENMESİ

Uçankuş, Tuğba

Yüksek Lisans, Çevre Mühendisliği Bölümü

Tez Yöneticisi : Prof. Dr. Kahraman Ünlü

Aralık 2005, 127 sayfa

Yeraltı su kaynaklarının petrol hidrokarbonları ile kirlenmesi yaygın bir çevre problemidir. Doğal Giderim akifer ortamındaki petrol hidrokarbonlarının temizlenmesinde etkili ve ucuz yöntem olarak yaygın şekilde kullanılmaktadır. Bu yöntemi doğal prosesleri kullanarak sahadaki mevcut kirleticilerin yayılması önlenmekte ve konsantrasyonların düşürülmesi sağlanmaktadır. Doğal giderim uygulamalarında karşılaşılan en önemli konulardan bir tanesi, yöntemin etkinliğini belirlemede en önemli parametre olan kirletici giderim oranlarının belirlenmesinin büyük ölçüde yeraltı suyu (YAS) akış rejimine bağlı olması ve YAS akış rejiminin de akifer heterojenliği tarafından kontrol ediliyor olmasıdır. Bu çerçevede bu tez çalışmasının temel amacı, petrol hidrokarbonlarının akifer ortamındaki doğal giderim oranları ile akifer heterojenliği arasındaki ilişkinin sayısal simülasyon yöntemi kullanılarak niceliksel olarak tanımlanmasıdır. Farklı düzeylerdeki akifer heterojenliğini temsil etmek üzere, farklı değişim katsayısı (CV) ve korelasyon uzunluğuna (h) sahip hidrolik iletkenlik dağılımları, 'Turning Bands Algoritması' kullanılarak istatistiksel yöntemle simüle edilmiştir. Visual MODFLOW, petrol

hidrokarbonlarının farklı hidroluk iletkenlik dađılımlarına sahip sahalarda taşınmasının modellemesi için kullanılmıştır. Giderim oranları, ‘Buscheck&Alcantar’ ve ‘Korunmalı İzleyici’ Metodları kullanılarak hesaplanmıştır. Sonuçlar, h sabitken, CV artarsa, kirliliđin yavaşladığını ve sistem içerisinde daha uzun süre kaldığını, bu yüzden kirliliđin alansal genişliğinin azaldığını göstermektedir. Anisotropik özelliđe sahip sahada kirlilik x- ve y-ekseninde daha fazla dađılır ve kirliliđin alansal gelişliđi daha büyük olur. Fizibilite etüdüleri sırasında, sırasıyla 100 % ve 10 m’ den küçük CV ve h deđerlerine sahip akifer heterojenliđi için, önerilen en küçük giderim oranı sabiti olarak  $0.02 d^{-1}$  kullanılabilirken, sırasıyla 100 % ve 10 m’ den büyük CV ve h deđerlerine sahip akifer heterojenliđi için, önerilen en küçük giderim oranı sabiti olarak  $0.06 d^{-1}$  önerilebilir.

Anahtar Kelimeler: Doğal Giderim, Petrol Hidrokarbonları, Hidroluk Geçirgenlik, Heterojenlik, Sayısal Simulasyon.

## **ACKNOWLEDGEMENTS**

I would like to express my sincerest appreciation and thanks to my adviser Prof. Dr. Kahraman Ünlü, for his skillful and scholarly guidance throughout this research. I would also appreciate his endless support during my graduate study.

I would also like to thank to committee members of my thesis defense; Prof. Dr. Ülkü YETİŞ, Asst. Prof. Dr. Ayşegül AKSOY, Prof. Dr. Erdal ÇOKÇA and Prof. Dr. Nurkan KARAHANOĞLU for their valuable advises and suggestions.

I am very grateful to my parents for their love and support during this thesis study. In addition, I would like to thank to my friends, Nuray ATEŞ for her helps and also Başak Önkal.

Finally, my deepest appreciation goes to one of the important people in my life, A. Hakan BÖLÜKBAŞI for his advises and endless support.

# TABLE OF CONTENTS

<b>PLAGIARISM.....</b>	<b>III</b>
<b>ABSTRACT.....</b>	<b>IV</b>
<b>ÖZ.....</b>	<b>VI</b>
<b>ACKNOWLEDGEMENTS.....</b>	<b>VIII</b>
<b>TABLE OF CONTENTS.....</b>	<b>IX</b>
<b>LIST OF TABLES .....</b>	<b>XII</b>
<b>LIST OF FIGURES .....</b>	<b>XIII</b>
<b>CHAPTER</b>	
<b>1. INTRODUCTION.....</b>	<b>1</b>
1.1. GENERAL .....	1
1.1.1. <i>Monitored Natural Attenuation</i> .....	2
1.1.2. <i>Processes of Natural Attenuation</i> .....	5
1.1.3. <i>Potential Advantages and Disadvantages of NA</i> .....	8
1.2. SCOPE AND OBJECTIVES .....	9
1.3. LITERATURE REVIEW .....	10
<b>2. MATERIALS AND METHODS.....</b>	<b>16</b>
2.1. RANDOM FIELD GENERATION.....	16
2.1.1. <i>Random Field Theory</i> .....	17
2.1.2. <i>Generation of Hydraulic Conductivity Fields</i> .....	19
2.2. MODELING FATE AND TRANSPORT OF BTEX .....	22
2.2.1. <i>Overview of Visual MODFLOW</i> .....	22
2.2.1.1. MODFLOW Package .....	23
2.2.1.2. RT3D Package.....	24
2.2.1.3. Governing Equations .....	25
2.2.1.4. Modules Available For Reaction Kinetics In RT3D .....	26
2.2.2. <i>Description of Simulated Aquifer System</i> .....	32
2.2.3. <i>Input Data File Preparation</i> .....	33

2.2.3.1.	Input Data for Flow Package .....	34
2.2.3.2.	Input Data for Fate and Transport Package.....	37
2.2.3.3.	Model Output.....	40
2.3.	CALCULATION OF BIODEGRADATION RATES .....	40
2.3.1.	<i>Buscheck-Alcantar Method</i> .....	40
2.3.2.	<i>Conservative Tracer Method</i> .....	43
<b>3.</b>	<b>RESULTS AND DISCUSSION.....</b>	<b>46</b>
3.1.	RANDOM HYDRAULIC CONDUCTIVITY FIELD .....	46
3.1.1.	<i>Validation of Generated Random Fields</i> .....	47
3.1.2.	<i>Isotropic Hydraulic Conductivity Fields</i> .....	49
3.1.3.	<i>Anisotropic Hydraulic Conductivity Fields</i> .....	53
3.2.	BTEX PLUME SIMULATIONS AND PLUME BEHAVIOUR .....	55
3.2.1.	<i>Plumes of Isotropic Random Fields</i> .....	55
3.2.2.	<i>Plumes of Anisotropic Random Fields</i> .....	67
3.3.	ASSESSMENT OF BIODEGRADATION RATES AS A FUNCTION OF HETEROGENEITY .....	71
3.3.1.	<i>BUSCHECK AND ALCANTAR METHOD</i> .....	73
3.3.1.1.	Isotropic Hydraulic Conductivity Field .....	74
3.3.1.2.	Anisotropic Hydraulic Conductivity Field.....	77
3.3.2.	<i>CONSERVATIVE TRACER METHOD</i> .....	78
3.3.2.1.	Isotropic Hydraulic Conductivity Field .....	79
3.3.2.2.	Anisotropic Hydraulic Conductivity Field.....	81
3.3.3.	<i>FUNCTIONAL RELATIONSHIP BETWEEN RATE CONSTANTS AND HETEROGENEITY</i> .....	83
<b>4.</b>	<b>SUMMARY AND CONCLUSION.....</b>	<b>86</b>
	<b>REFERENCES.....</b>	<b>91</b>
	<b>APPENDICES</b>	
	<b>A. INPUT DATA OF RANDOM FIELD GENERATOR.....</b>	<b>95</b>
	<b>B. STATISTICAL PARAMETER GRAPHS OF RANDOM FIELD GENERATOR.....</b>	<b>98</b>
	<b>C. HEAD DISTRIBUTIONS OF SIMULATED FIELDS .....</b>	<b>108</b>
	<b>D. BTEX PLUMES AT THE END OF THE SIMULATION PERIOD .....</b>	<b>112</b>
	<b>E. OBSERVATION WELL TRANSECTS.....</b>	<b>116</b>

<b>F. LINEAR REGRESSION ANALYSIS GRAPHS FOR BUSCHECK AND ALCANTAR METHOD.....</b>	<b>120</b>
<b>F. LINEAR REGRESSION ANALYSIS GRAPHS FOR CONSERVATIVE TRACER METHOD.....</b>	<b>124</b>

## LIST OF TABLES

### TABLES

Table 2.1. Mean $m_{ln}$ and standard deviation $\sigma_{ln}$ values of ln-hydraulic conductivity field for different coefficient of variation, CV and correlation length, h.....	22
Table 2.2. Yield values for hydrocarbon destruction with decay processes .....	32
Table 2.3. The dimensional description and discretization of the aquifer system.....	33
Table 2.4. Constant concentration boundary of the system at the west boundary.....	36
Table 2.5. Source definition .....	36
Table 2.6. The material property values of the aquifer system.....	37
Table 2.7 Input parameters (Initial concentrations, degradation rates, saturation constants, inhibition constants) used in the BTEX degradation kinetics model.	39
Table 3.1. The downgradient distances of observation wells .....	72
Table 3.2. The Groundwater and Contaminant Velocities of the fields.....	73
Table 3.3. BTEX concentrations observed in monitoring wells .....	74
Table 3.5. Biodegradation and overall attenuation rates and $\lambda / k$ ratios of BTEX at anisotropic fields calculated by Buscheck and Alcantar Method .....	77
Table 3.6. Corrected BTEX concentrations observed in monitoring wells. ....	78
Table 3.7. Biodegradation rates of BTEX calculated by Conservative Tracer Method .....	80
Table 3.8. Biodegradation rates of BTEX at anisotropic fields calculated.....	82
by Conservative Tracer Method.....	82
Table 3.9. Biodegradation rates of BTEX calculated by two different methods. ....	83

# LIST OF FIGURES

## FIGURES

Figure 2.1. Boundary conditions, source area and grid system of the simulated domain.....	35
Figure 3.1. Mean, Variance and Covariance estimate for isotropic hydraulic conductivity field having CV = 50 % and h = 5 m. ....	48
Figure 3.2. Hydraulic conductivity distribution for (a) h = 5 m , (b) h = 10 m, and (c) h = 20 m when CV = 50 %.....	50
Figure 3.3. Hydraulic conductivity distribution for (a) h = 5 m , (b) h = 10 m , and (c) h = 20 m when CV = 100 %.....	51
Figure 3.4. Hydraulic conductivity distribution for (a) h = 5 m , (b) h = 10 m , and (c) h = 20 m when CV = 150 %.....	52
Figure 3.5. Hydraulic conductivity distribution for anisotropic field having CV = 50 %, $h_x = 20$ m and $h_y = 4$ m. ....	54
Figure 3.6. Hydraulic conductivity distribution for anisotropic field having CV = 150 %, $h_x = 10$ m and $h_y = 2$ m. ....	54
Figure 3.7. BTEX plume at 50 and 1000 days for Uniform Field .....	57
Figure 3.8. BTEX plumes at 50 and 800 days for isotropic fields having (a) h = 5 m, (b) h = 10 m, (c) h = 20 m, when CV = 50 % .....	58
Figure 3.9. BTEX plumes at 50 and 800 days for isotropic fields having (a) h = 5 m, (b) h = 10 m, (c) h = 20 m, when CV = 100 % .....	59
Figure 3.10. BTEX plumes at 50 and 800 days for isotropic fields having (a) h = 5 m, (b) h = 10 m, (c) h = 20 m, when CV = 150 % .....	60
Figure 3.11. The location of peak concentrations versus time graph for different CV values when (a) h = 5 m, (b) h = 10 m, (c) h = 20 m .....	63
Figure 3.12. Peak concentration versus location of peak concentration graph for different h values when (a) h = 5 m, (b) h = 10 m, (c) h = 20 m. ....	64

Figure 3.13. Peak concentration versus time graph for different h values when (a) h = 5 m, (b) h = 10 m, (c) h = 20 m.....	65
Figure 3.14. The location of plume front versus time graph for different CV values when (a) h = 5 m, (b) h = 10 m, (c) h = 20 m. ....	66
Figure 3.15. BTEX plumes at 50 and 800 days for anisotropic fields having CV = 50 %, $h_x = 20$ m and $h_y = 4$ m. ....	68
Figure 3.16. BTEX plumes at 50 and 800 days for anisotropic fields having CV = 150 %, $h_x = 10$ m and $h_y = 2$ m. ....	68
Figure 3.17. The location of peak concentrations versus time graph for two different anisotropic fields .....	69
Figure 3.18. Peak concentration versus location of peak concentration graph for two different anisotropic fields .....	69
Figure 3.19. Peak concentration versus time graph for two different anisotropic fields .....	69
Figure 3.20. The location of plume front versus time graph for two different anisotropic fields .....	70
Figure 3.21. Biodegradation rate versus correlation length for CV = 50 %, CV = 100 %, and CV = 150 %. ....	76
Figure 3.23. Biodegradation rate versus correlation length for CV = 50 %, CV = 100 %, and CV = 150 %. ....	80
Figure 3.24 Biodegradation rate versus CV for h = 5 m, h = 10 m, and h = 20 m ....	81
Figure 3.25 3-Dimensional surface plot of biodegradation rates for Buscheck and Alcantar Method. ....	84
Figure 3.26 3-Dimensional surface plot of biodegradation rates for Conservative Tracer Method.....	84

# CHAPTER 1

## INTRODUCTION

### 1.1. General

The organic or inorganic chemicals which affect the quality of the groundwater in the subsurface environment are described as contaminants. Generally, subsurface environments have been contaminated by synthetic organic chemicals (PCB's or pesticides), metals, pathogens (bacteria or viruses), and mostly by hydrocarbons (PAH's, BTEX or chlorinated solvents). Groundwater pollution by petroleum-derived hydrocarbons released from underground storage tanks and pipelines is a common and widespread problem throughout the industrialized world. Moreover, groundwater contamination poses a serious risk to human health and the environment, since the petroleum hydrocarbons can migrate through the underlying aquifer and discharge at water supply wells and surface water bodies.

Petroleum hydrocarbons, which affect the groundwater quality, contain benzene, toluene, ethylbenzene, and xylene isomers (BTEX), which are considered to be priority pollutants regulated by many nations. BTEX are of concern because of their toxicity and relatively high solubility. BTEX components ultimately reached to the groundwater do not readily mixed with aqueous phase, instead, they remain as a separate phase. In general, any materials that exhibit this phenomenon are known as non - aqueous phase liquid (NAPL). Typically, BTEX components, released into the subsurface as other oily-phase liquids, are less dense or lighter than water. Therefore, they are commonly referred to as "light nonaqueous-phase liquids," or LNAPLs. The

greatest mass of contaminant hydrocarbons are associated with these LNAPL source areas, not with groundwater. As groundwater moves through the LNAPL source areas, soluble components partition into the moving groundwater to generate the plume of dissolved contamination (Wiedemeier et al., 1995).

Groundwater remediation is a complex process relying on the implementation of a variety of technologies to effectively degrade the contamination. Remediation relies on the knowledge of the physical, chemical and hydrogeological properties of the subsurface. Active remediation technologies may sometimes not be an effective solution to widespread plumes, because of hydrogeological constraints, contaminant properties or the physical/chemical interaction of the contaminants in the subsurface. In these instances, natural attenuation with monitoring or institutional controls may be the most feasible solution for contaminated aquifers (Dale, 2001).

#### **1.1.1. Monitored Natural Attenuation**

Having understood the nature and extent of petroleum contamination in a site, taking an effective remedial action usually becomes necessary. Besides, understanding the nature and extent of contamination, site characterization is also important when choosing an appropriate remedial option. Under proper site conditions, natural attenuation can be a viable remedial option for contaminated aquifers.

Over the last decades, environmental professionals have recognized the importance of natural processes in affecting contaminant attenuation. In order to achieve the remediation goals of natural attenuation, a well designed monitoring program is required in the site remediation.

Monitored natural attenuation (MNA), as defined by EPA, is the reliance on natural attenuation processes, within the context of a carefully controlled and monitored site cleanup, to achieve site-specific remedial objectives within a reasonable time frame. MNA, sometimes named as intrinsic remediation, is one of the in-situ bioremediation

methods. MNA consists of many different physical, chemical and biological processes such as biodegradation, dispersion, dilution, adsorption, volatilization, and chemical or biological stabilization, transformation, or destruction of contaminants.

Contamination found in the site can be remediated by the help of some processes occurred in the subsurface environment. In MNA, contaminant mass can be reduced through destructive processes (such as biodegradation and chemical transformation); while concentration of contaminants can be decreased by simple dilution or dispersion mechanisms. Also, contaminant molecules can be bound to the soil surface by adsorption mechanism so that the contamination does not spread or mitigate far away from the source of the contamination.

Despite the common sense, MNA is not a “do nothing approach” to the site clean up; it is, in fact, a proactive method, because MNA comprises characterizing of the fate and transport of contamination (e.g. petroleum hydrocarbons, chlorinated solvents), evaluating the factors that will affect the long-term performance of MNA, and monitoring of the natural processes to ensure their effectiveness. Additionally, MNA also ensures that natural attenuation processes reduce the mass, toxicity, and mobility of contamination, without any human intervention.

Being a cost effective alternative, MNA should be evaluated as a remedial approach at petroleum hydrocarbon sites. It can be applied as a stand-alone technology or together with or a follow upto other remedial technologies (such as source reduction, air sparging, enhanced bioremediation, etc.), in order to reduce overall remediation costs.

MNA is based on the verification, monitoring and quantitatively documenting the natural processes at a contaminated site. In other words, MNA is a “knowledge-based” remedy, instead of active engineered remediations. The evaluation of MNA should be performed to some extend at every site, preferably at early stages in the site investigation processes. In order to determine that the natural attenuation can be

a viable option for a contaminated groundwater, before monitored natural attenuation can be proposed, the contaminated site must be characterized and the risk to human health and the environment should be assessed. With a well – documented monitored natural attenuation, the contaminant concentration can be reduced to the desired target levels within a reasonable time frame without risking the human health and environment.

Every site uses the benefits of MNA to some extent. However, depending on the site conditions, MNA may not be able to accomplish the cleanup goals in a desirable time period. In such a case, incorporation of natural and active remediation techniques (e.g. source reduction, air sparging) usually enhances the performance for little additional cost.

Application of MNA has to be justified by using “lines of evidence” which prove that MNA reduces the contaminant concentration to regulatory cleanup levels within a reasonable time frame with no human health and environmental risks. The lines of evidence are as;

- Documented reduction of contaminant mass at the site,
- Presence and distribution of geochemical and biochemical indicators of natural attenuation,
- Direct microbiological evidence.

Typically, the first line of evidence (i.e., loss of contaminants) is documented by reviewing historical trends in contaminant concentration and distribution in conjunction with the site geology and hydrogeology to show that a reduction in the total mass of contaminants is occurring at the site. This mass loss may be in the source area and/or along the groundwater flowpath. Biodegradation rates are more site-specific (e.g., dependent on redox conditions, electron donor concentration). Therefore, it is more important to estimate a biodegradation rate at contaminated sites from field data (Buscheck and Alcantar, 1995, Weaver et al, 1996).

The second line of evidence involves the use of chemical analytical data to show that reduction in contaminant and electron acceptor (such as dissolved oxygen, nitrate and sulfate) concentrations can be directly correlated to increases in metabolic byproduct (such as dissolved iron, manganese and methane) concentrations (Wiedemeier et al., 1995). These chemical indicators can be used to estimate the site-specific potential for contaminants to be destroyed by biodegradation.

The third line of evidence, direct microbiological evidence, can be used to show that indigenous biota are capable of degrading site contaminants (Wiedemeier et al., 1995). Microbiological evidence can demonstrate that native bacteria can biodegrade contaminants of concern under controlled conditions.

Ideally, the first two lines of evidence listed above should be used in the natural attenuation demonstration. A “weight-of-evidence” approach will greatly increase the likelihood of successfully implementing natural attenuation at sites where natural processes are restoring the environmental quality of groundwater contaminated with fuel hydrocarbons. The need to collect the third line of evidence is evaluated on a case-by-case basis and is generally only required when field data supporting the first two lines of evidence are insufficient to adequately support natural attenuation (ITRC, 1999).

### **1.1.2. Processes of Natural Attenuation**

Natural Attenuation is an effective remedial approach for petroleum hydrocarbons, such as BTEX. In order to understand the behavior of BTEX plumes in groundwater it is important to determine how the various physical, chemical, and biological processes interact.

One of the natural attenuation processes is sorption. As the groundwater migrates through the pores, contaminant molecules can be sorbed on to the soil and sediment

particle surfaces. Sorption retards the contaminant molecules, so the movement of the contaminant slows or stops. This process can reduce the likelihood that the contaminants will reach a receptor (such as a drinking water supplies or surface water bodies), where the contaminants would affect human or environmental health.

Dispersion and dilution are other two processes of natural attenuation of BTEX. As the contaminant move far away from the source, the contaminant can disperse and dilute to the lower concentrations over time. Since the contaminant concentration is decreased by these processes, the exposure risk of human and environment will be minimized.

Many petroleum hydrocarbons can evaporate or volatilize readily into the atmosphere, reducing the concentration. In some cases, this means of natural attenuation may be useful, since the hydrocarbons can be broken down by sunlight. Vapors in contact with soil microorganisms may be biodegraded.

The most important process of natural attenuation is biodegradation, which is the change in form of compounds carried out by microorganisms. Biodegradation processes are the major mechanisms that account for both containment of the petroleum hydrocarbon plume and reduction of the contaminant concentration. Under appropriate conditions, microorganisms can cause or assist chemical reactions that change the form of the contaminants so that little or no health risk remains. Biodegradation is important because many important components of petroleum hydrocarbon contamination can be destroyed by this process.

Biodegradation is largely based on microbial activity. Microorganisms transform nutrients into forms useful for energy and cell production by facilitating the transfer of electrons from electron donors to electron acceptors. Petroleum hydrocarbons can serve as electron donors. Electron acceptors are compounds that exist in the groundwater in relatively oxidized states. The most commonly occurring electron

acceptors in groundwater include *dissolved oxygen, nitrate, manganese (IV), iron (III), sulfate, and carbon dioxide.*

Biologically mediated degradation reactions are Reduction/Oxidation (*REDOX*) reactions, involving the transfer of electrons from the organic contaminant compound to an electron acceptor. Oxygen is the electron acceptor for aerobic metabolism, whereas nitrate, ferric iron, sulfate, and carbon dioxide can serve as electron acceptors for alternative anaerobic pathways, such as denitrification, manganese reduction, iron reduction, sulfate reduction, or methanogenesis (Newell et al., 1996).

In the presence of organic substrate and dissolved oxygen (*DO*), microorganisms capable of aerobic metabolism will predominate over anaerobic forms. However, *DO* is rapidly consumed in the interior of contaminant plumes, converting these areas into anoxic (low oxygen) zones. Under these conditions, anaerobic bacteria begin to utilize other electron acceptors to metabolize dissolved hydrocarbons. The principal factors influencing the utilization of the various electron acceptors by fuel-hydrocarbon-degrading bacteria include the relative biochemical energy provided by the reaction, the availability of individual or specific electron acceptors at a particular site, and the kinetics of the microbial reaction associated with the different electron acceptors.

The biochemical energy associated with alternative degradation pathways can be represented by the redox potential of the alternative electron acceptors: the more positive the redox potential, the more energetically favorable the reaction (Bioscreen, 1996). In general, rates of biodegradation follow the order of favorable electron acceptor availability:  $O_2 > NO_3^- > FeIII > SO_4^{2-} > CO_2$ . Based on thermodynamic considerations, the most preferred reaction should take place in the plume until all of the required electron acceptor is depleted. At that point, the next most-preferred reaction should begin and continue until that electron acceptor is consumed, leading to a pattern where preferred electron acceptors are consumed one at a time, in sequence (Newell et al., 1996).

### **1.1.3. Potential Advantages and Disadvantages of NA**

The potential advantages of natural attenuation can be listed as follows:

- Generation of a reduced volume of remediation wastes, as compared to that obtained when contaminated groundwater is treated “above ground”.
- Reduction in potential cross contamination of uncontaminated groundwater because pumping is not required.
- Reduction in the risk of human exposure to contamination, by keeping contaminants below ground.
- Fewer surface structures are required, so there is less disruption to the site and less ecological destruction due to construction activities.
- Can be combined with active remedial measures or used to remediate a portion of the site
- Overall remediation cost may be lower than active remediation

On the contrary, the potential limitations of NA are as follows:

- Longer time period may be required to achieve the cleanup goals, compared to active remediation
- Site characterization may be more complex and time consuming.
- Long-term monitoring and associated cost can be excessive for some sites
- Intermediate breakdown compounds may be more toxic than initial contaminants.
- If natural attenuation rates are too slow, contaminants may migrate before they are degraded
- Land and groundwater use controls are often required.

## 1.2. Scope and Objectives

The objectives of this study are

- to assess the effect of aquifer heterogeneity on the plume behavior and natural attenuation rates of BTEX compounds; and
- to develop a quantitative relationship between natural attenuation rates of BTEX compounds and aquifer heterogeneity, characterized by the coefficient of variation and correlation length of hydraulic conductivity field.

In order to achieve these objectives, first, hydraulic conductivity fields having different heterogeneity levels are generated using a FORTRAN Program called turning bands random field algorithm. The program simulates the hydraulic conductivity distributions according to the specified coefficient of variation and spatial correlation length to achieve the desired level of aquifer heterogeneity. The generated hydraulic conductivity field is used in another program, Visual MODFLOW with RT3D Transport Package, to simulate the flow field and the fate and transport of BTEX compounds in the aquifer. After the simulations of BTEX plumes subject to different hydraulic conductivity fields, the differences in plume behaviours were evaluated and then the biodegradation rates were calculated in order to quantify natural attenuation of BTEX compounds in different fields. For the calculation of these biodegradation rates, two different methods were used, namely Buscheck and Alcantar and Conservative Tracer Methods, which are commonly used in many field studies. Finally, a multiple non-linear regression analyses were conducted to identify and quantify the relationship between biodegradation rate constants and the parameters of aquifer heterogeneity, coefficient of variation and spatial correlation length of hydraulic conductivity.

This thesis is structured as follows: Chapter 2 gives information about the materials and methods used in the thesis. That is, the algorithm for random field generation, the modeling of BTEX transport in aquifers and the methods of calculating natural

attenuation rate constants, Buscheck-Alcantar Method and Conservative Tracer Methods are presented.

Chapter 3 presents the results and discussions. First, results for random hydraulic conductivity field are presented. Then, the simulation results for BTEX plume from Visual MODFLOW are provided. After the simulations, the biodegradation rates are calculated by using Buscheck and Alcantar Method and Conservative Tracer Method. Finally, multiple non-linear regression analyses are performed to find a functional relationship between biodegradation rates and level of heterogeneity; and overall results are discussed.

Chapter 4 provides the summary and conclusions from this work. The major findings of this thesis are presented in this section.

### **1.3. Literature Review**

Groundwater pollution by petroleum-derived hydrocarbons is a widespread problem throughout the industrialized world. Although active remedial technologies were used in past, environmental professionals have recognized the importance of natural processes in affecting contaminant attenuation. The applicability of monitored natural attenuation depends on both contaminant and site characterization. Recently, a large body of research results is reported in the literature to evaluate the effectiveness of natural attenuation processes. A review of these studies is summarized in the following sections.

The model development of Natural Attenuation of BTEX contamination is presented in Lu et al. (1999). The field studied in the paper is in a sandy aquifer near a petroleum oil and lubricant facility at Hill Air-Force Base in Utah. The observations at the studied field indicate that the BTEX contamination is degraded by using multiple terminal electron-accepting processes including aerobic respiration, denitrification, iron reduction, sulfate reduction, and methanogenesis. The developed

model agrees well with the field observations. It is shown in the study that the total amount of BTEX mass present in the aquifer is sensitive to hydraulic conductivity, first order degradation rate constant, and recharge. The shape of the BTEX plume is sensitive to the hydraulic conductivity and aquifer thickness ahead of the plume front. Dispersivity is also found to be a sensitive parameter with respect to the plume shape, but not total mass of BTEX. It is stated that, anaerobic degradation is responsible for the %70 of total BTEX degradation; the remaining part of the removal is handled by aerobic degradation.

The attenuation of BTEX plume (from an aircraft crash site) due to intrinsic bioremediation is studied by Chen et al. (1997). In the paper, a site specific field scale model describing the fate and transport of selected target compounds at the Wurtsmith Air Force Base is studied using a robust mechanistic two-dimensional simulator (the Michigan Unsaturated/Saturated Transformation (MUST) Model). The modeled processes include advective and dispersive transport mass transfer between constituent phases, and monod-type microbial transformation and growth under various redox conditions. The results indicate that the value of apparent biodegradation rate in the aerobic plume is  $0.018 \text{ day}^{-1}$ , which is within the range reported for other BTEX contaminated sites.

Field Investigation of the natural attenuation and intrinsic biodegradation rates at an underground storage tank site is reported by Kao and Wang (2001). A mass flux approach, which is accomplished by using the differences in total contaminant mass flux across two cross sections of the contaminant plume, is used to calculate the contaminant mass reduction and field-scale decay rate at a gasoline spill site. The mass flux calculation indicates that 88% of the dissolved in BTEX removal was observed by NA processes. A first order decay model was applied for the NA and intrinsic biodegradation rate calculations; the results indicate that intrinsic biodegradation processes were the major cause of the BTEX reduction and iron reduction is the dominant biodegradation pattern within the plume. The results show

that 99 % of the BTEX mass was removed by the natural attenuation processes; and intrinsic biodegradation process was responsible for the 87 % of the total removal.

Another field scale intrinsic bioremediation investigation, which was conducted at a gasoline spill site in Dublin, North Carolina, USA, is presented by Kao and Wang (1999). Due to the appearance of nonaqueous phase liquid (NAPL), dissolved BTEX are released into the groundwater with a total concentration of 60 mg/L. At the spill site, a cropland extends from the mid-plume area of the downgradient of the plume. Due to the usage of fertilizer, 15 mg/L nitrate was detected in the groundwater beneath the cropland area. In this study, a three year research was performed to characterize a BTEX contaminated aquifer and a spatial variations in aqueous phase geochemistry, to assess the mechanisms of intrinsic bioremediation, to calculate the mass flux and field scale degradation rate, and to assess the effects of the intrinsic bioremediation as a remedial alternative. Results show that BTEX concentrations drop to below detection level before reaching the downgradient monitoring well. Iron reduction, denitrification and aerobic degradation take place in the contaminated area, with mass flux removal of 93.1 %, 5.6 %, and 1.3 %, respectively. It is concluded from this paper that the iron reduction is the dominant degradation process within highly contaminated area.

A stochastic analysis of in-situ bioremediation within a heterogeneous porous media is studied by Lee et al. (1997). Numerical modeling techniques are performed to demonstrate how geologic complexity may affect the pump-and-treat and in-situ bioremediation of organic contaminated groundwater. Lee et. al. (1997) use turning bands method to generate two-dimensional random permeability fields, which is described by mean, variance, and the horizontal and vertical correlation length. This study integrates the BIOPLUME II (Rifai et al., 1989) computer model and turning bands method to assess the influence of the spatial variability in the permeability on the transport and degradation of organic plume. The results of this study shows that as the media become more heterogeneous, longer time is required for complete aquifer decontamination by pump-and-treat and in-situ bioremediation methods. Low

conductivity zones can trap significant amounts of pollutants and later release them into the groundwater. This effect can significantly increase the cost and time for complete cleanup. The irregular plume transport and biodegradation patterns in heterogeneous permeability fields differ markedly from the somewhat regular pattern shown in homogeneous aquifer.

An accurate and efficient numerical solution for the transport of biodegradable organic solutes is developed by MacQuarrie and Sudicky (1990a). A dual-Monod relationship, combined with the advection-dispersion equation, is used to represent the biological and physical processes affecting the organic solute, electron acceptor, and microbial population. In the paper, the three resulting differential equations are nonlinearly coupled through the Monod decay terms. By employing an iterative principal direction finite-element technique, efficiency is achieved by decoupling each of the two-dimensional transport equations into a series of one-dimensional equations. The principal direction Galerkin finite-element technique is used to iteratively solve the two-dimensional form of the resulting non-linear transport equations. Model results are compared to the results of a one-dimensional laboratory experiment to assess the applicability of the theoretical formulation of the problem. Finally, a two-dimensional example is presented to elucidate plume behavior in a uniform flow field and to demonstrate the favorable numerical characteristics of the iterative principal direction technique. The simulation results obtained for the case of a small dissolved organic source in a uniform horizontal flow field demonstrated that the behavior of an organic plume is significantly and rapidly affected by biodegradation. In a natural aquifer, oxygen availability in and around the plume controls the contaminant mass loss, the rate of spatial spreading, and the bulk rate of translation of the organic plume. It is also shown that, mass loss is initially rapid but slows with time due to the decrease in the organic and dissolved oxygen concentrations.

The numerical organic solute transport model developed by MacQuarrie and Sudicky (1990a) is used to examine the various physical, chemical and biochemical factors

which affect the behavior of organic plumes in a natural aquifer system (MacQuarrie et al, 1990b). MacQuarrie and Sudicky select a two-dimensional, shallow, unconfined, sandy aquifer with horizontal groundwater flow, while toluene and the dissolved oxygen are selected as organic solute and electron acceptor, respectively. This study is performed in both homogeneous and heterogeneous hydraulic conductivity fields. To generate the heterogeneous hydraulic conductivity fields, turning band algorithm was used in this study. It has been demonstrated that the physical and chemical parameters controlling the aerobic biodegradation of organic plume include the initial concentration of contaminant and dissolved oxygen, the average linear groundwater velocity, the retardation factor of organic solute, and the heterogeneity of the porous medium. In a uniform flow field, the rate of mass loss was observed to decrease with time since the organic and dissolved oxygen decreased with time due to biodegradation and dispersion processes. Low background concentration of dissolved oxygen also causes organic mass loss to decrease. Moreover, it is concluded that large groundwater velocity results in increase the rate of organic mass loss, because of increased mechanical mixing of contaminant and electron acceptor. The retardation effect on biodegradation shows that as the retardation factor increases the rate of mass loss decreases. In heterogeneous fields, the rate of spreading of the organic plume was found to dependent on the local scale transport parameters (such as groundwater velocity), and the rate of mass loss shows the same behavior observed in uniform flow field.

Natural attenuation processes include advection, dispersion, sorption, and biodecay. The contribution of those processes to the overall attenuation of petroleum hydrocarbons is studied by Buscheck & Alcantar (1995) by applying some well-known regression techniques and analytical solutions. In the paper, the regression of concentration versus distance for stable plumes was coupled with an analytical solution for one-dimensional, steady-state, contaminant transport. The mechanism of biodegradation is complex, and the rate is most likely controlled by the mixing of the contaminant and electron acceptors in a three-dimensional, heterogeneous aquifer. Therefore, the assumption of a first order decay is made in order to simplify the

analysis. The results show that, given a constant source, sorption and dispersion alone are not likely to account for a stable plume. According to the analysis, sorption only retards the velocity, whereas dispersion results in further spreading of the contaminant, reducing concentrations. It is indicated that, biodecay (biodegradation of BTEX compounds) is the most significant mechanism that accounts for mass loss in a dissolved contaminant plume.

When used with accurate estimates of dispersivity and groundwater flow and solute transport velocity, Buscheck and Alcantar method gives reasonable first-order biodegradation rates. However, Walt et. al. (1998) that the estimation of natural attenuation and degradation rates, using B&A method, is subject to significant imprecision and the analysis can be misinterpreted, especially when few number of monitoring points (or wells) are used. The reason behind this argument is that, when analyzing a small number of data points, it is often possible to fit a straight line through log concentration versus distance data with a high degree of correlation even when biotransformation is insignificant or absent altogether, resulting in incorrect biotransformation rate estimations.

## CHAPTER 2

### MATERIALS AND METHODS

The theoretical background for the generation of spatially correlated random hydraulic conductivity fields, the simulation of the fate and transport of BTEX Plumes and the software programs used are explained in this section.

#### 2.1. Random Field Generation

In porous media, the physical properties (such as porosity and hydraulic conductivity) change continuously from one location to another. Spatial heterogeneity, the variation of a physical property in 2- or 3-dimensional space, affects the flow and transport processes in groundwater. The generation of spatially correlated samples of random fields plays a fundamental role in the numerical analysis of stochastic processes - whether they are 1-, 2-, or 3-dimensional.

The stochastic analysis is the quantitative measure describing the uncertainty of the best estimate of the hydraulic properties, such as hydraulic conductivity. The purpose of random field simulation is to create numerical samples or "realizations" of stochastic processes with well-defined properties.

The random field generator used in this study is the Turning Bands Algorithm. The principal advantage of this method is that it reduces the generation of a 2- or 3-dimensional, random, spatially correlated process to the generation of one-dimensional, correlated line processes.

The turning bands method has been used to create artificial fields of physical quantities (such as rainfall distribution, hydraulic conductivities or other subsurface flow parameters) perceived to be random in various sorts of statistical or stochastic models of natural processes (Tompson et al., 1987).

There are several reasons for having the ability to simulate random fields. Firstly, the in-situ distribution of variable quantities is extremely difficult to measure in detail over large spatial or temporal distances. Secondly, the ability to mathematically represent spatially and temporally variable parameters as correlated random fields can allow larger scale mean effects and manifestations of this variability to be predicted through some sort of stochastic model. Since complete and detailed parameter measurements over space and time can be difficult (or impossible) to find, artificial distributions can be used in place of reality in simulations carried out to check the theoretical results (Tompson et al., 1987).

The success of the turning bands method lies in its efficiency at generated fields. The algorithm involves the generation of a series of one-dimensional random processes along lines radiating from a coordinate origin and their subsequent projection and combination at arbitrary points in space, yielding discrete values or realization of the field. An important advantage of the method lies in its computational efficiency, which is primarily derived from the conversion of a two- or three- dimensional problem to a series of one-dimensional problems (Tompson et al., 1987, Tompson et al., 1989).

### **2.1.1. Random Field Theory**

The concept of a random field derives directly from simple definition of a random variable. The turning bands method can be used to generate a second order, stationary random field whose marginal density functions are all normal of mean zero and variance one (Tompson et al., 1987). We define  $z(x)$  as the desired three-

dimensional normally distributed  $N(0, \sigma^2)$  field realization. Such a field could easily be transformed into another normal field  $z^*(x)$  with mean  $F$  and variance  $\sigma_f^2$  as;

$$z^*(x) = \sigma_f z(x) + F \quad (2.1)$$

or a lognormal field, such as a hydraulic conductivity  $K(x)$  distribution, as

$$K(x) = \exp(z^*(x)) = e^F e^{\sigma_f z(x)} = K_G e^{f(x)} \quad (2.2)$$

where  $K_G$  is the geometric mean of  $K(x)$ , that is  $K_G = e^F$ , and  $f(x)$  is equal to

$$f(x) = \sigma_f z(x) = z^*(x) - F \quad (2.3)$$

where  $F$  is the expected value of the transformed normal field, namely  $z^*(x)$ , i.e.  $F = E[z^*(x)]$ . From equation (2.2),  $z^*(x)$  is equal to  $\ln(K(x))$ , hence,  $f(x)$  in equation (2.3) is expressed as;

$$f(x) = \ln(K(x)) - E[\ln(K(x))] \quad (2.4)$$

The turning bands method can be used for the generation of both 2-dimensional and 3-dimensional random fields. The program codes have been written in FORTRAN. There are two different codes for each of 2-dimensional or 3-dimensional generation.

The required data are read in “subroutine input” in two groups. The first group contains physical information regarding the number of grid points, grid spacing, and statistical properties of log-normally distributed hydraulic conductivity field to be generated, namely spatial correlation length, and mean and variance. The second group of input data contains parametric data related to simulation itself and theoretical standpoint of line processes. This data set consists of choosing number

and orientation of lines, number of Monte Carlo Simulations, and properties of the ensemble histogram of the simulated normal field.

### 2.1.2. Generation of Hydraulic Conductivity Fields

Turning bands method is designed to generate a realization of stationary, correlated, multi-dimensional random fields from a normal distribution with zero mean and specified covariance structure (Tompson et al., 1989). Such a field is easily transformed to one with different characteristics (Tompson et al., 1987). In this study for the generation of randomly distributed isotropic hydraulic conductivity fields, an exponential covariance structure of the following form was used:

$$c(l) = \sigma^2 e^{-l/h} \quad (2.5)$$

where  $\sigma^2$  is the variance;  $l$  is the spatial lag distance; and  $h$  is the spatial correlation length. For anisotropic hydraulic conductivity fields, equation (2.5) takes the form;

$$c(l) = \sigma^2 \exp\left\{-\left[\left(l/h_x\right)^2 + \left(l/h_y\right)^2\right]^{1/2}\right\} \quad (2.6)$$

where  $h_x$  and  $h_y$  are correlation lengths in x- and y- directions, respectively.

In turning bands algorithm, the mean, variance, and the spatial correlation length of the generated random field are the important parameters that determine the degree of heterogeneity within the generated random field. The effect of mean and variance in field heterogeneity is stated by a ratio, called ‘‘Coefficient of Variation (CV)’’, which can be defined as:

$$CV = \frac{\sigma}{m} \quad (2.7)$$

In this study, as a result of stationarity assumption, the mean value of the hydraulic conductivity ( $K$ ) in the contaminated aquifer is taken as constant. For different coefficient of variation values (CV), different standard deviation values ( $\sigma$ ) can be calculated using the mean conductivity value to generate with different statistical properties.

As mentioned before, the turning bands algorithm generates lognormally distributed random fields. Since the generator produces a lognormal field, using a normal distribution, the mean and variance of this normal distribution have to be input to the program accordingly in order to generate a field with the specified mean and variance. For lognormally distributed variables, the following conversion formulas are used to determine the log mean  $m_{\ln}$  and log variance  $\sigma_{\ln}^2$  as

$$m_{\ln} = \ln(m) - \frac{\sigma_{\ln}^2}{2} \quad (2.8)$$

$$\sigma_{\ln}^2 = \ln\left(\frac{\sigma^2}{m^2} + 1\right) \quad (2.9)$$

where  $m$  and  $\sigma^2$  are the mean and variance of the original (non-transformed) log-normal random variable, respectively. The values of  $m_{\ln}$  and  $\sigma_{\ln}^2$  are used to generate the lognormal random variables from the transformed normal distribution  $N(m_{\ln}, \sigma_{\ln}^2)$  (Ünlü, 1994).

In turning bands algorithm,  $\sigma_{ln}$  is the input parameter of the random field generator. There is another input parameter,  $K_G$ , which is the median value of the random field, and calculated from  $m_{ln}$  value as:

$$K_G = e^{m_{\ln}} \quad (2.10)$$

In this research, nine different isotropic and two anisotropic hydraulic conductivity fields are generated by using turning bands methods. The mean hydraulic conductivity value is taken as constant for all isotropic and anisotropic fields, but the Coefficient of Variation and correlation length values vary from field to field.

The values of statistical input parameters, namely mean, variance, and correlation length, to be used in the generation of random hydraulic conductivity field are selected based on reported field observations (Carsel and Parrish, 1988; Ünlü et al, 1990; and Gelhar et al, 1992). The mean hydraulic conductivity is taken as 6.25 m/d, while CV as 50 %, 100 %, and 150 % and the correlation length as 5 m, 10 m, and 20 m, for the isotropic fields. Two anisotropic fields are generated to assess the anisotropy effects on the removal of contaminants. In the generation of anisotropic hydraulic conductivity fields, anisotropy ratio, in terms of correlation length, is taken as 5 (i.e.  $h_x / h_y = 5 / 1$ ). Two different anisotropic hydraulic conductivity fields are generated. For the first one, CV,  $h_x$ ,  $h_y$  are taken as 50 %, 20 m 4 m, respectively; for the second one, CV,  $h_x$ ,  $h_y$  are taken as 150 %, 10 m 2 m, respectively.

The conversion of the mean ( $m$ ) and standard deviation ( $\sigma$ ) of the original hydraulic conductivity field to the corresponding parameters of  $m_{ln}$  and  $\sigma_{ln}$  of normal hydraulic conductivity field are accomplished using equations (2.8) and (2.9). Calculated values of  $m_{ln}$  and  $\sigma_{ln}$ , as input to the turning bands algorithm, are summarized in Table 2.1.

The generated hydraulic conductivity fields are two dimensional, having a size of 150 m in x-direction and 100 m in y-direction with a grid spacing value of  $\Delta x = \Delta y = 0.5$  m. The complete physical and parametric input data of random field generator, for each of nine generated fields are given in Appendix A.

Table 2.1. Mean  $m_{ln}$  and standard deviation  $\sigma_{ln}$  values of ln-hydraulic conductivity field for different coefficient of variation, CV and correlation length, h.

	h = 5 m		h = 10 m		h = 20 m	
	$m_{ln} (m)$	$\sigma_{ln} (\sigma)$	$m_{ln} (m)$	$\sigma_{ln} (\sigma)$	$m_{ln} (m)$	$\sigma_{ln} (\sigma)$
CV = 50 %	-9.6457 (7.234x10 <sup>-5</sup> )	0.47238 (3.617x10 <sup>-5</sup> )	-9.6457 (7.234x10 <sup>-5</sup> )	0.47238 (3.617x10 <sup>-5</sup> )	-9.6457 (7.234x10 <sup>-5</sup> )	0.47238 (3.617x10 <sup>-5</sup> )
CV = 100 %	-9.8807 (7.234x10 <sup>-5</sup> )	0.83255 (7.234x10 <sup>-5</sup> )	-9.8807 (7.234x10 <sup>-5</sup> )	0.83255 (7.234x10 <sup>-5</sup> )	-9.8807 (7.234x10 <sup>-5</sup> )	0.83255 (7.234x10 <sup>-5</sup> )
CV = 150 %	-10.123 (7.234x10 <sup>-5</sup> )	1.0857 (1.085x10 <sup>-4</sup> )	-10.123 (7.234x10 <sup>-5</sup> )	1.0857 (1.085x10 <sup>-4</sup> )	-10.123 (7.234x10 <sup>-5</sup> )	1.0857 (1.085x10 <sup>-4</sup> )

## 2.2. Modeling Fate and Transport of BTEX

The fate and transport of BTEX contamination in the aquifer having the generated random hydraulic conductivity field are modeled using a computer program, called Visual MODFLOW. An overview of Visual MODFLOW, its input requirements and the modeling approach are explained in this section.

### 2.2.1. Overview of Visual MODFLOW

Visual MODFLOW is a 3-D groundwater flow and contaminant transport modeling program. It includes various flow and transport packages. Among these, MODFLOW and RT3D packages were used in this study. MODFLOW package is used to simulate of groundwater flow regime while, the RT3D package is used to simulate the fate and transport of BTEX plume in the aquifers.

Visual MODFLOW is currently the most complete and relatively easy-to-use modeling environment for practical applications in three dimensional groundwater flow and contaminant transport simulations (Waterloo Hydrogeologic Inc., 2002). Visual MODFLOW consists of a menu structure that guides a user to build input files, calibrate and evaluate a groundwater flow and contaminant transport model output.

### 2.2.1.1. MODFLOW Package

MODFLOW is a computer program that numerically solves the three-dimensional groundwater flow equation for a porous medium by using a finite-difference method (Harbaugh et al., 2002). The modular structure of MODFLOW consists of a Main Program and a series of highly-independent subroutines called modules. The modules are grouped in packages. Each package deals with a specific feature of the hydrologic system which is to be simulated, such as flow from rivers or flow into drains. The division of MODFLOW into modules permits the user to examine specific hydrologic features of the model independently (Harbaugh et al., 2002).

A large amount of information and a complete description of the flow system are required to make the most efficient use of MODFLOW. To use MODFLOW, the region to be simulated must be divided into cells with a rectilinear grid resulting in layers, rows and columns. Files must then be prepared that contain hydraulic parameters (hydraulic conductivity, transmissivity, specific yield, etc.), boundary conditions (location of impermeable boundaries and constant heads), and stresses (pumping wells, recharge from precipitation, rivers, drains, etc.) (Harbaugh et al., 2002).

In MODFLOW, the following groundwater flow equation is solved using the finite-difference approximation. The general form of the groundwater flow equation for 3-dimensional subsurface systems is described by the partial differential equation:

$$\frac{\partial}{\partial x} \left( K_{xx} \frac{\partial H}{\partial x} \right) + \frac{\partial}{\partial y} \left( K_{yy} \frac{\partial H}{\partial y} \right) + \frac{\partial}{\partial z} \left( K_{zz} \frac{\partial H}{\partial z} \right) - W = S_s \frac{\partial H}{\partial t} \quad (2.11)$$

where  $K_{xx}$ ,  $K_{yy}$  and  $K_{zz}$  are the hydraulic conductivity values along x, y, and z directions which are assumed to be parallel to the major axis of hydraulic conductivity, ( $LT^{-1}$ );  $H$  is the potentiometric head, (L);  $W$  is the volumetric flux per

unit volume of aquifer and represents sources/sinks, ( $T^{-1}$ );  $S_s$  is the specific storage of the aquifer, ( $L^{-1}$ ); and  $t$  is time, (T).

In MODFLOW, the flow region is subdivided into blocks in which the medium properties are assumed to be uniform. In plan view, the blocks are made from a grid of mutually perpendicular lines that may be variably spaced. Model layers can have varying thickness. A flow equation is written for each block, called a cell. Several solvers are provided for solving the resulting matrix problem; the user can choose the best solver for the particular problem. Flow-rate and cumulative-volume balances from each type of inflow and outflow are computed for each time step (Harbaugh et al., 2002).

#### **2.2.1.2. RT3D Package**

RT3D (The Reactive Transport in 3-Dimensions) is a computer code used for modeling the contaminant fate and transport in groundwater systems. This computer code solves the coupled partial differential equations that describe transport of multiple, mobile and/or immobile reactive species in three-dimensional groundwater. In RT3D, there are specified reaction kinetics for the specified species; petroleum hydrocarbons and chlorinated solvents.

The current version of RT3D uses the advection and dispersion solvers and requires the groundwater flow code MODFLOW simulations for computing spatial and temporal variations in groundwater velocity distribution.

The RT3D code is unique in that it includes an implicit reaction solver that makes the code sufficiently flexible for simulating various types of chemical and microbial reaction kinetics. It supports seven pre-programmed reaction modules that can be used to simulate different types of reactive contaminants including benzene-toluene-xylene mixtures (BTEX), and chlorinated solvents (PCE - TCE). In addition, RT3D

has a user-defined reaction option that can be used to simulate any other types of user-specified reactive transport systems (Sun et al., 1998).

### 2.2.1.3. Governing Equations

RT3D is a finite – difference code, which is developed to solve the multi-species reactive transport equations given as (Clement, 1997);

$$\frac{\partial C_k}{\partial t} = \frac{\partial}{\partial x_i} \left( D_{ij} \frac{\partial C_k}{\partial x_j} \right) - \frac{\partial}{\partial x_i} (v_i C_k) + \frac{q_s}{\phi} C_{s_k} + r_c \quad \text{where } k = 1, 2, \dots, m \quad (2.12)$$

where  $m$  is the total number of aqueous-phase (mobile) species;  $C_k$  is the aqueous-phase concentration of the  $k^{\text{th}}$  species [ $\text{ML}^{-3}$ ];  $D_{ij}$  the hydrodynamic dispersion coefficient [ $\text{L}^2\text{T}^{-1}$ ];  $v$  is the pore velocity [ $\text{LT}^{-1}$ ];  $\phi$  is the soil porosity;  $q_s$  is the volumetric flux of water per unit volume of aquifer representing sources and sinks [ $\text{T}^{-1}$ ];  $C_s$  is the concentration of source/sink [ $\text{ML}^{-3}$ ];  $r_c$  is the rate of all reactions that occur in the aqueous phase [ $\text{ML}^3\text{T}^{-1}$ ].

The mobile species transport given in equation (2.12) can be divided into four different equations:

The advection equation, 
$$\frac{\partial C}{\partial t} = - \frac{\partial (v_i C)}{\partial x_i} \quad (2.13)$$

The dispersion equation, 
$$\frac{\partial C}{\partial t} = \frac{\partial}{\partial x_i} \left( D_{ij} \frac{\partial C}{\partial x_j} \right) \quad (2.14)$$

The source-sink mixing equation, 
$$\frac{\partial C}{\partial t} = \frac{q_s}{\phi} C_s \quad (2.15)$$

The reaction equation, 
$$\frac{dC}{dt} = r \quad (2.16)$$

In immobile transport species equation, all terms, except the reaction term, are equal to zero. Then the equation (2.12) becomes following equation:

$$\frac{d\tilde{C}_{im}}{dt} = \tilde{r}_c \quad \text{where } im = 1, 2, \dots, (n-m) \quad (2.17)$$

where  $n$  is the total number of species;  $m$  is the total number of aqueous-phase (mobile) species (thus,  $n$  minus  $m$  is the total number of solid-phase or immobile species),  $\tilde{C}_{im}$  is the solid-phase concentration of the  $im^{\text{th}}$  species [either  $\text{MM}^{-1}$  (contaminant mass per unit mass of porous media) or  $\text{ML}^{-3}$  (contaminant mass per unit aqueous-phase volume) unit basis can be used],  $\tilde{r}_c$  is the rate of all reactions that occur in the soil-phase [either  $\text{MM}^{-1}\text{T}^{-1}$  or  $\text{ML}^3\text{T}^{-1}$  can be used].

#### 2.2.1.4. Modules Available For Reaction Kinetics In RT3D

The RT3D code always requires a reaction module to define the problem-specific reactions (i.e., how the contaminants react with each other and with the subsurface). RT3D Modules are used for simulating different types of reactive contaminants. In RT3D, seven pre-programmed reaction modules and a user-defined reaction module are available. Among these, three of the modules can be used to model BTEX degradation. These modules are Instantaneous Aerobic Decay of BTEX, Instantaneous Degradation of BTEX using Multiple Electron Acceptors, and Kinetic-Limited Degradation of BTEX using Multiple Electron Acceptors.

Due to the complex nature of the subsurface systems, multi-species reactive transport simulation is generally needed both to accurately reflect existing site conditions and to quantify the effectiveness of the biodegradation processes (Lu et al., 1999). Therefore, in this study, the third module, Kinetic-limited degradation of BTEX

using multiple electron acceptors, is used to model BTEX degradation. This module uses kinetic-limited reactions rather than the instantaneous reactions. The kinetic-limited reactions occur in the sequential order as seen in the natural groundwater systems. This module also predicts the rate of hydrocarbon decay, which is directly proportional to the species concentrations.

The following section provides details of the kinetic – limited BTEX degradation model.

### **Kinetic-Limited Degradation of BTEX Using Multiple Electron Acceptors**

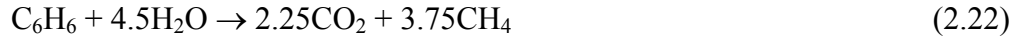
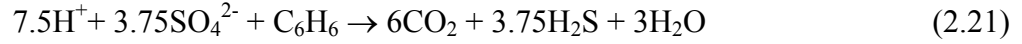
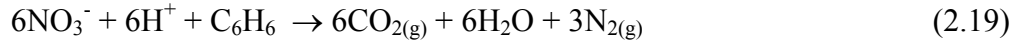
BTEX biodegradation is essentially an oxidation-reduction process where the BTEX (electron donor) are oxidized and the electron acceptor (e.g. O<sub>2</sub>, NO<sub>3</sub><sup>-</sup>, Fe<sup>+3</sup>, SO<sub>4</sub>, or CO<sub>2</sub>) is reduced. The following conceptual biochemical model can be used to represent various degradation reactions taking place in real subsurface systems (Lu et al., 1999);



where ED is the electron donor; EA is the electron acceptor; mo is the microorganism.

The reactive transport model considered here simulates the transport and rate-limited degradation of hydrocarbon through five different degradation pathways: aerobic respiration, denitrification, iron reduction, sulfate reduction, and methanogenesis. The stoichiometry of these degradation reactions is described by the following equations (Wiedemeier et al., 1999);





The reactions given in equations (2.18) to (2.22) are assumed to occur in a sequential order, as listed above. This sequential order is based on thermodynamic consideration. In a contaminated aquifer, first, the aerobic respiration occurs until the dissolved oxygen is depleted. Lastly, methanogenesis occurs.

The form of transport equations solved by this module is described by the following equations:

$$R_{HC} \frac{\partial[HC]}{\partial t} = \frac{\partial}{\partial x_i} \left( D_{ij} \frac{\partial[HC]}{\partial x_j} \right) - \frac{\partial(v_i[HC])}{\partial x_i} + \frac{q_s}{\phi} [HC]_s + r_{HC} \quad (2.23)$$

$$R_{O_2} \frac{\partial[\Theta_2]}{\partial t} = \frac{\partial}{\partial x_i} \left( D_{ij} \frac{\partial[O_2]}{\partial x_j} \right) - \frac{\partial(v_i[O_2])}{\partial x_i} + \frac{q_s}{\phi} [O_2]_s + r_{O_2} \quad (2.24)$$

$$R_{NO_2} \frac{\partial[NO_3]}{\partial t} = \frac{\partial}{\partial x_i} \left( D_{ij} \frac{\partial[NO_3]}{\partial x_j} \right) - \frac{\partial(v_i[NO_3])}{\partial x_i} + \frac{q_s}{\phi} [NO_3]_s + r_{NO_3} \quad (2.25)$$

$$R_{Fe^{2+}} \frac{\partial[Fe^{2+}]}{\partial t} = \frac{\partial}{\partial x_i} \left( D_{ij} \frac{\partial[Fe^{2+}]}{\partial x_j} \right) - \frac{\partial(v_i[Fe^{2+}])}{\partial x_i} + \frac{q_s}{\phi} [Fe^{2+}]_s + r_{Fe^{2+}} \quad (2.26)$$

$$R_{SO_4} \frac{\partial[SO_4]}{\partial t} = \frac{\partial}{\partial x_i} \left( D_{ij} \frac{\partial[SO_4]}{\partial x_j} \right) - \frac{\partial(v_i[SO_4])}{\partial x_i} + \frac{q_s}{\phi} [SO_4]_s + r_{SO_4} \quad (2.27)$$

$$R_{CH_4} \frac{\partial[CH_4]}{\partial t} = \frac{\partial}{\partial x_i} \left( D_{ij} \frac{\partial[CH_4]}{\partial x_j} \right) - \frac{\partial(v_i[CH_4])}{\partial x_i} + \frac{q_s}{\phi} [CH_4]_s + r_{CH_4} \quad (2.28)$$

In this model, a kinetic reaction framework is used to model the reaction terms. In the kinetic model, the rate of hydrocarbon decay is assumed to be directly proportional to hydrocarbon concentration (i.e. the decay is a first-order reaction). A Monod-type term is used to account for the presence (or absence) of various electron acceptors, and an inhibition model is used to simulate inhibition due to the presence of any of the earlier EAs (i.e. an EA with higher energy in the reaction chain) (Lu et al., 1999).

The kinetic expressions used for modeling hydrocarbon decay are:

$$r_{HC,O_2} = -k_{O_2} [HC] \frac{[O_2]}{K_{O_2} + [O_2]} \quad (2.29)$$

$$r_{HC,NO_3} = -k_{NO_3} [HC] \frac{[NO_3]}{K_{NO_3} + [NO_3]} \frac{K_{i,O_2}}{K_{i,O_2} + [O_2]} \quad (2.30)$$

$$r_{HC,Fe^{2+}} = -k_{Fe^{3+}} [HC] \frac{[Fe^{3+}]}{K_{Fe^{3+}} + [Fe^{3+}]} \frac{K_{i,O_2}}{K_{i,O_2} + [O_2]} \frac{K_{i,NO_3}}{K_{i,NO_3} + [NO_3]} \quad (2.31)$$

$$r_{HC,SO_4} = -k_{SO_4} [HC] \frac{[SO_4]}{K_{SO_4} + [SO_4]} \frac{K_{i,O_2}}{K_{i,O_2} + [O_2]} \frac{K_{i,NO_3}}{K_{i,NO_3} + [NO_3]} \frac{K_{i,Fe^{3+}}}{K_{i,Fe^{3+}} + [Fe^{3+}]} \quad (2.32)$$

$$r_{HC,CH_4} = -k_{CH_4} [HC] \frac{[CH_4]}{K_{CH_4} + [CH_4]} \frac{K_{i,O_2}}{K_{i,O_2} + [O_2]} \frac{K_{i,NO_3}}{K_{i,NO_3} + [NO_3]} \frac{K_{i,Fe^{3+}}}{K_{i,Fe^{3+}} + [Fe^{3+}]} \frac{K_{i,SO_4}}{K_{i,SO_4} + [SO_4]} \quad (2.33)$$

where  $r_{HC,O_2}$  is the hydrocarbon destruction rate utilizing oxygen;  $r_{HC,NO_3}$  is the destruction rate utilizing nitrate;  $r_{HC,Fe^{2+}}$  is the destruction rate utilizing  $Fe^{3+}$  (or producing  $Fe^{2+}$ );  $r_{HC,SO_4}$  is the destruction rate utilizing sulfate;  $r_{HC,CH_4}$  is the destruction rate via methanogenesis;  $[O_2]$  is oxygen concentration  $[ML^{-3}]$ ;  $k_{O_2}$  is the first-order degradation rate constant for hydrocarbon utilizing oxygen as the electron acceptor  $[T^{-1}]$ ;  $K_{O_2}$  is the Monod half-saturation constant  $[ML^{-3}]$ ;  $K_{i,O_2}$  is the oxygen inhibition constant  $[ML^{-3}]$ ; and similar nomenclature is used for all subsequent reactions. The inhibition constants are typically set to some arbitrarily small values to simulate the sequential electron acceptor utilization process.

Since the concentration of  $Fe^{3+}$  and  $CO_2$  cannot be measured under normal field conditions, these concentration terms were replaced with “assimilative capacity terms” (for iron reduction and methanogenesis) defined as:

$$[Fe^{3+}] = [Fe^{2+}_{max}] - [Fe^{2+}] \quad (2.34)$$

$$[MC] = [CO_2] = [CH_{4,max}] - [CH_4] \quad (2.35)$$

where  $[Fe^{2+}_{max}]$  and  $[CH_{4,max}]$  are the maximum levels (or expected levels) of  $Fe^{2+}$  and  $CH_4$ , respectively, measured in the field, and represent the aquifer’s total

capacity for iron reduction and methanogenesis; and  $[MC]$  is the methanogenic capacity of the aquifer.

Since methane production is a fermentation process, there is no external electron transfer process involved in this reaction step. Therefore, the concentration term for  $CO_2$ , used in equation (2.33), should be considered as a hypothetical term that simply indicates the methanogenic capacity (MC) of the aquifer. Similarly, the concentration term for  $Fe^{3+}$ , used in (2.31), should also be considered as a hypothetical term representing the iron reduction capacity (bioavailable iron) of the aquifer. Using transformation equations (2.34) and (2.35), the unquantifiable concentration levels of the species  $Fe^{3+}$  and  $CO_2$  are related back to field-measurable  $Fe^{2+}$  and  $CH_4$  concentrations.

The total rate of hydrocarbon destruction via all decay processes is written as:

$$r_{HC} = r_{HC,O_2} + r_{HC,NO_3} + r_{HC,Fe^{2+}} + r_{HC,SO_4} + r_{HC,CH_4} \quad (2.36)$$

Rates of electron acceptor utilization (or product formation) are given by the rates of hydrocarbon destruction multiplied by an appropriate yield coefficient (Y):

$$r_{O_2} = Y_{O_2/HC} r_{HC,O_2} \quad (2.37)$$

$$r_{NO_3} = Y_{NO_3/HC} r_{HC,NO_3} \quad (2.38)$$

$$r_{Fe^{2+}} = -Y_{Fe^{2+}/HC} r_{HC,Fe^{2+}} \quad (2.39)$$

$$r_{SO_4} = Y_{SO_4/HC} r_{HC,SO_4} \quad (2.40)$$

$$r_{CH_4} = -Y_{CH_4/HC} r_{HC,CH_4} \quad (2.41)$$

Assuming that BTEX represents all fuel contaminants, the yield value for hydrocarbon destruction with all decay processes are tabulated in Table 2.2.

Table 2.2. Yield values for hydrocarbon destruction with decay processes

Process	$Y_{O_2/HC}$	$Y_{NO_3/HC}$	$Y_{Fe^{2+}/HC}$	$Y_{SO_4/HC}$	$Y_{CH_4/HC}$
Yield Value*	3.14	4.9	21.8	4.7	0.78

\* all yield values are based on mg/L basis

It should be noted that the kinetic model described above assumes that degradation reactions occur only in the aqueous phase, which is a conservative assumption. The model includes six mobile (aqueous phase) components, namely BTEX, oxygen, nitrate, iron (II), sulfate, and methane.

### 2.2.2. Description of Simulated Aquifer System

In this study, a real contaminated Petroleum, Oil, and Lubricant (POL) Facility, in Hill Air Force Base (AFB), in Utah, USA was considered (Lu et al., 1999). At this site, a BTEX spill into the groundwater from an Underground Storage Tank (UST) occurred. The soil and groundwater contamination at the site was realized during the removal of UST. Because of this, the actual source of the contamination and the total amount of fuel leaked into the subsurface was not known exactly. A mobile LNAPL was present, and the distribution of the LNAPL was used to characterize the BTEX source, at this site.

This contamination situation was simulated in field with a dimension of 150 m to 100 m. The field domain was discretized using a numerical grid with 300 columns and 200 rows, having grid spacing of 0.5 m. Most of the site and plume data is taken from Hill AFB site, however, some of the unavailable required parameters for the Visual MODFLOW program are chosen independently, but realistically.

As the first step of the numerical model building, the 2-dimensional flow field was discretized into square grids, in the same manner as the discretization of generated random fields. In other words, generated random hydraulic conductivity field and groundwater flow field use the same grid system in order to assign model hydraulic conductivity values and to preserve the spatial random structure of the hydraulic conductivity field. During discretization of the flow field, square grid size selected taking into account of the numerical concern that at a minimum of 5 nodal hydraulic conductivity values should fall within the specified correlation length. This concern is important to maintain the numerical robustness of generated random fields. Table 2.3 shows the dimensions and the characteristics of the grid system selected for numerical flow and transport simulations.

Table 2.3. The dimensional description and discretization of the aquifer system.

<i>The length in x-direction</i>	
x-min (m)	0
x-max (m)	150
<i>The length in y-direction</i>	
y-min (m)	0
y-max (m)	100
<i>Grid spacing</i>	
$\Delta x$ (m)	0.5
$\Delta y$ (m)	0.5
<i>Number of columns</i>	300
<i>Number of rows</i>	200
<i>Number of layers</i>	1

### 2.2.3. Input Data File Preparation

Following the discretization of the domain, the input data files to characterize the groundwater flow system and the source and transport behavior of BTEX plume are prepared. The data for groundwater flow characterization are input to the program using Input Menu. The data required for the fate and transport of BTEX can be input

to the program by the help of Transport Engine in Setup Menu. All input data requirement of the program are explained in detail, in the following sections.

### **2.2.3.1. Input Data for Flow Package**

Using Input menu of Visual MODFLOW, all input data describing the groundwater flow system is specified. This data include the material properties of the aquifer and flow and transport boundary conditions. Further explanation for these input data are presented in the following sections.

#### *Flow Boundary*

The object of defining flow boundary in the system is to characterize the groundwater flow, by using velocity and head distribution. In Hill AFB, the measured groundwater levels indicate that the average groundwater flow direction and the gradient remained fairly constant. In the system, the constant linear head boundary condition is selected for the west and the east boundaries. The hydraulic gradient between west and the east boundaries is taken as  $5 \times 10^{-3}$  m/m. Therefore, the groundwater head difference across the flow domain is 0.75 m. The other boundaries (north and south boundaries) are selected as no flow boundary in order to obtain linear velocity field. Figure 2.1 shows the assigned boundary conditions, contaminant source and grid system of the simulated domain.

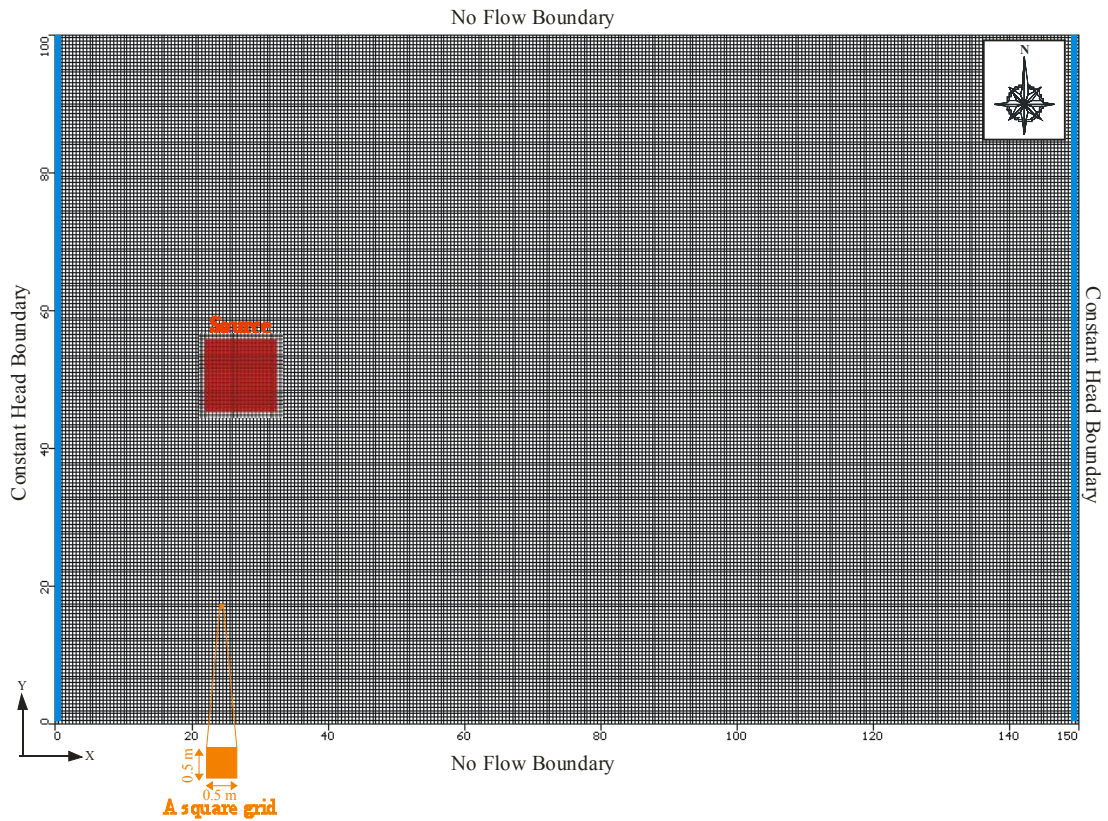


Figure 2.1. Boundary conditions, source area and grid system of the simulated domain.

### *Recharge Boundary and Source Boundary*

At Hill Air Force Base, the recharge is mainly controlled by the soil properties. The amount of recharge into the system is specified as 45 mm/year, as observed for Hill Air Force Base (Lu et al., 1999). The chemical composition of the recharging water is also specified for the system; it is taken same as the initial composition of unpolluted groundwater (see Table 2.7). In other words, the recharging water is assumed to be free of BTEX.

To define the entry of BTEX and other species into the system through the upgradient boundary (i.e. through the recharging groundwater), the west boundary was selected as constant concentration transport boundary, as shown in Table 2.4. At

the north, south and east boundaries, in order to allow the solutes to move freely out of the domain, default boundary condition, meaning no mass flux boundary, of the program are used.

Table 2.4. Constant concentration boundary of the system at the west boundary.

<b>Time (days)</b>	<b>BTEX (mg/L)</b>	<b>O<sub>2</sub> (mg/L)</b>	<b>Nitrate (mg/L)</b>	<b>Fe<sup>+2</sup> (mg/L)</b>	<b>Sulfate (mg/L)</b>	<b>Methane (mg/L)</b>
0-1000	0	6	17	0.001	100	0.0001

Additionally, the source of the system is characterized by constant concentration boundary condition. The size of the source is chosen as  $10\text{ m}$  in both  $x$  and  $y$ -direction, with an area of  $100\text{ m}^2$ . Table 2.5 gives the source definition in the system. As seen from Table 2.5, the source behaves as a pulse with a moderate duration. Source concentration is taken as the solubility of BTEX compounds, since after the spill, some free product (as LNAPL) was found at Hill Air Force Base Site (Lu et. al., 1999). The concentrations of the electron acceptors are also assigned at the source, according to the concentrations of the free product found at Hill Air Force Base Site (Lu et. al., 1999).

Table 2.5. Source definition

<b>Time (days)</b>	<b>BTEX (mg/L)</b>	<b>O<sub>2</sub> (mg/L)</b>	<b>Nitrate (mg/L)</b>	<b>Fe<sup>+2</sup> (mg/L)</b>	<b>Sulfate (mg/L)</b>	<b>Methane (mg/L)</b>
0-250	125	1	1	50.5	2	2
250-275	12.5	1	1	50.5	2	2
275-1000	0	1	1	50.5	2	2

### *Material Properties*

In this sub-menu of the program, material properties of the aquifer are specified. Table 2.6 shows the values of aquifer material properties used in the numerical simulations.

Table 2.6. The material property values of the aquifer system.

<i>Material Property</i>	<i>Symbol</i>	<i>Values</i>
<b>Hydraulic Conductivity**</b>	$K_x=K_y^*$	$7.234 \times 10^{-5}$ m/s
<b>Specific Storage</b>	$S_s$	$1 \times 10^{-7}$ m
<b>Specific Yield</b>	$S_y$	0.22
<b>Total Porosity**</b>	$\phi$	0.25
<b>Longitudinal Dispersivity**</b>	$\sigma_x$	8.5 m
<b>Transverse Dispersivity**</b>	$\sigma_y$	0.85 m
<b>Diffusion Coefficient</b>	$D_o$	$1 \times 10^{-5}$ m <sup>2</sup> /d

\*  $K_x = K_y = 7.234 * 10^{-5}$  is used only for the uniform case.

\*\* Lu et al. (1999).

For the isotropic and anisotropic, heterogeneous media, the hydraulic conductivity fields generated in the random field generator were imported to the program and these hydraulic conductivity distributions were used in the simulations.

### 2.2.3.2. Input Data for Fate and Transport Package

In Visual MODFLOW, transport engine is used in order to input contaminant properties and possible degradation mechanisms. In this part, also a numeric engine is selected to perform the numeric calculations required for the solution of the finite difference equations of groundwater flow and mass transport.

For this study, RT3D is selected as the numeric engine for simulation of the fate and transport of BTEX. For the sorption of contaminant, linear equilibrium sorption model was selected with a distribution coefficient,  $K_d = 4.41 \times 10^{-8}$  L / mg. Additionally, biodegradation kinetics of BTEX was selected as Kinetic Limited Multi-Path Degradation. This kinetic model was developed to describe degradation reactions of BTEX, under different conditions. This model assumes that all BTEX decay reactions are first-order degradation reactions. Therefore, the first-order

hydrocarbon decay rates are used as input to the kinetic model. The values of the degradation rate constants were selected based on literature data (Lu et al., 1999).

Initial concentrations of the contaminant and the electron acceptors in groundwater, before the spill occurs, are the important inputs for the system. It was assumed that initially no BTEX was present in the aquifer. Initial concentrations of electron acceptor species are selected considering the natural geochemistry of groundwater and presented in Table 2.7.

In this module, the inhibition model is used to simulate inhibition due to the presence of earlier electron acceptors having higher free energy. The inhibition constants are set to small values in order to simulate pure sequential electron acceptor processes. If the inhibition constants are assigned to very large values, larger than the value of electron acceptor species, then the simultaneous use of electron acceptors can be simulated. As seen in Table 2.7, all inhibition constants, except for iron reaction was set at 1 mg/L. The inhibition constant for iron was set at 10 mg/L to allow simultaneous iron- and sulfate-use reactions (Lu et al., 1999).

Similarly, half saturation constants were set to the small values, so that, zero-order dependency with respect to the electron donor, and the first order degradation model with respect to BTEX can be simulated. All saturation constants were set at 0.05 mg/L, as seen in Table 2.7.

Additionally, the stoichiometric yield values for BTEX are needed as input to the kinetic model. Since this kinetic model assumes that BTEX represents all fuel contaminants in aqueous phase, the yield value for hydrocarbon destruction with all decay processes, which is tabulated in Table 2.2 in the previous section, are also input to the program.

Table 2.7 Input parameters (Initial concentrations, degradation rates, saturation constants, inhibition constants) used in the BTEX degradation kinetics model.

<b>Kinetic Parameter</b>	<b>Symbol</b>	<b>Units</b>	<b>Value</b>
Initial Conc. of Oxygen	$C_{0,O_2}$	mg/L	6
Initial Conc. of Nitrate	$C_{0,NO_3}$	mg/L	17
Initial Conc. of $Fe^{3+}$	$C_{0,Fe^{3+}}$	mg/L	0.001
Initial Conc. of Sulfate	$C_{0,SO_4}$	mg/L	100
Initial Conc. of Methane	$C_{0,CH_4}$	mg/L	0.0001
Max. Conc. of $Fe^{+2}$	$Fe_{max}^{+2}$	mg/L	50.5
Max. Conc. of Methane	$CH_{4,max}$	mg/L	2.05
Aerobic Hydrocarbon Decay Rate	$k_{O_2}$	d <sup>-1</sup>	0.051
Hydrocarbon Decay Rate via Denitrification	$k_{NO_3}$	d <sup>-1</sup>	0.031
Hydrocarbon Decay Rate via Iron Reduction	$k_{Fe^{3+}}$	d <sup>-1</sup>	0.005
Hydrocarbon Decay Rate via Sulfate Reduction	$k_{SO_4}$	d <sup>-1</sup>	0.004
Hydrocarbon Decay Rate via Methanogenesis	$k_{CH_4}$	d <sup>-1</sup>	0.002
Half Saturation Constant for Oxygen	$K_{O_2}$	mg/L	0.5
Half Saturation Constant for Nitrate	$K_{NO_3}$	mg/L	0.5
Half Saturation Constant for $Fe^{3+}$	$K_{Fe^{3+}}$	mg/L	0.5
Half Saturation Constant for Sulfate	$K_{SO_4}$	mg/L	0.5
Half Saturation Constant for Methane	$K_{CH_4}$	mg/L	0.5
Inhibition Coefficient for Oxygen Reduction	$Ki_{O_2}$	mg/L	1
Inhibition Coefficient for Nitrate Reduction	$Ki_{NO_3}$	mg/L	1
Inhibition Coefficient for $Fe^{3+}$ Reduction	$Ki_{Fe^{3+}}$	mg/L	10
Inhibition Coefficient for Sulfate Reduction	$Ki_{SO_4}$	mg/L	1
Inhibition Coefficient for Methane Reduction	$Ki_{CH_4}$	mg/L	1

### **2.2.3.3. Model Output**

For modeling fate and transport of BTEX, through various flow fields of different level of heterogeneity, RT3D and MODFLOW are run at transient state for *1000 days*. The output of the Visual MODFLOW Program provides the visualization of the simulation results. The outputs consist of hydraulic head, velocity, and concentration distributions in the model domain.

## **2.3. Calculation of Biodegradation Rates**

The first-order attenuation rate constant is an important parameter for evaluating natural attenuation processes at groundwater contamination sites. The overall impact of natural attenuation processes at a given site can be assessed by evaluating the rate at which contaminant concentrations are decreasing both spatially and temporally.

There are two methods reported in the literature regarding the calculation of BTEX biodegradation rates. These methods are called Buscheck-Alcantar and Conservative Tracer Method, and briefly explained in the following sections.

### **2.3.1. Buscheck-Alcantar Method**

The mechanism of biodegradation is complex, and the degradation rate is controlled by mixing of contaminant and the electron acceptors. The assumption of a first order decay is the most useful approximation of this complex phenomenon.

The Buscheck and Alcantar method (Buscheck, Alcantar, 1995) is based on a derived relationship that allows calculation of an approximate biodegradation rate constant. An important assumption of the methodology is that the contaminant plume has reached a steady-state configuration. A stable plume is characterized by contaminant concentrations remaining constant over time.

The first-order decay reaction of the contaminant,  $C$ , as a function of distance,  $x$ , can be derived from (Kemblowski et al., 1987);

$$C(x) = C_0 e^{-k \frac{x}{v_x}} \quad (2.42)$$

where  $C_0$  is the concentration at the source;  $k$  is the first-order mass attenuation rate coefficient; and  $v_x$  is the average groundwater velocity. Note that the term “ $x/v_x$ ” is the residence time for the pore water to move some distance,  $x$ , from the source.

Buscheck and Alcantar method involves coupling a linear regression analysis, involving a semi-log concentration versus downgradient distance plots, to an analytical solution of one-dimensional, steady-state, contaminant transport equation that includes advection, dispersion, sorption, and biodegradation.

It is assumed that degradation occurs in the aqueous and sorbed phases at the same rate (Buscheck, Alcantar, 1995). The steady state solution of the one-dimensional transport is expressed as (Bear, 1979);

$$C(x) = C_0 \exp \left[ \frac{x}{2\alpha_x} \left[ 1 - \left( 1 + \frac{4\lambda\alpha_x}{v_c} \right)^{\frac{1}{2}} \right] \right] \quad (2.43)$$

where  $C_0$  is the concentration at the source;  $x$  is distance;  $\alpha_x$  is the dispersivity along the flow direction;  $\lambda$  is the total biodegradation rate constant; and  $v_c$  is the contaminant velocity, which is defined as  $v_c = v_x / R$ , where  $R$  is the retardation factor.

It should be noted that both equation (2.42) and equation (2.43) are of the same form

$$C(x) = C_0 e^{mx} \quad (2.44)$$

where  $m$  is the slope of the log-linear data, i.e. that is;

$$m = \frac{k}{v_x} = \left( \frac{1}{2\alpha_x} \right) \left[ 1 - \left( 1 + \frac{4\lambda\alpha_x}{v_c} \right)^{1/2} \right] \quad (2.45)$$

From equation (2.45), the biodegradation rate,  $\lambda$ , which is a measure of natural attenuation, can be found in terms  $m$  as (Buscheck, Alcantar, 1995);

$$\lambda = \frac{v_c}{4\alpha_x} \left( (1 - 2\alpha_x m)^2 - 1 \right) \quad (2.46)$$

where  $\alpha_x$  is the dispersivity along the flow direction, (L);  $v_c$  is the contaminant velocity, (L/T);  $m$  is slope of the regression line. The substitution of  $m$  in equation (2.46) can be substituted by  $(-k/v_x)$  yields;

$$\lambda = \frac{v_c}{4\alpha_x} \left( \left( 1 + 2\alpha_x \frac{k}{v_x} \right)^2 - 1 \right) \quad (2.47)$$

When used with accurate estimates of dispersivity, groundwater flow and solute transport velocity, this method gives first-order biodegradation rate with a reasonable accuracy.

### 2.3.2. Conservative Tracer Method

In this method, in order to calculate biodegradation rates accurately, first measured contaminant concentrations must be normalized or corrected for the effects of dispersion, dilution and sorption, using measured concentration of an appropriate tracer. At sites where petroleum hydrocarbon plumes are present, TMB (trimethyl benzene), which can be biological recalcitrant under some geochemical conditions, is generally used as a tracer when estimating biodegradation rates of BTEX (Wiedemeier et al., 1995).

Measured concentration of tracer and BTEX from a minimum of two points along the flow path can be used to estimate the amount of contaminant that would be expected to remain at each point if biodegradation were the only attenuation process operating to reduce the contaminant concentration. The tracer is affected by dilution and dispersion to same degree as the contaminant of interest and is not affected by biological process. The following equation (2.48) uses these assumptions to solve for the expected downgradient contaminant concentration if biodegradation had been only attenuation process operating between the two points along the flow path:

$$C_{B,corr} = C_B \left( \frac{T_A}{T_B} \right) \quad (2.48)$$

where  $C_{B,corr}$  is the corrected contaminant concentration at a downgradient point;  $C_B$  is the measured contaminant concentration at downgradient point;  $T_A$  is the tracer concentration at an upgradient point; and  $T_B$  is the tracer concentration at a downgradient point. A series of corrected contaminant concentrations along the flow direction can be used to estimate the first-order biodegradation rate constant.

The corrected concentration is the concentration that would be expected at one point (B) located downgradient from another point (A) if the process of dispersion and dilution had not been occurring between these two points. The biodegradation rate

can be estimated between any two points (A and B) of a corrected data set (where point A is upgradient of point B) as:

$$C_{B,corr} = C_A e^{-\lambda t} \quad (2.49)$$

where  $C_{B,corr}$  is the corrected contaminant concentration at downgradient point B;  $C_A$  is the measured contaminant concentration at upgradient point A;  $\lambda$  is the first-order biological decay rate constant; and  $t$  is the contaminant travel time between points A and B. It should be noticed that,  $\lambda$  in this equation is not the total attenuation rate; it is the biological decay rate constant, because the effects of advection, dispersion, dilution from recharge, and sorption have been removed. The above equation can be rearranged for  $\lambda$  as follows:

$$\lambda = -\frac{\ln\left(\frac{C_{B,corr}}{C_A}\right)}{t} \quad (2.50)$$

The travel time,  $t$ , between two points is given by:

$$t = \frac{x}{v_c} \quad (2.51)$$

where  $x$  is travel distance, L; and  $v_c$  is contaminant velocity, L/T.

If a number of sampling points (more than 2) are available along the flow path, all the locations should be included in calculations of biodegradation rate. The simplest way to determine the first-order rate constant from the entire set of corrected concentration data is to make a log-linear plot of corrected contaminant concentrations versus travel time. If the plot of data follows a straight line, the relationship is first-order and a linear regression analysis can be performed. The

equation of the linear regression analysis gives the line of best fit for the data in the form of;

$$\ln y = b + mt \quad (2.52)$$

where  $y$  is corrected contaminant concentration plotted on log-linear  $y$  axis,  $M/L^3$ ;  $b$  is the intercept of  $y$  axis;  $m$  is the slope of the regression line, which gives the first-order biodegradation rate constant; and  $t$  is the downgradient travel time along the flow direction.

## CHAPTER 3

### RESULTS AND DISCUSSION

For the BTEX contamination, the random heterogeneous hydraulic conductivity distributions are generated by the help of random field generator. Then, these generated distributions are used in Visual MODFLOW program in order to observe the plume behavior and quantify the fate and transport of the BTEX contamination in the aquifer. The results are presented and discussed in the following sections.

#### **3.1. Random Hydraulic Conductivity Field**

Two dimensional randomly distributed hydraulic fields are generated by using Turning Bands Method. All the physical and parametric data required for the turning bands are given in related sections.

Under most field conditions, hydraulic conductivity is not uniform, rather exhibits a large spatial variation. Therefore, randomly distributed spatially correlated hydraulic conductivity fields are generated to represent the field conditions realistically.

Nine different isotropic hydraulic conductivity fields are generated having the same mean but different variance and spatial correlation length. In addition to nine isotropic hydraulic conductivity fields, in order to assess the anisotropy effect of hydraulic conductivity on contaminant fate and transport, two anisotropic hydraulic conductivity fields are generated.

### 3.1.1. Validation of Generated Random Fields

Before using the generated hydraulic conductivity fields in flow and transport simulations, the fields must be validated. The objective of the validation procedure is to make sure that the generated spatially variable random hydraulic conductivity fields have preserved the statistical properties prescribed prior to generation; that is the mean, variance and the spatial correlation lengths estimated from the generated hydraulic conductivity fields should be same as the theoretical specified values. For this purpose, the turning bands program performs Monte Carlo Runs to calculate the mean and the variance of each Monte Carlo realization called “Base Distribution”. Base distribution is the distribution of the random numbers having zero mean and unit variance. This distribution is transformed to log-normal hydraulic conductivity fields, using equations 2.1 to 2.4, as presented earlier. Therefore, it is expected that each realization of base distributions should have a mean and variance close to 0 and 1, respectively.

Another measure for the validation of generated field is the comparison of the theoretical covariance function (calculated using equation 2.5 for isotropic and 2.6 for anisotropic fields) with the estimated covariance function (calculated from the generated hydraulic conductivity distributions). For validation of the generated hydraulic conductivity fields, it is expected that both theoretical and estimated covariance function should be close to each other. Figure 3.1 illustrates the validation of generated hydraulic conductivity field with  $CV = 50\%$  and  $h = 5$  m. Similar validation tests are performed for all other isotropic and anisotropic generated hydraulic conductivity fields and results are presented in Appendix B.

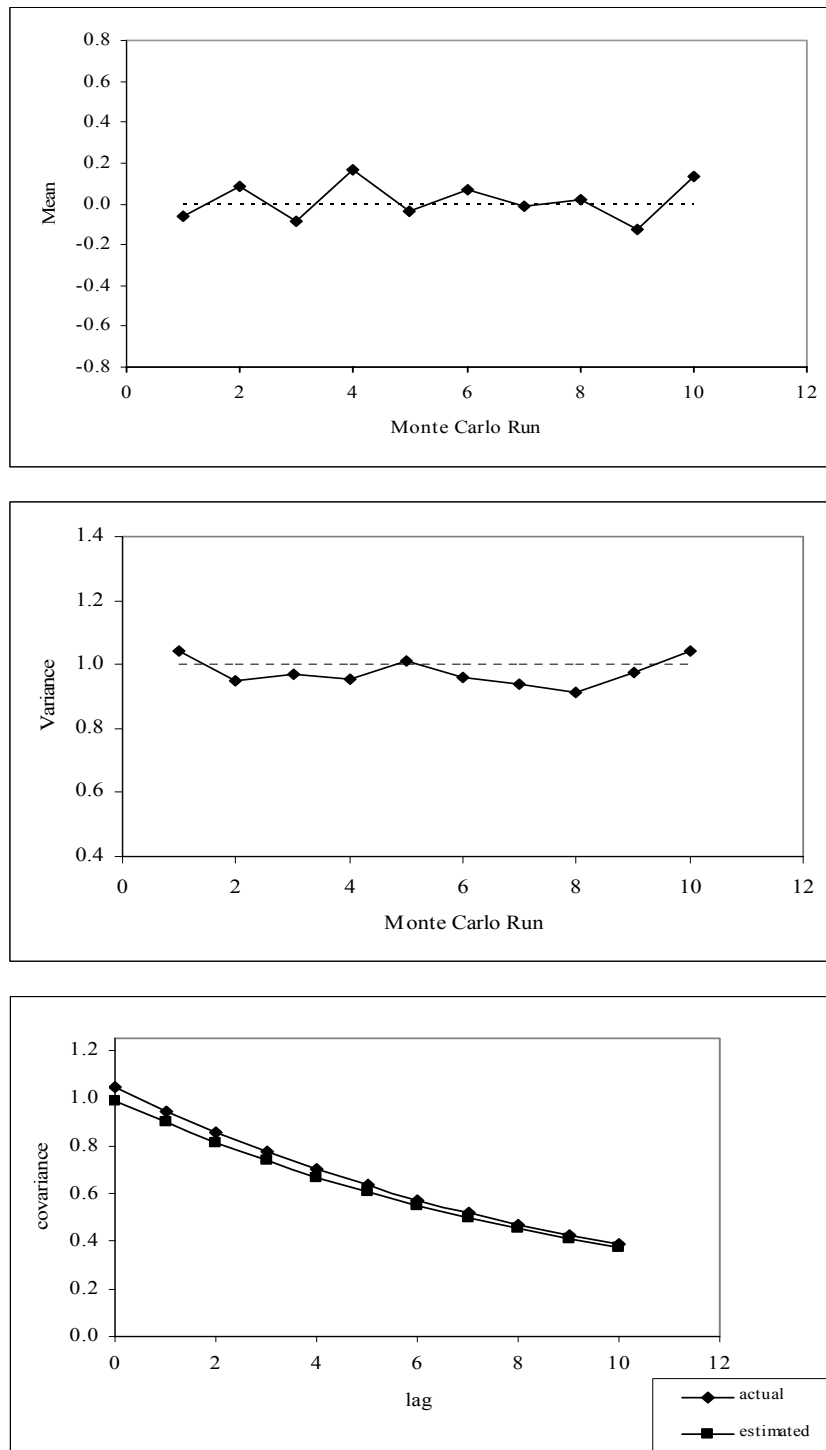


Figure 3.1. Mean, Variance and Covariance estimate for isotropic hydraulic conductivity field having CV = 50 % and h = 5 m.

### 3.1.2. Isotropic Hydraulic Conductivity Fields

Figure 3.2, 3.3, and 3.4 show the generated hydraulic conductivity fields and their frequency histograms for correlation lengths of 5, 10, and 20 m when CV was taken as 50, 100, and 150 %, respectively. From these figures, it can be seen that for a given CV, as the correlation length increases, the contrast of high and low conductivity zones are observed in longer distances; in other words, smaller size areas of high and low conductivity zones are spread across the entire flow field when correlation length is short. This behavior becomes much more evident as CV increases. On the other hand, for a given correlation length, as CV increases, the size of the high conductivity zones becomes larger and conductivity contrasts become much more evident.

The effect of correlation length and CV on hydraulic conductivity fields can also be observed from the frequency histograms. As seen from the following figures, all generated isotropic hydraulic conductivity fields are log-normally distributed. These frequency histograms give information about minimum and maximum hydraulic conductivity, and also frequency of these values in nodal places of the grid system. It is clear that the hydraulic conductivity data spread over a larger range, as CV increases, at a given correlation length. The lowest and highest conductivity values of the field having smaller CV is not repeated so much in that field, but the same value is repeated at the field having highest CV. For the field having CV of 50 % and h of 5 m, the lowest ( $K_{\min} = 9 \times 10^{-6}$  m/s) and the highest ( $K_{\max} = 4.65 \times 10^{-4}$  m/s) hydraulic conductivities are seen in only one cell, whereas same lowest and highest hydraulic conductivities are repeated in 5 and 668 cells respectively. Therefore, the high and the low conductivity zones can be seen more clearly at the field having CV of 150 %, h of 20 m than the fields having CV of 50 %, h of 5 m.

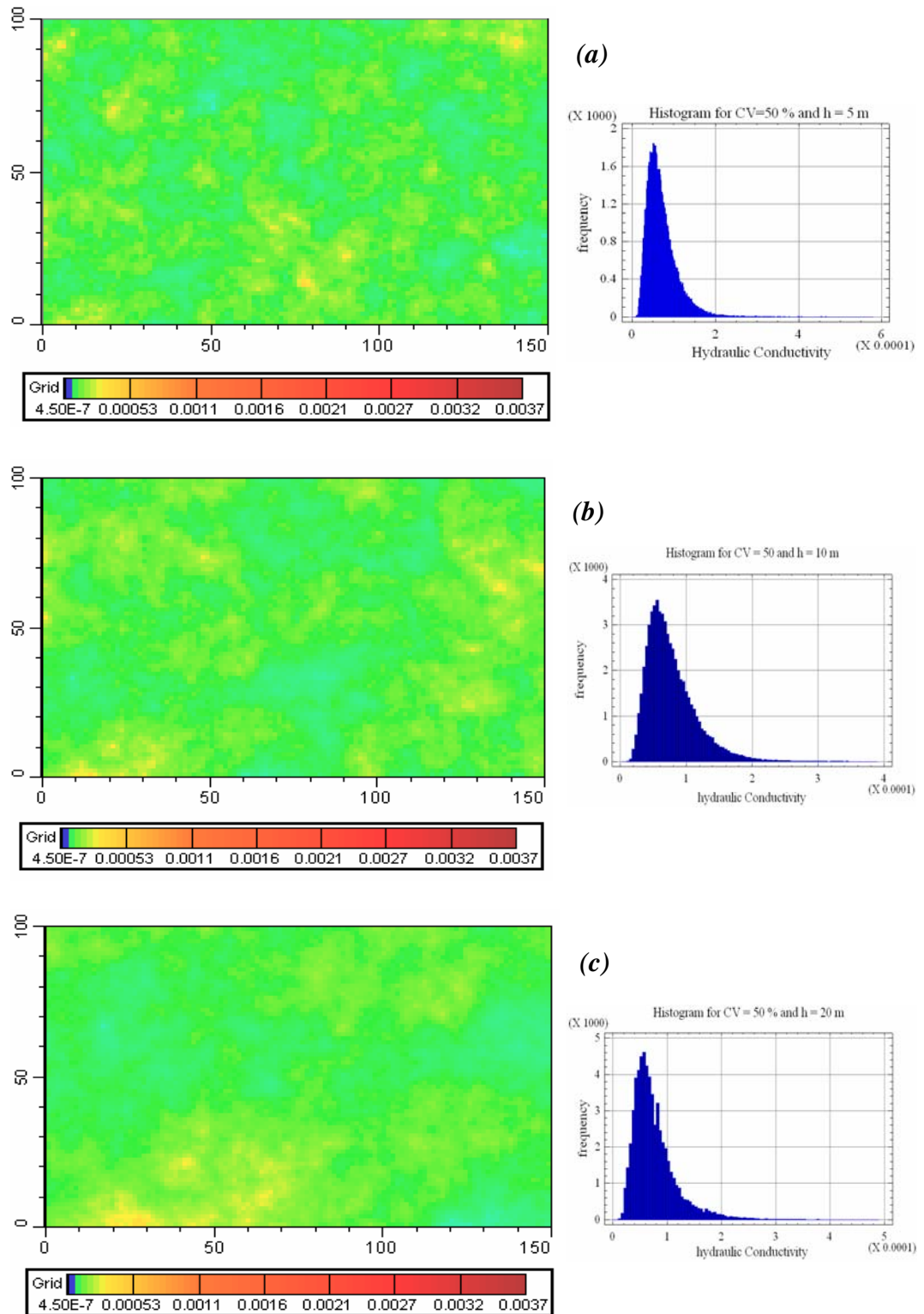


Figure 3.2. Hydraulic conductivity distribution for (a)  $h = 5$  m , (b)  $h = 10$  m, and (c)  $h = 20$  m when  $CV = 50\%$ .

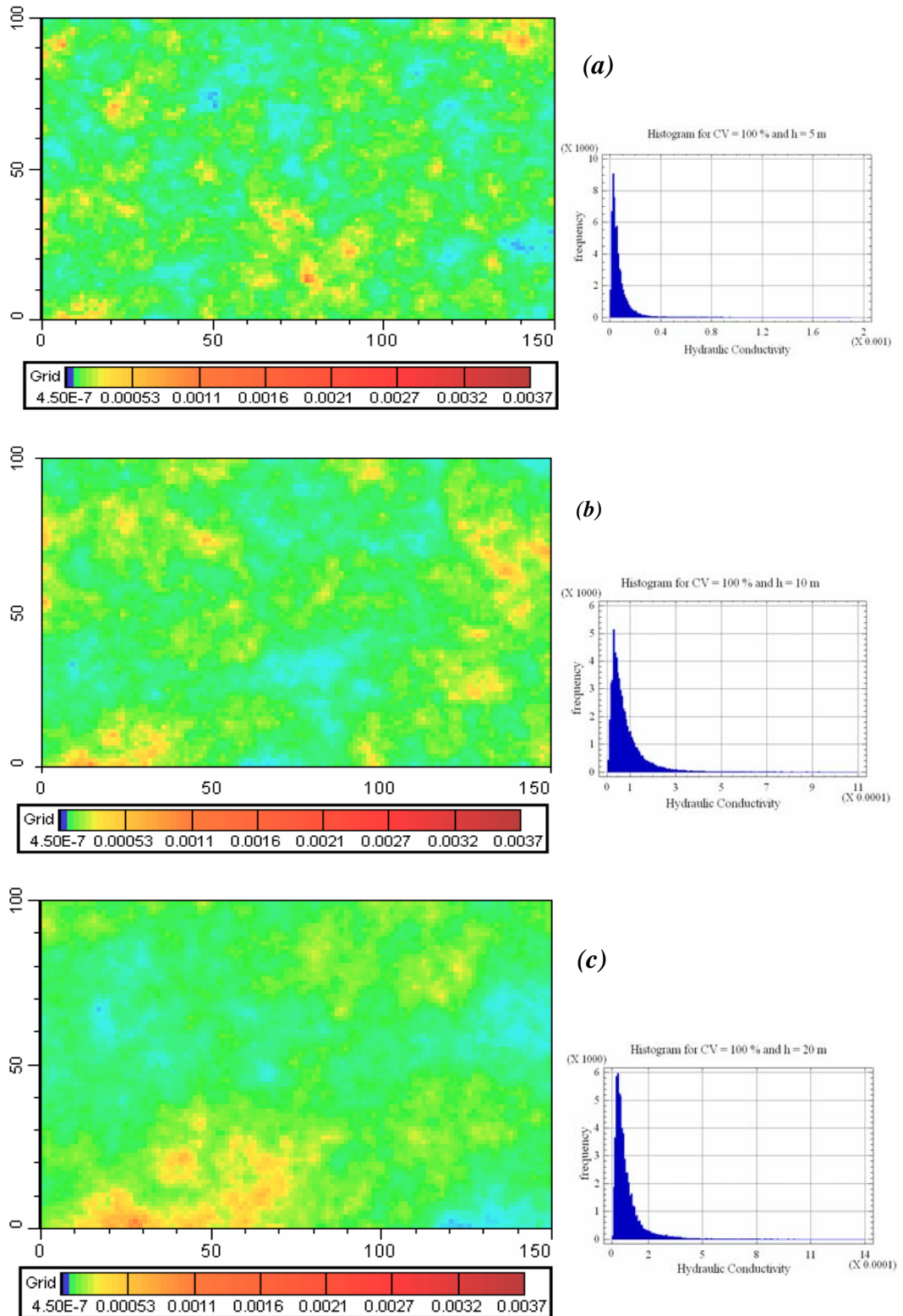


Figure 3.3. Hydraulic conductivity distribution for (a)  $h = 5$  m , (b)  $h = 10$  m , and (c)  $h = 20$  m when  $CV = 100\%$ .

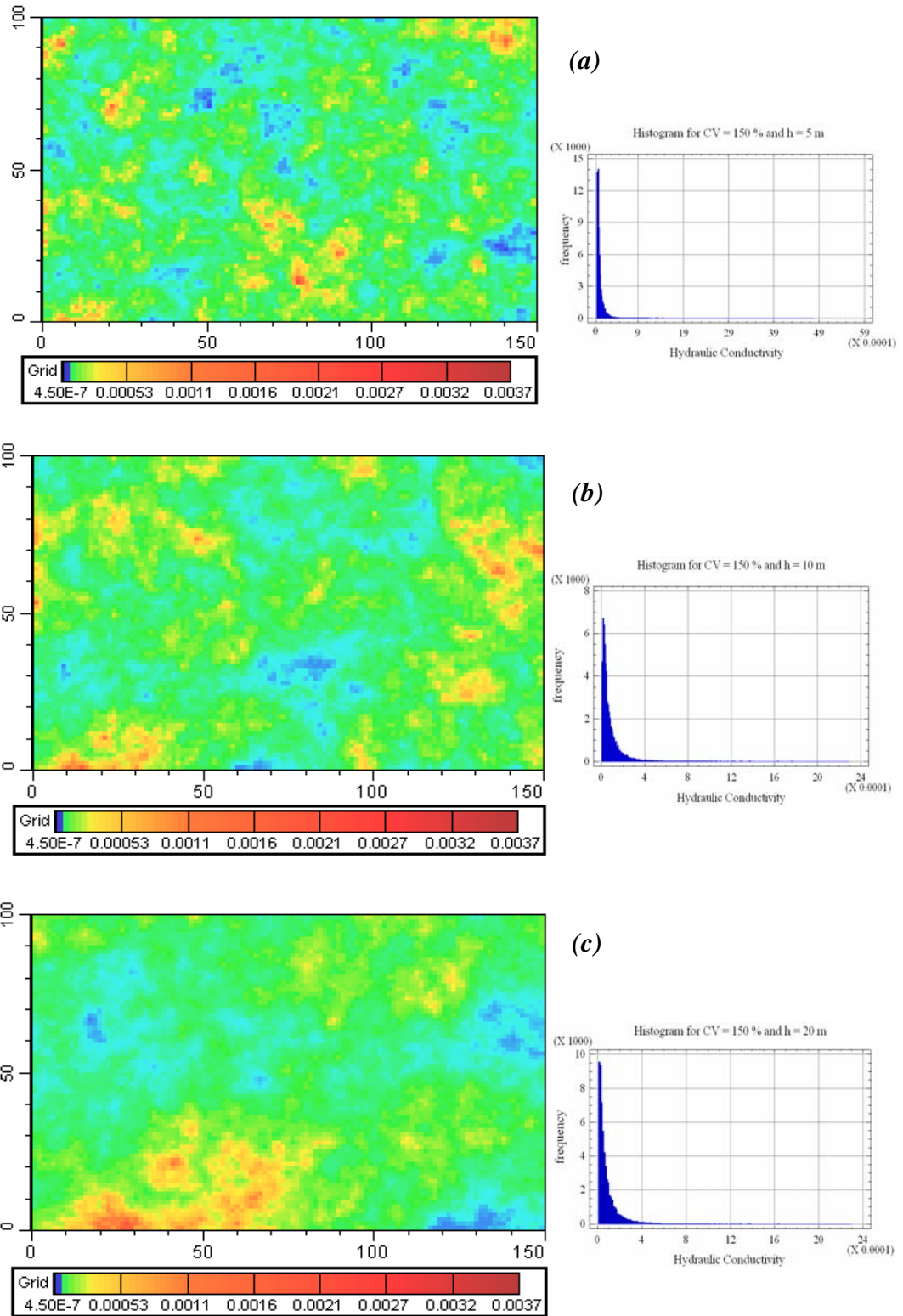


Figure 3.4. Hydraulic conductivity distribution for (a)  $h = 5 \text{ m}$  , (b)  $h = 10 \text{ m}$  , and (c)  $h = 20 \text{ m}$  when  $CV = 150 \%$ .

### 3.1.3. Anisotropic Hydraulic Conductivity Fields

Two anisotropic hydraulic conductivity fields are generated. In the generation of anisotropic fields, anisotropy ratio, with respect to correlation length, is taken as 5. For the first anisotropic field, CV,  $h_x$ , and  $h_y$  are taken as 50 %, 20 m, 4 m, respectively; and for the second one, CV,  $h_x$ , and  $h_y$  are taken as 150 %, 10 m, 2 m, respectively. Figure 3.5 and 3.6 show the generated anisotropic hydraulic conductivity fields and their frequency histograms for CV of 50 % and 150 %, respectively.

In anisotropic fields, since the assigned correlation lengths are different in x- and y-directions, the distributions of hydraulic conductivities are totally different from the isotropic ones. The smaller the correlation length in y-direction than in x-direction, the greater the changes in hydraulic conductivities in short distances in y-direction. Thus, the high and low conductivity zones are seen as squeezed in y-direction and extended in x-direction. This behavior of high and low conductivity zones are easily seen when the anisotropic fields having CV of 50 % and 150 % are compared to the isotropic fields having the same CV values, respectively. Furthermore, in anisotropic fields, the areal extents of high and low conductivity zones are small and spread across the entire flow field when correlation length is short.

When looked at the frequency histograms, in the following figures, it can be seen that the histograms are similar to the corresponding isotropic fields, that is, the statistical parameters (such as mean, variance, minimum and maximum values) of anisotropic fields are close to the isotropic fields having same CV values. However, the spatial distributions of hydraulic conductivity within the flow field are different.

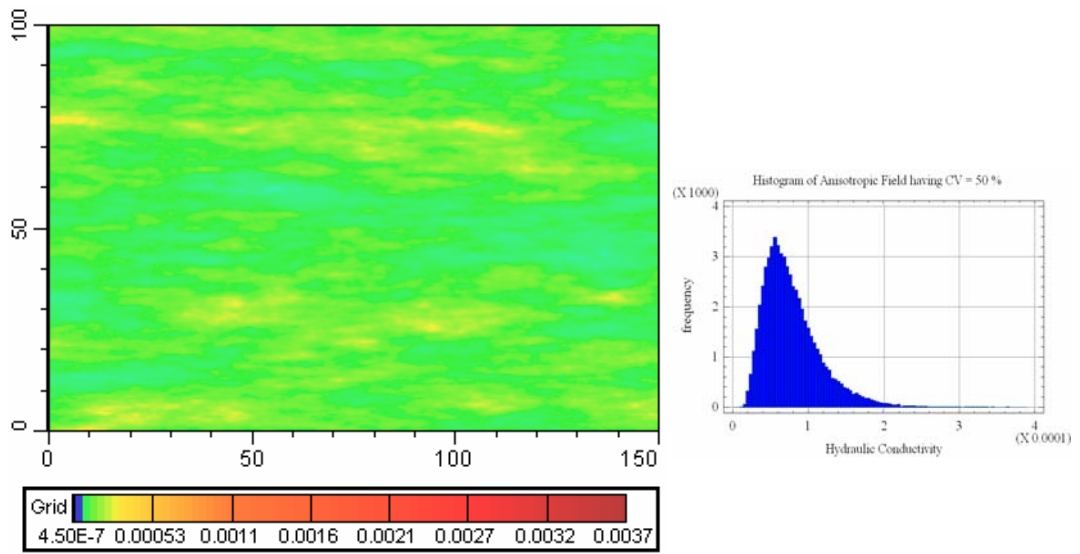


Figure 3.5. Hydraulic conductivity distribution for anisotropic field having CV = 50 %,  $h_x = 20$  m and  $h_y = 4$  m.

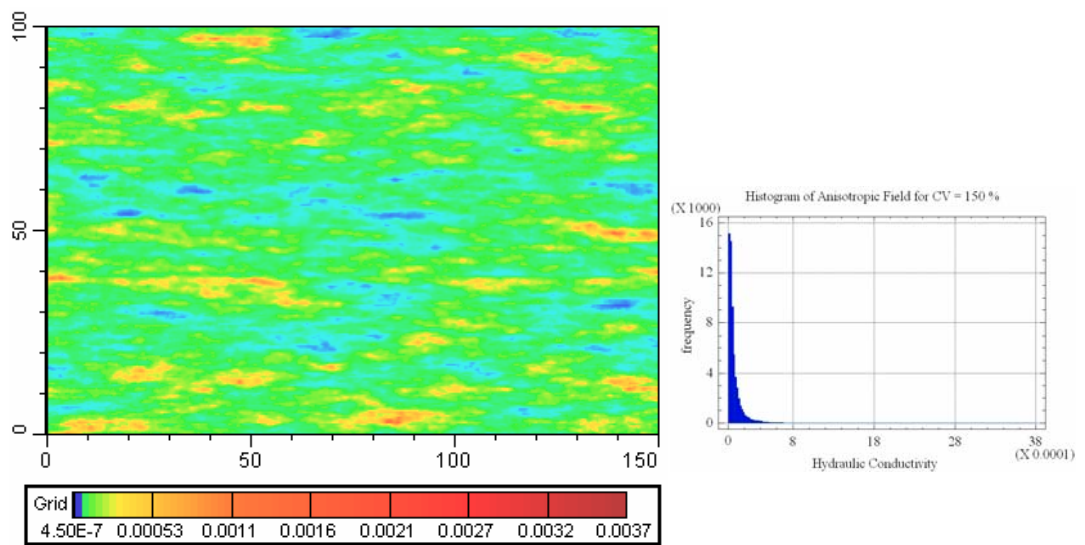


Figure 3.6. Hydraulic conductivity distribution for anisotropic field having CV = 150 %,  $h_x = 10$  m and  $h_y = 2$  m.

## **3.2. BTEX PLUME SIMULATIONS AND PLUME BEHAVIOUR**

The BTEX plume behaviors are simulated at twelve different fields. All the input parameters, except the hydraulic conductivity, are same in all simulated fields. The first field is uniform field with respect to hydraulic conductivity distribution, nine of them are isotropic heterogeneous fields, and two of them are anisotropic heterogeneous fields. The mean hydraulic conductivity values are same for all fields. Each of the generated hydraulic conductivity fields consists of numerical values of hydraulic conductivity assigned to each nodes of 300 by 200 grid system. Prior to simulation runs, hydraulic conductivity field was imported to the Visual MODFLOW program.

After all the input parameters are supplied to the program, MODFLOW and RT3D are run for all of the fields. MODFLOW model simulates groundwater flow and gives the head distribution and the velocity field within the system domain. RT3D model simulates the fate and transport of the contaminant and gives the contaminant plume distribution in the model domain.

### **3.2.1. Plumes of Isotropic Random Fields**

Hydraulic conductivity is the measure of an aquifer's ability to transmit water. Therefore, it is the most important parameter governing fluid flow in the subsurface (Wiedemeier et al., 1999). The head distributions and in turn groundwater velocity are affected by the hydraulic conductivity distributions, since both are controlled by groundwater flux. As the hydraulic conductivity changes from location to location, both the groundwater velocity and the head distribution change. Different head distributions corresponding to generated isotropic random hydraulic conductivity fields and a uniform conductivity field are shown in the figures given in Appendix C.

For uniform flow field, the mean hydraulic conductivity ( $7.234 \times 10^{-5}$  m/s) is assigned to the entire flow domain, i.e. hydraulic conductivity is constant across the flow field. Therefore, hydraulic head is changing only along the x-direction and there

is a one-dimensional groundwater flow in the model domain. In uniform flow field, head contours are placed at equal distance and parallel to each other.

However, in the isotropic heterogeneous conductivity fields, depending on the hydraulic conductivity distribution, head distribution and velocity fields change across the entire flow fields. The behavior of head and velocity distributions differ according to the shape, size, and relative position of high and low conductivity zones. The high conductivity zones generate higher groundwater velocities, whereas the low conductivity zones generate low groundwater velocities. At high conductivity zones, groundwater flows faster until reaching the low conductivity zones, so, head contours are placed sparsely within high conductivity zones; on the other hand, they are closer to each other at low conductivity zones. Moreover, high and low conductivity zones affect the flow direction, and the groundwater tends to flow towards the high conductivity zones. Hence, instead of uniform one-dimensional flow field, two-dimensional non-uniform flow is observed in the different hydraulic conductivity fields. Because of the directional change in the velocity vectors, as seen in the figures given in Appendix C, the head contours have irregular shape and the irregularity of these contours increase as CV increases, while  $h$  is constant. The most irregular head contours are observed in the field having CV of 150 %. Change in the correlation length does not affect the shape and spacing of head contours but affects the position of a given head contour within the flow domain.

BTEX plumes were simulated for a period of 1000 days for all of the generated random hydraulic conductivity fields and a uniform field. To delineate the plume boundaries the outer most concentration contours are defined as 0.05 mg / L in Figures 3.7-3.10. Moreover, assigning a constant value to the outer most concentration contours makes it easier to observe and compare the differences in plume shapes and the fate and transport of BTEX at fields having different hydraulic conductivity distributions. Figure 3.7 shows the plumes for the uniform field at the beginning (50 days) and at the end (1000 days) of the simulation period, while

Figures 3.8-3.10 show the similar plumes for the random isotropic hydraulic conductivity fields. At uniform field, because of constant hydraulic conductivity, the contaminant plume has a regular shape. Figure 3.7 illustrates that, since there is a one dimensional flow in the x-direction, the plume moves along the x - direction and it is affected by the advection process along with the other natural attenuation processes. However, in y-direction, advection no longer affects the plume at uniform field; the dispersion and dilution processes affect the plume behavior and plume is dispersed along the y-direction.

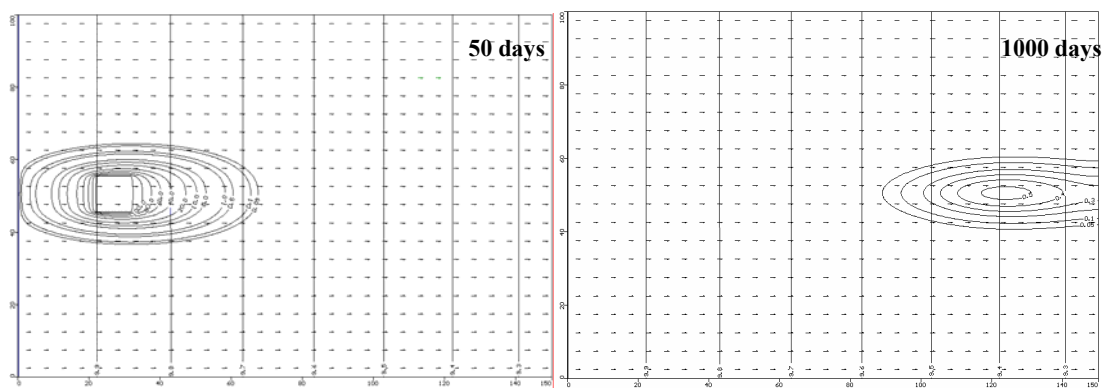


Figure 3.7. BTEX plume at 50 and 1000 days for Uniform Field

Figures 3.8-3.10 demonstrate that the plume behaviors are different at different isotropic hydraulic conductivity fields. The plumes at 50 days and 800 days are shown in these figures, since at some of the fields, after 800 days, the concentration of the contaminant decreases below the assigned outer contour concentration (0.05 mg/L). The simulation results at 1000 days are given in Appendix D.

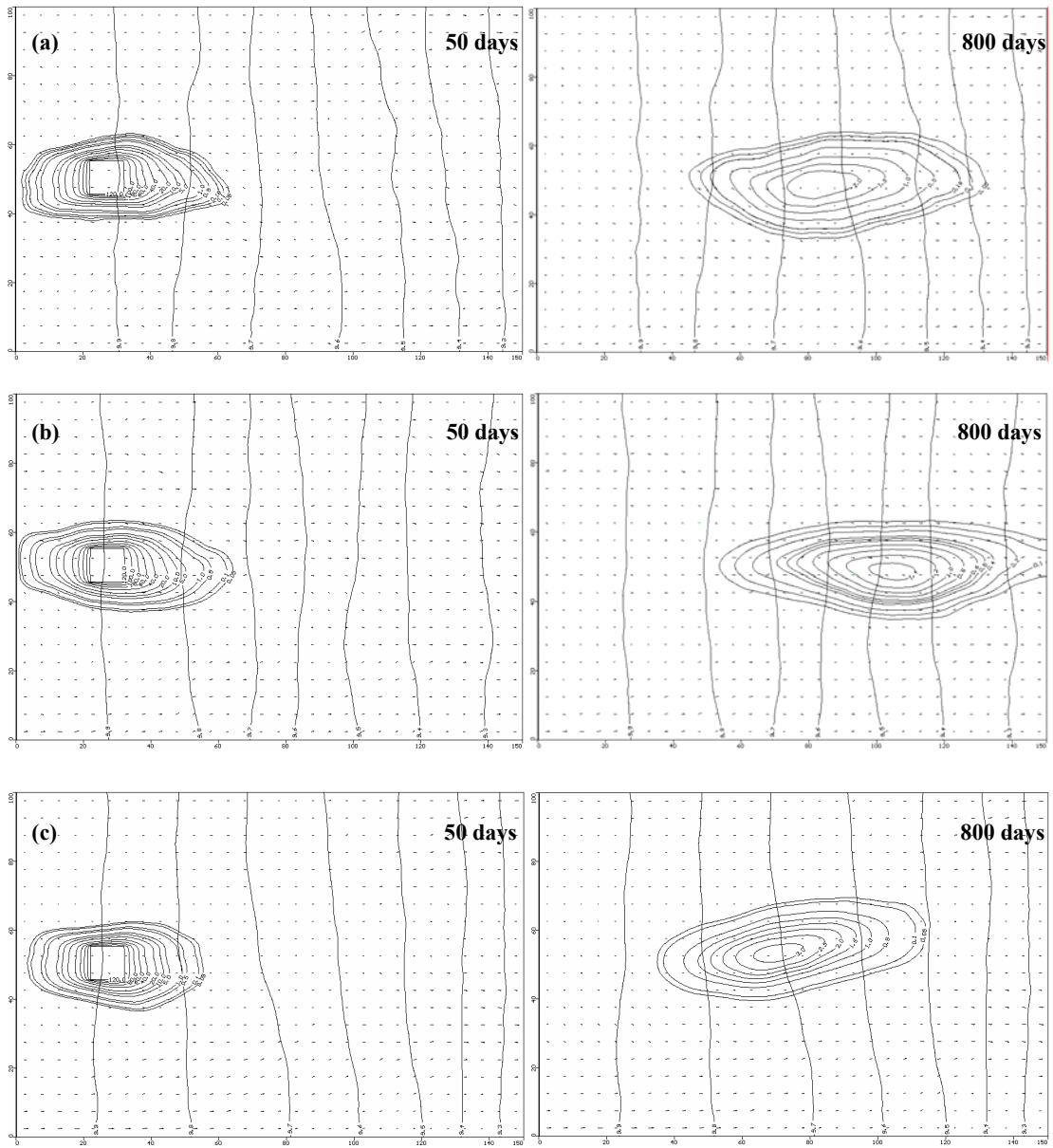


Figure 3.8. BTEX plumes at 50 and 800 days for isotropic fields having  
 (a)  $h = 5$  m, (b)  $h = 10$  m, (c)  $h = 20$  m, when  $CV = 50\%$

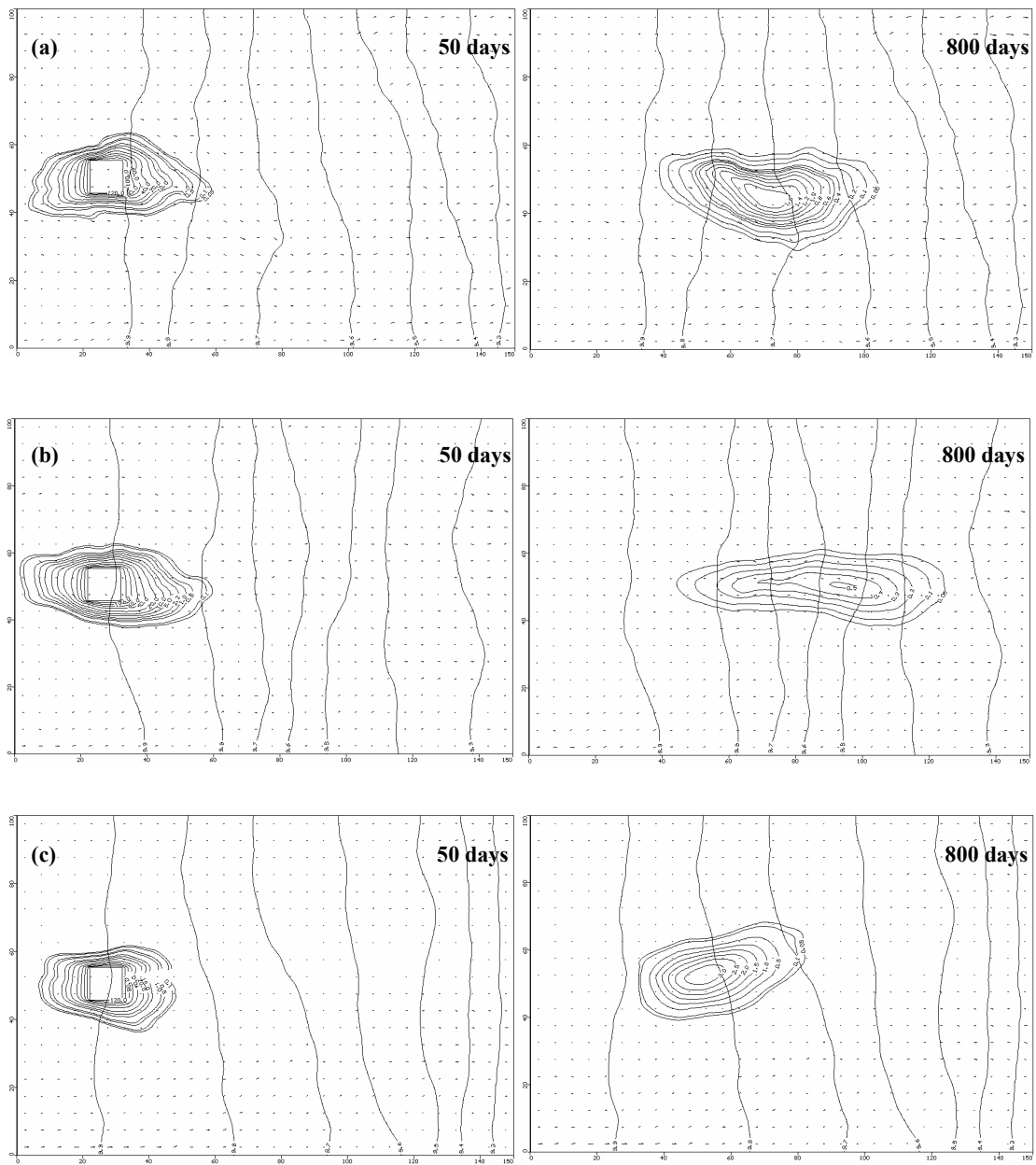


Figure 3.9. BTEX plumes at 50 and 800 days for isotropic fields having  
 (a)  $h = 5$  m, (b)  $h = 10$  m, (c)  $h = 20$  m, when  $CV = 100\%$

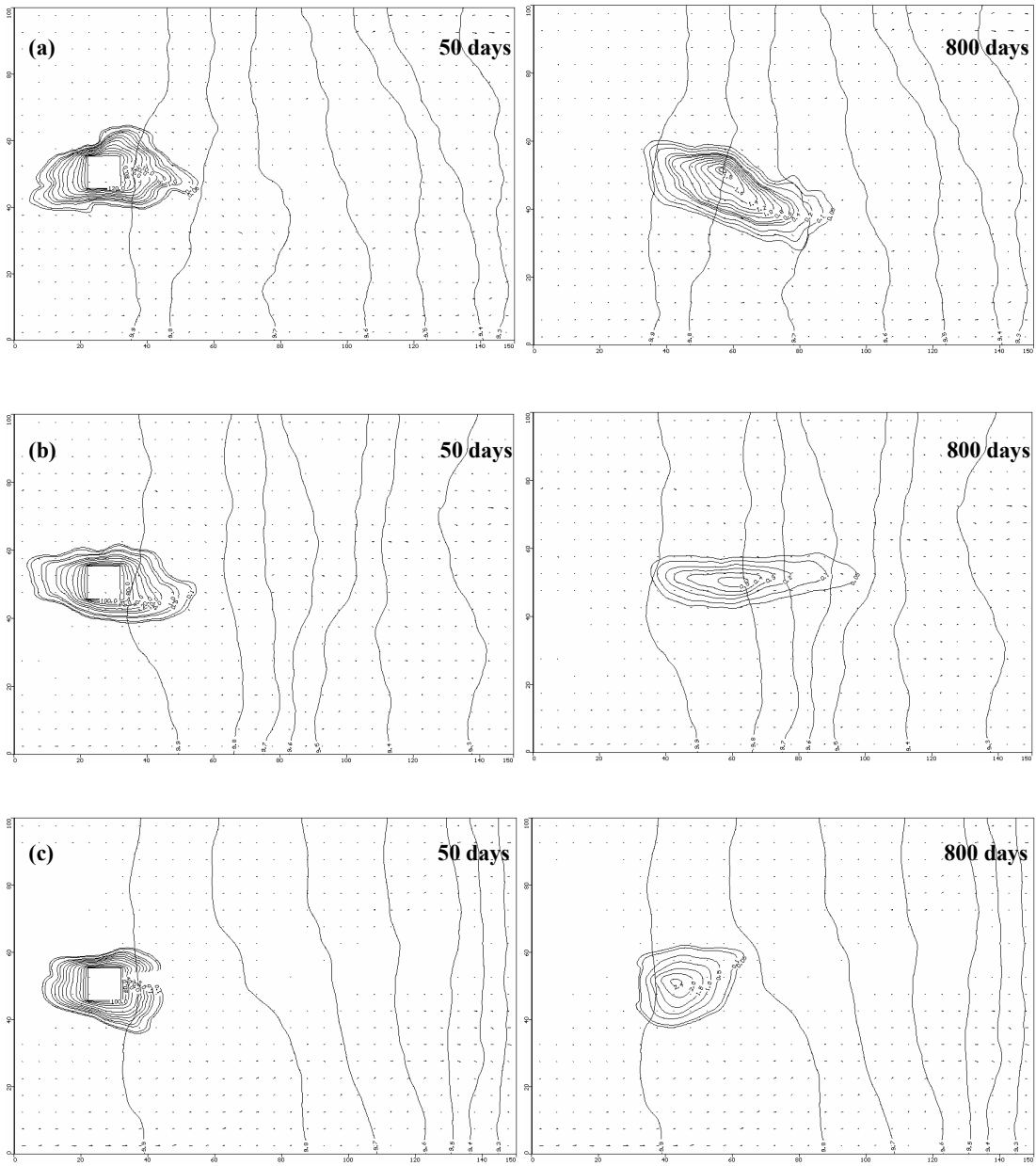


Figure 3.10. BTEX plumes at 50 and 800 days for isotropic fields having  
 (a)  $h = 5$  m, (b)  $h = 10$  m, (c)  $h = 20$  m, when  $CV = 150\%$

As seen from Figures 3.8 through 3.10, the shapes and the sizes of the plumes change as CV and h of the hydraulic conductivity distributions change. In the uniform field, the plume has a regular shape, but in different hydraulic conductivity distributions, the shapes of the plumes are somewhat irregular and distorted. The shape of the plume is more affected by the CV. As CV increases, the irregularity and distortion of the plume shape increases. As both CV and h increases plume size shrinks; this shrinkage becomes much more apparent with time. CV affects the plume size more than h. The smallest plume at a given time (e.g.,  $t = 800$  days) developed in the hydraulic conductivity field with  $CV = 150\%$  and  $h = 20$  m, while the largest plume occurred in hydraulic conductivity field with  $CV = 50\%$  and  $h = 5$  m.

While CV is constant, the plumes move faster in the fields having correlation length of 10 m than the plumes in the other fields. Because the plumes move slowly at correlation lengths of 5 m and 20 m, the plumes stay longer at the system and go through the degradation processes for longer times, when CV is constant. Therefore, the plumes at fields having correlation lengths of 5 m and 20 m are smaller than the plumes at fields having correlation length of 10 m.

On the other hand, when correlation length is constant, as CV increases, the plume slows down and stays longer at the model domain, so that areal extent of the plume decreases. Therefore, smaller plumes are observed at hydraulic conductivity fields having higher CV at a constant correlation length value.

Figures 3.11-3.14 show the location of peak concentration versus time, peak concentration versus location of peak concentration, peak concentration versus time, and the location of plume front versus time graphs, respectively, for all random hydraulic conductivity fields.

The plume speed decreases when CV increases, regardless of the correlation length. Furthermore, the effect of correlation length on the location of peak concentration,

which indicates the location of the center of mass of the plume, decreases when CV increases.

As seen in Figure 3.11, the location of peak concentration does not change with CV value until the source is depleted. After that time, the center of mass of each plume begins to move within the domain. The displacements of the plumes differ from field to field with changing CV and h values. The greater displacement is observed when CV is 50 %, while the smallest displacement is observed when CV is 150 %. This situation indicates that groundwater and the plume velocities decrease as CV increases. In other words, the plume (or the center of mass) slows down, as CV increases, when h is constant. When CV is constant, a regular behavior can not be seen with decreasing or increasing values of the correlation length. The plume moves faster within the domain, when h is equal 10 m, i.e. the greater displacement is observed at h of 10 m, while the smallest displacement is seen at h of 20 m.

Figure 3.12 shows the location of the center of mass with its concentration. The maximum concentration of the contaminant plume is first seen in the source and decreases as the plume moves through the field. The same behavior is observed in all fields. However, when h is constant, at highest CV (150 %), peak concentration decreases within a shorter distance, while at smallest CV (50 %), it decreases within a longer distance, since the speed of the plume decreases with increasing CV, at constant correlation length. The peak concentration and its location do not seem to be affected by h. Figure 3.13 demonstrates that the peak concentration decreases with time in a similar manner in all fields, regardless of CV and h. As seen from Figure 3.12 and 3.13, the rate of the reduction in the peak concentration decreases both with time and distance from the source. This situation indicates that the efficiency of the attenuation mechanisms, especially biodegradation, decreases with time. The biodegradation effectiveness generally depends on the electron acceptor concentration, so as time increases, the concentration of the electron acceptors decrease in all fields having different heterogeneity levels.

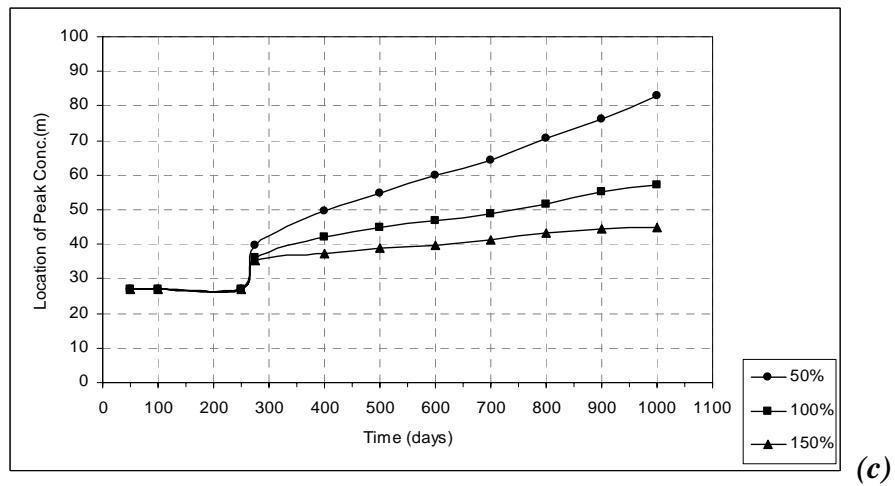
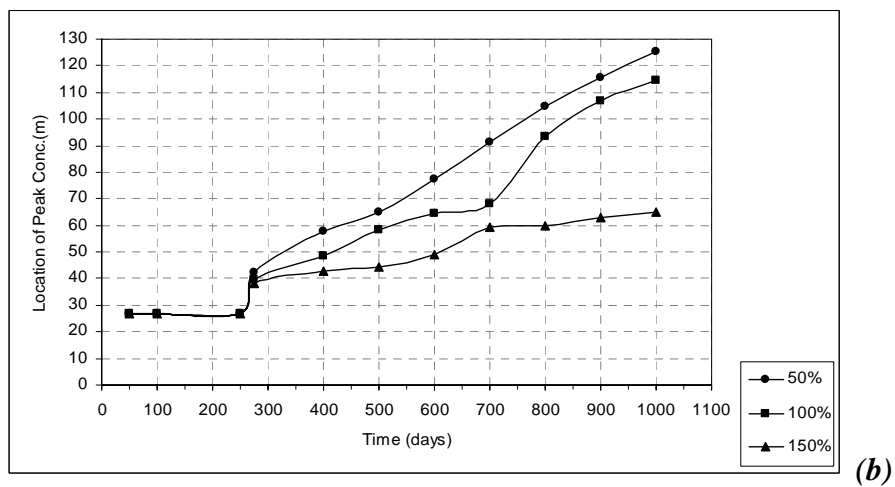
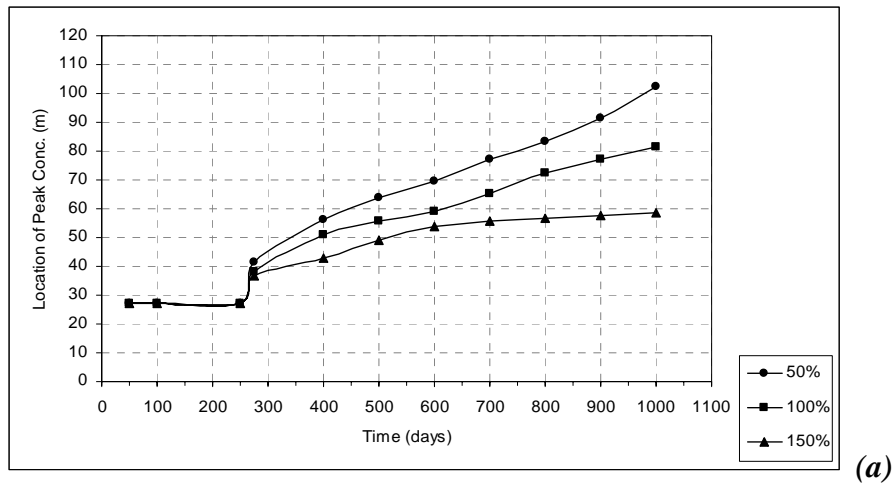


Figure 3.11. The location of peak concentrations versus time graph for different CV values when (a)  $h = 5$  m, (b)  $h = 10$  m, (c)  $h = 20$  m.

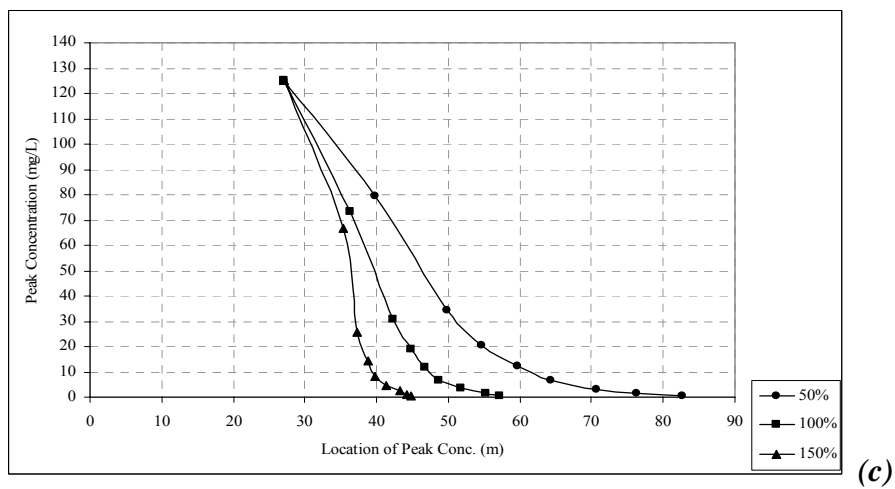
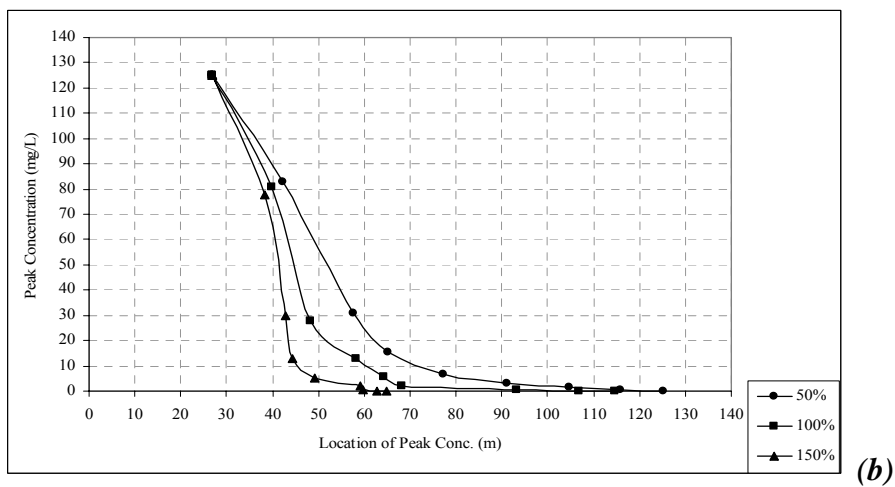
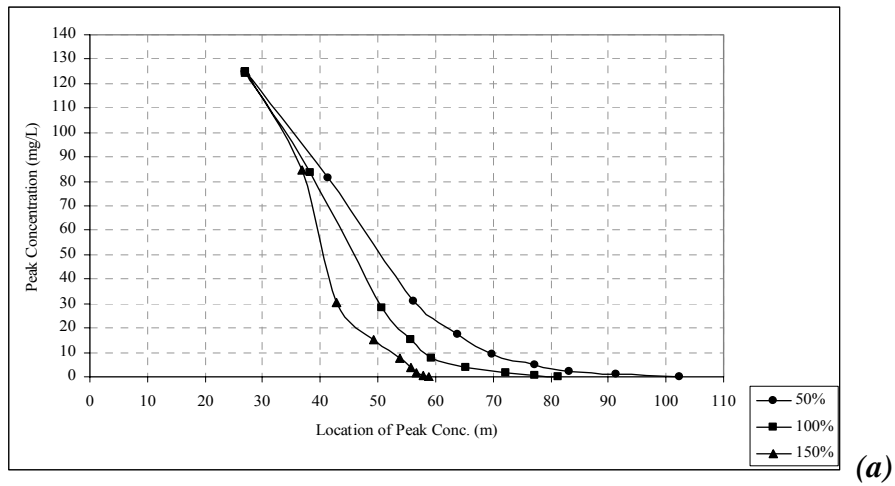


Figure 3.12. Peak concentration versus location of peak concentration graph for different  $h$  values when (a)  $h = 5$  m, (b)  $h = 10$  m, (c)  $h = 20$  m.

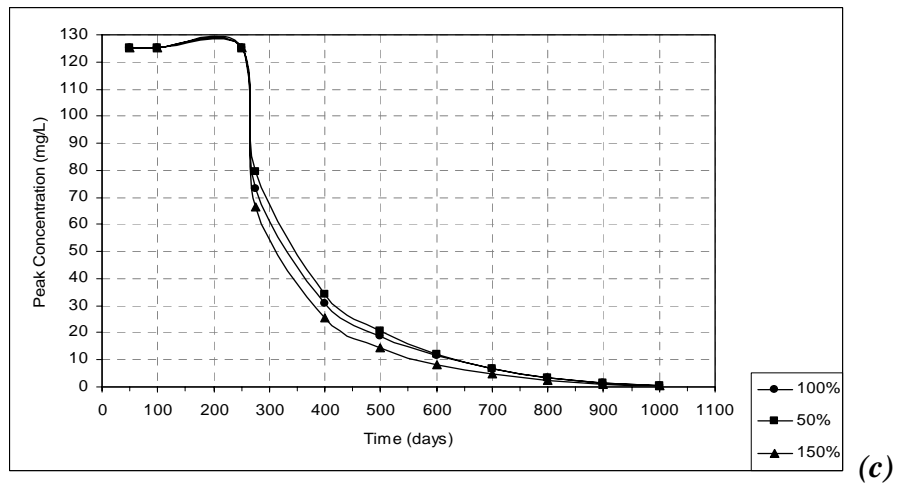
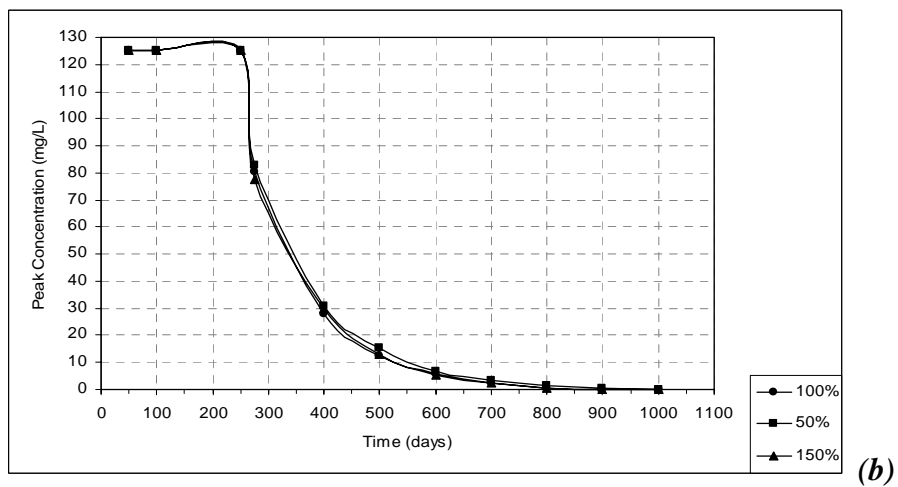
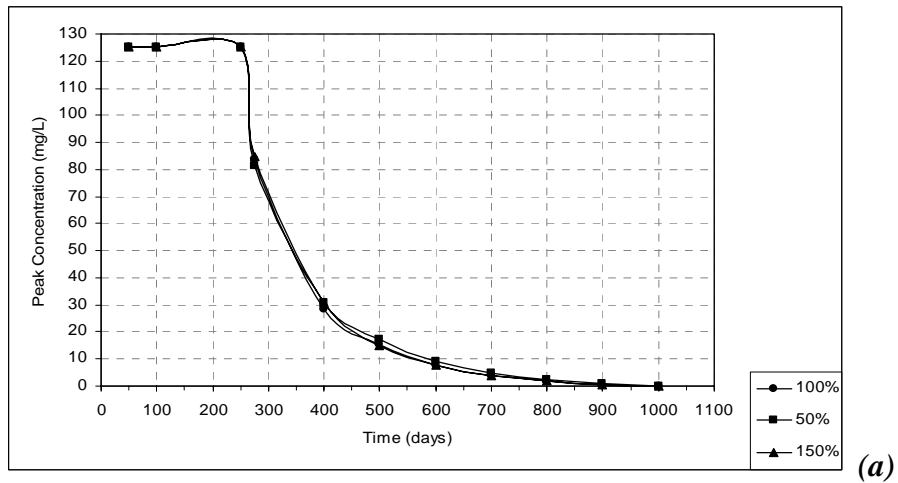


Figure 3.13. Peak concentration versus time graph for different  $h$  values when (a)  $h = 5$  m, (b)  $h = 10$  m, (c)  $h = 20$  m.

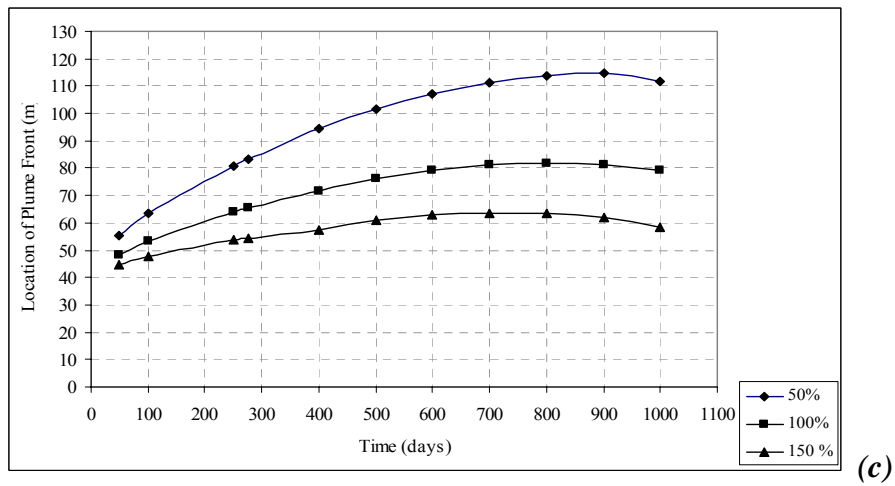
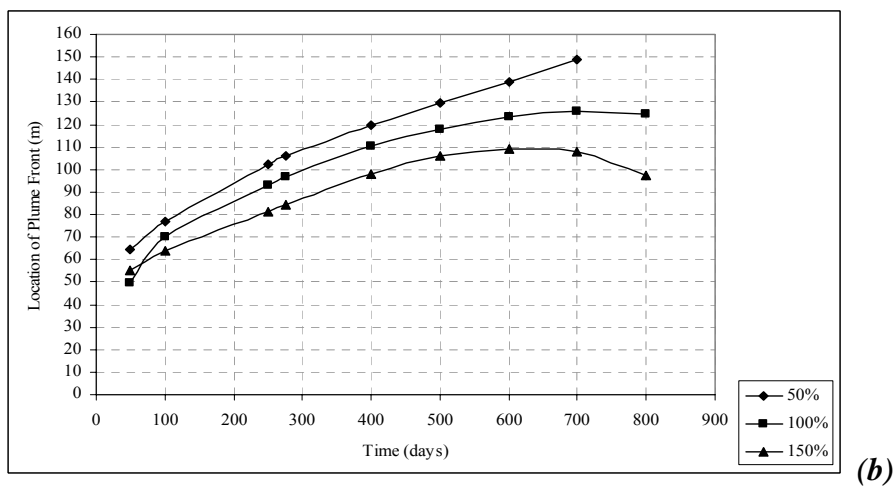
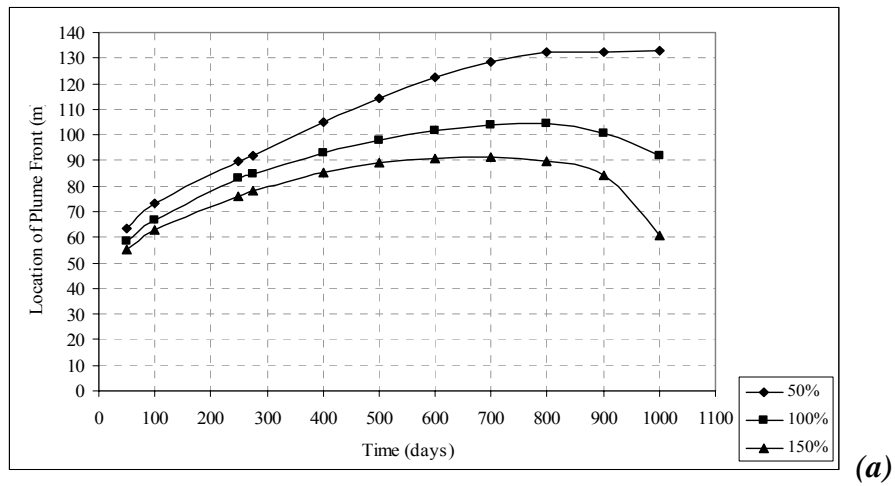


Figure 3.14. The location of plume front versus time graph for different CV values when (a)  $h = 5$  m, (b)  $h = 10$  m, (c)  $h = 20$  m.

The plume front of the contaminant shows the dispersion and the displacement of the plume along the flow direction within the model domain. Figure 3.14 illustrates that, as CV increases, the advancement of the plume front decreases, since at smaller CV, the plume has a greater velocity. The plume front moves ahead with time, because of the advection and dispersion processes. Almost in all fields having different heterogeneity level, up to a certain time, the plume is transported and degraded at the same time. The transport of the plume decreases with time, but the degradation mechanisms still take place within the plume. Therefore, shrinkage in the areal extent of the plumes is observed. At a given correlation length, as CV increases, the areal extent of the plumes decreases, i.e. more shrinkage in the areal extent is observed.

### **3.2.2. Plumes of Anisotropic Random Fields**

Two anisotropic simulations are performed, in this study, in order to observe the anisotropy effect of hydraulic conductivity on the fate and transport of BTEX contamination. The CV and  $h_x$  values for the anisotropic hydraulic conductivity field simulations are determined according to the isotropic simulation results. When choosing anisotropic simulations, the areal extent of the plumes at the end of the simulation time period at every isotropic field is examined and the fields, where the largest and the smallest plumes have been occurred, are chosen; that is CV = 50 %,  $h = 20$  m and CV = 150 %,  $h = 10$  m, respectively.

Figures 3.15 and 3.16 demonstrate the plume behaviors at two anisotropic hydraulic conductivity fields. The plumes at 50 days and 800 days are shown in these figures. The simulation results at 1000 days are given in Appendix D. The shape of the plume in the field having CV of 50 % is more regular than the shape of the plume in the field having CV of 150 %. Moreover, the displacements of the plumes are different in different anisotropic fields. From Figures 3.15 and 3.16, it can be seen that the plume in the field having CV of 50 % and  $h_x$  of 20 m moves faster than the plume in the field having CV of 150 % and  $h_x$  of 10 m.

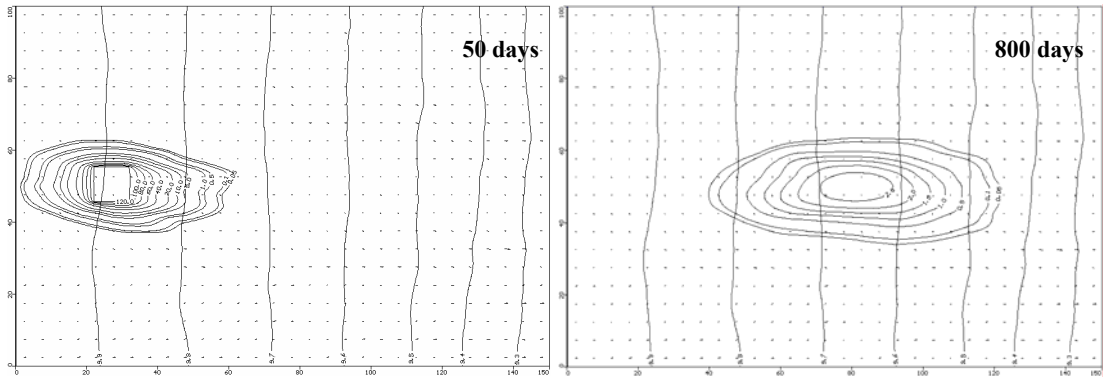


Figure 3.15. BTEX plumes at 50 and 800 days for anisotropic fields having  $CV = 50 \%$ ,  $h_x = 20$  m and  $h_y = 4$  m.

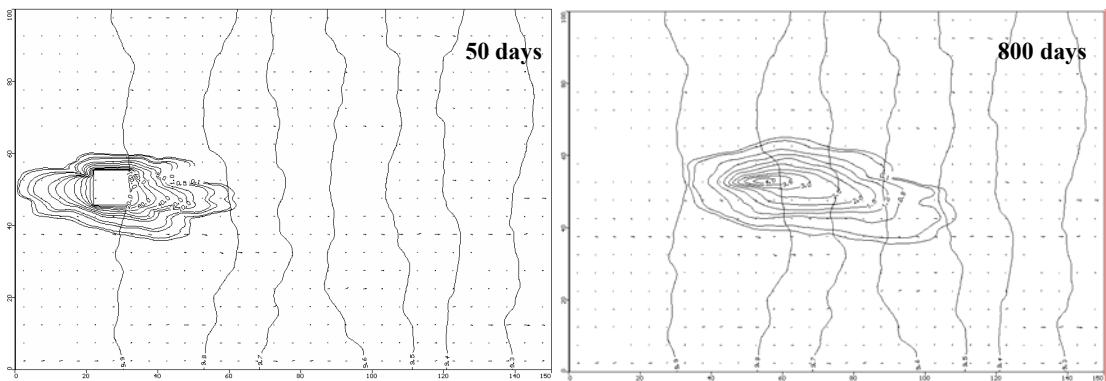


Figure 3.16. BTEX plumes at 50 and 800 days for anisotropic fields having  $CV = 150 \%$ ,  $h_x = 10$  m and  $h_y = 2$  m.

Figures 3.17-3.20 show the location of peak concentration versus time, peak concentration versus location of peak concentration, peak concentration versus time graphs, and the location of plume front versus time graphs, respectively, for different anisotropic hydraulic conductivity fields. Figure 3.17 illustrates that the displacement of the plume in the field having CV of 50 % is greater than the displacement of the plume in the field having CV of 150 %. The behavior of Figures 3.18 and 3.19 are similar to the figures that represent the isotropic fields. Therefore, in the flow domain, the peak concentrations of the plumes decrease with time, and the center of masses, where the peak concentrations are seen, have transported along the flow field when the source is depleted.

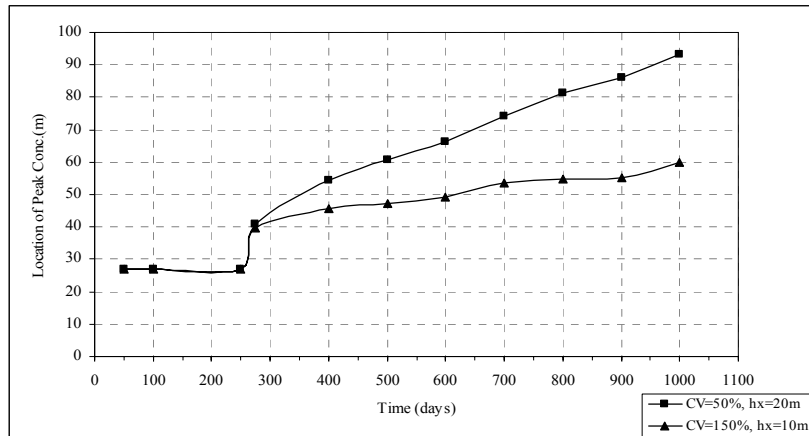


Figure 3.17. The location of peak concentrations versus time graph for two different anisotropic fields

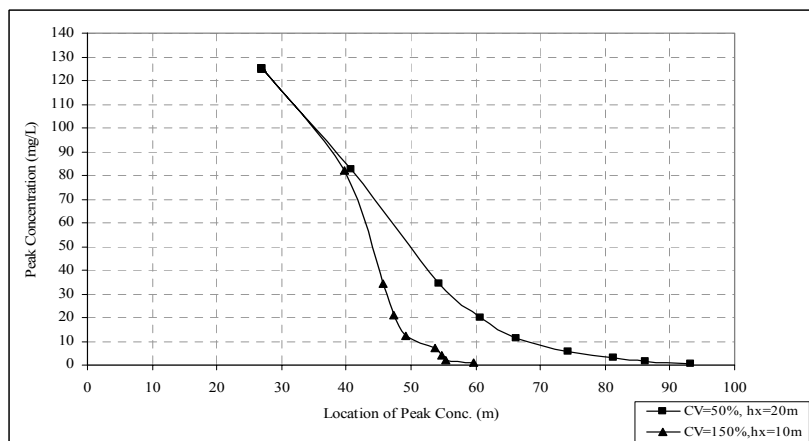


Figure 3.18. Peak concentration versus location of peak concentration graph for two different anisotropic fields.

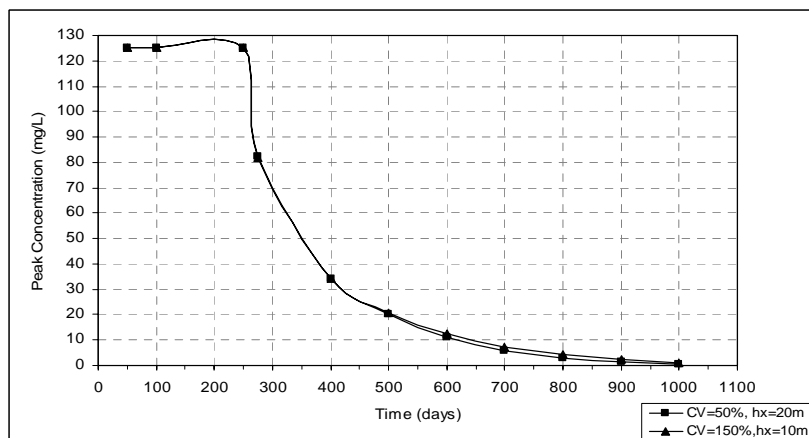


Figure 3.19. Peak concentration versus time graph for two different anisotropic fields

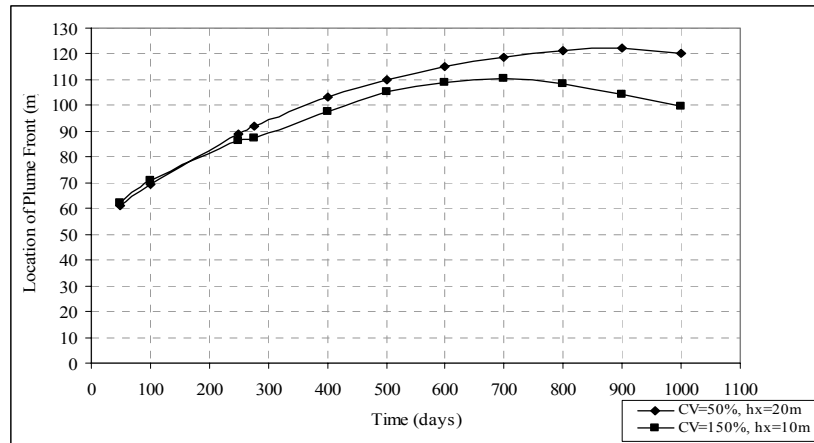


Figure 3.20. The location of plume front versus time graph for two different anisotropic fields.

As stated before, the plume front of the contaminant shows the dispersion and the displacement of the plume along the flow direction. Figure 3.20 illustrates that the displacement of the plume front in the field having CV of 50 % is higher than that of the plume front at field having CV of 150 %. After a certain time (or travel distance), the plumes tend to shrink, and the areal extent of the plume decreases with time, because of the natural attenuation mechanisms. For CV = 150 % field, plume shrinks after 700 days or a travel distance of 55 m from the source, whereas for CV = 50 % field, plume shrinks after 900 days or a travel distance of 85 m from the source.

When isotropic and anisotropic fields having the same CV and  $h_x$  values are compared, it can be said that, the behavior of the plumes are totally different for isotropic and anisotropic fields. For instance, areal extents of the plumes are different. The areal extents of the plumes at anisotropic fields are more regular than the areal extents of the plumes at isotropic fields.

Anisotropic fields are more conservative fields than the isotropic ones. The plume does not move as fast as the plumes of isotropic fields. Moreover, the plumes are more dispersed along the x-direction, so the dispersion mechanism is more important in anisotropic fields than the isotropic fields. As CV increases, the effect of

anisotropy on the areal extent of plume (longer elongation of the plume along the flow direction) becomes more apparent.

### **3.3. ASSESSMENT OF BIODEGRADATION RATES AS A FUNCTION OF HETEROGENEITY**

For all different random hydraulic conductivity fields, the biodegradation rates of BTEX contamination were calculated using Buscheck and Alcantar and Conservative Tracer Methods.

For determination of biodegradation rates, a BTEX sampling transect along the flow direction was determined for each plume. This sampling transect is chosen when the plume is reached the steady state in terms of its size. Based on this analysis, the sampling transects are determined using the plumes of 400 days. The figures that show the selected transects in the plumes are given in Appendix E. The beginnings of the pathways are taken as the center of mass and the other observation wells are placed at equal distances along the x-direction according to plume shape and plume length. Table 3.1 shows the downgradient distances of observation wells located at the corresponding plumes of each field. From these observation wells, the contaminant concentrations are determined and they are used in the calculations of biodegradation rates.

For the biodegradation rate calculations, a contaminant velocity is required. Visual MODFLOW program gives the groundwater velocity field as a file, having the magnitude of directional velocity components in both x- and y- direction. The mean groundwater velocity for each hydraulic conductivity field is calculated from these files. Then, the mean groundwater velocity is used to calculate the mean contaminant velocity as;

$$v_c = \frac{v_x}{R} \quad (3.1)$$

where  $v_c$  is the contaminant velocity (L/T);  $v_x$  is the groundwater velocity (L/T);  $R$  is the retardation factor, which is calculated from;

$$R = 1 + \frac{\rho_b K_d}{\phi} \quad (3.2)$$

where  $\rho_b$  is the bulk density of aquifer media ( $M/L^3$ );  $K_d$  is the soil-water partition coefficient ( $L^3/M$ );  $\phi$  is the porosity. From the material properties of the aquifer system, retardation factor ( $R$ ) is calculated for BTEX as 1.30. Table 3.2 tabulates the calculated mean groundwater and contaminant velocities for each hydraulic conductivity field. These contaminant velocities are used in Buscheck and Alcantar Method in order to calculate the biodegradation rate and in Conservative Tracer Method in order to calculate the downgradient travel time.

Table 3.1. The downgradient distances of observation wells

		Downgradient Distance of The Observation Wells in Plumes (m)								
		OW1*	OW2	OW3	OW4	OW5	OW6	OW7	OW8	OW9
<b>Uniform</b>		0	5.5	15.5	25.5	35.5	45.5	55.5	65.5	75.5
<b>CV = 50 %</b>	<b>h = 5 m</b>	0	11.2	21.3	31.4	41.5	51.6	61.6	71.6	-
	<b>h = 10 m</b>	0	9.0	19.0	29.0	39.0	49.0	59.0	69.0	79.0
	<b>h = 20 m</b>	0	7.0	17.1	27.2	37.4	47.6	57.6	67.6	-
<b>CV = 100 %</b>	<b>h = 5 m</b>	0	7.4	18.8	29.3	39.3	50.7	61.3	-	-
	<b>h = 10 m</b>	0	12.4	22.4	32.4	42.5	52.5	62.5	72.5	-
	<b>h = 20 m</b>	0	4.6	15.1	26.0	36.5	-	-	-	-
<b>CV = 150 %</b>	<b>h = 5 m</b>	0	11.2	22.6	33.0	43.2	-	-	-	-
	<b>h = 10 m</b>	0	13.0	23.1	33.3	43.4	53.4	63.4	-	-
	<b>h = 20 m</b>	0	9.8	21.0	32.4	-	-	-	-	-
<b>CV = 50 %</b>	<b>hx = 20 m hy = 4 m</b>	0	10	20	30	40	50	60	70	-
<b>CV = 150 %</b>	<b>hx = 10 m hy = 2 m</b>	0	10.2	20.2	30.2	41	51.2	61.2	71.2	-

\* located at the center of mass of the plume

Table 3.2. The Groundwater and Contaminant Velocities of the fields

Hydraulic Conductivity Fields		Groundwater Velocity (m/s)	Contaminant Velocity (m/s)
Uniform		$1.643 \times 10^{-06}$	$1.264 \times 10^{-06}$
CV = 50 %	h = 5 m	$1.434 \times 10^{-06}$	$1.103 \times 10^{-06}$
	h = 10 m	$1.601 \times 10^{-06}$	$1.232 \times 10^{-06}$
	h = 20 m	$1.598 \times 10^{-06}$	$1.229 \times 10^{-06}$
CV = 100 %	h = 5 m	$1.119 \times 10^{-06}$	$8.609 \times 10^{-07}$
	h = 10 m	$1.393 \times 10^{-06}$	$1.072 \times 10^{-06}$
	h = 20 m	$1.404 \times 10^{-06}$	$1.080 \times 10^{-06}$
CV = 150 %	h = 5 m	$8.703 \times 10^{-07}$	$6.695 \times 10^{-07}$
	h = 10 m	$1.091 \times 10^{-06}$	$8.393 \times 10^{-07}$
	h = 20 m	$1.173 \times 10^{-06}$	$9.025 \times 10^{-07}$
CV = 50 %	hx = 20 m hy = 4 m	$1.718 \times 10^{-06}$	$1.321 \times 10^{-06}$
CV = 150 %	hx = 10 m hy = 2 m	$1.259 \times 10^{-06}$	$9.685 \times 10^{-07}$

### 3.3.1. BUSCHECK AND ALCANTAR METHOD

In this method, the biodegradation rates were calculated by using equation (2.46). The details of this method are explained in Chapter 2. Table 3.3 shows BTEX concentrations observed along the sampling transects (i.e., observed in monitoring wells) at each plume of the corresponding random hydraulic conductivity field. Using these concentration values, a linear regression analysis, involving  $(\ln C)$  versus downgradient distance plots, were conducted for each data set to calculate slope (m) of the regression line. Regression plots for Buscheck and Alcantar Method are presented in Appendix F. Calculated m values are used in equation (2.46) to calculate the biodegradation rate constants for each hydraulic conductivity field. Moreover,

overall attenuation rates are calculated by using  $m$  values from equation (2.45). The results of Buscheck and Alcantar Method for isotropic and anisotropic fields are given in the following sections.

Table 3.3. BTEX concentrations observed in monitoring wells.

Hydraulic Conductivity Fields		BTEX Concentrations Observed in Monitoring Wells (mg/L)								
		OW1*	OW2	OW3	OW4	OW5	OW6	OW7	OW8	OW9
<b>Uniform</b>		36.92	34.65	23.17	12.17	4.93	1.08	0.13	0.01	$2 \times 10^{-3}$
<b>CV = 50 %</b>	<b>h = 5 m</b>	30.87	22.75	10.67	2.71	0.33	0.03	$3 \times 10^{-3}$	$2 \times 10^{-4}$	-
	<b>h = 10 m</b>	30.70	25.99	16.48	8.89	3.74	0.86	0.10	0.01	$1 \times 10^{-3}$
	<b>h = 20 m</b>	34.42	28.18	12.73	3.68	0.42	0.03	$1 \times 10^{-3}$	-	-
<b>CV = 100 %</b>	<b>h = 5 m</b>	28.41	24.64	11.78	3.10	0.33	0.01	$5 \times 10^{-3}$	-	-
	<b>h = 10 m</b>	31.62	24.63	14.18	6.57	2.02	0.29	0.03	$3 \times 10^{-3}$	-
	<b>h = 20 m</b>	30.79	24.37	6.62	0.35	0.01	-	-	-	-
<b>CV = 150 %</b>	<b>h = 5 m</b>	30.61	28.30	17.08	5.16	0.59	0.03	-	-	-
	<b>h = 10 m</b>	29.47	17.86	7.95	2.23	0.39	0.06	0.01	-	-
	<b>h = 20 m</b>	25.63	7.53	0.08	$5.3 \times 10^{-4}$	-	-	-	-	-
<b>CV = 50 %</b>	<b><math>h_x = 20</math> m <math>h_y = 4</math> m</b>	24.17	25.10	12.44	3.90	0.54	0.04	0.001	-	-
<b>CV = 150 %</b>	<b><math>h_x = 10</math> m <math>h_y = 2</math> m</b>	34.26	28.47	17.43	6.93	0.52	0.07	0.009	$1 \times 10^{-3}$	-

\* located at the center of mass of the plume

### 3.3.1.1. Isotropic Hydraulic Conductivity Field

Table 3.4 shows the calculated biodegradation and overall attenuation rates for BTEX contamination at all isotropic fields. Table 3.4 also shows the  $\lambda / k$  ratio, which is the contribution of biodegradation to the overall attenuation rate, for all isotropic fields. As seen in Table 3.4, there is one order of magnitude difference between the calculated biodegradation rates, but there is no such difference between

the overall attenuation rates. The highest biodegradation rate ( $1.05 \times 10^{-1} \text{ d}^{-1}$ ) and overall attenuation rate ( $3.47 \times 10^{-2} \text{ d}^{-1}$ ) are observed for the field having CV value of 150 %, correlation length of 20 m, while the smallest biodegradation rate ( $1.69 \times 10^{-2} \text{ d}^{-1}$ ) and overall attenuation rate ( $1.02 \times 10^{-2} \text{ d}^{-1}$ ) are observed for field having CV value of 150 %, correlation length of 5 m. Moreover, the highest  $\lambda / k$  ratio is obtained for the field having CV value of 150 %, correlation length of 20 m, while the smallest  $\lambda / k$  ratio is obtained for the field having CV value of 50 %, correlation length of 10 m. It can be said that the highest  $\lambda / k$  ratio is obtained in the field having the smallest plume, while smallest  $\lambda / k$  ratio is obtained in the field having largest plume, at 400 days, when the plumes reach steady-state in terms of areal extent. Therefore, it is stated that  $\lambda / k$  ratios, obtained at a contaminated site, are related to the areal extent of the plume.

Table 3.4. Biodegradation and overall attenuation rates and  $\lambda / k$  ratios of BTEX at isotropic fields calculated by Buscheck and Alcantar Method

		Biodegradation Rates, $\lambda$ (1/d)	Overall Attenuation Rate, $k$ (1/d)	$\lambda / k$ (%)
<b>Uniform</b>		$3.08 \times 10^{-2}$	$1.88 \times 10^{-2}$	163.7 %
<b>CV = 50 %</b>	<b>h = 5 m</b>	$4.01 \times 10^{-2}$	$2.12 \times 10^{-2}$	188.9 %
	<b>h = 10 m</b>	$2.89 \times 10^{-2}$	$1.79 \times 10^{-2}$	161.5 %
	<b>h = 20 m</b>	$4.64 \times 10^{-2}$	$2.42 \times 10^{-2}$	191.7 %
<b>CV = 100 %</b>	<b>h = 5 m</b>	$3.34 \times 10^{-2}$	$1.72 \times 10^{-2}$	193.6 %
	<b>h = 10 m</b>	$2.51 \times 10^{-2}$	$1.55 \times 10^{-2}$	161.9 %
	<b>h = 20 m</b>	$6.54 \times 10^{-2}$	$2.84 \times 10^{-2}$	230.1 %
<b>CV = 150 %</b>	<b>h = 5 m</b>	$1.69 \times 10^{-2}$	$1.02 \times 10^{-2}$	165.7 %
	<b>h = 10 m</b>	$2.03 \times 10^{-2}$	$1.24 \times 10^{-2}$	163.2 %
	<b>h = 20 m</b>	$1.05 \times 10^{-1}$	$3.47 \times 10^{-2}$	301.1 %

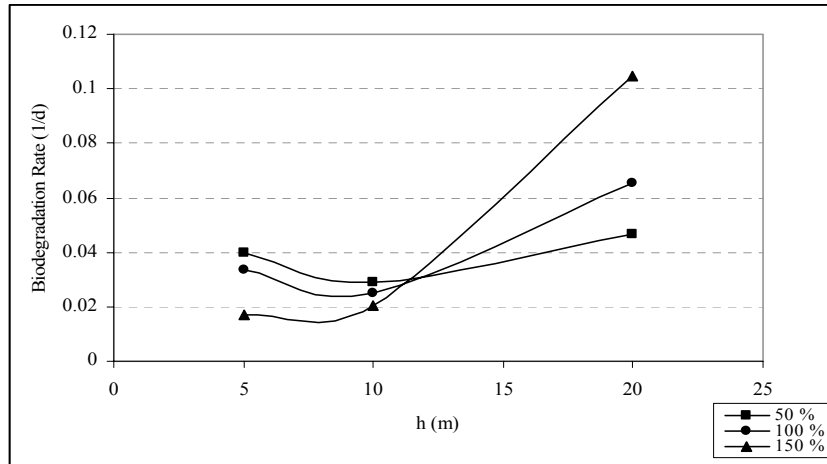


Figure 3.21. Biodegradation rate versus correlation length for CV = 50 %, CV = 100 %, and CV = 150 %.

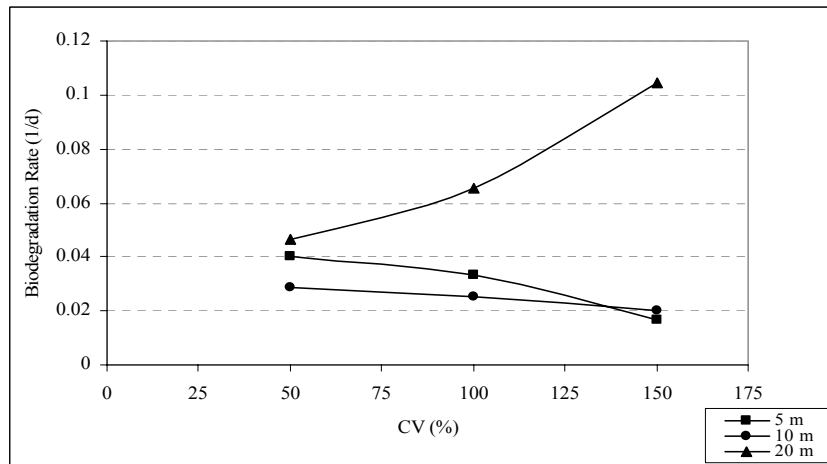


Figure 3.22. Biodegradation rate versus CV for h = 5 m, h = 10 m, and h = 20 m.

Figure 3.21 shows biodegradation rates versus correlation length graph for CV = 50 %, 100 %, and 150 %; and Figure 3.22 illustrates biodegradation rate versus CV graph for h = 5 m, 10 m, and 20 m. As seen from these figures, when h = 10-12 m, the biodegradation rate has a relatively mild variability between 0.02–0.04 d<sup>-1</sup>, regardless of CV. However, when h ≈ 20 m, biodegradation rate increases drastically with increasing CV, implying that the affect of heterogeneity is becoming much more apparent when CV > 100 % and h ≈ 20 m. For h is 5 m and 10 m cases, biodegradation rate decreases when CV increases. However, for h is 20 m case

biodegradation rate increases as CV increases. The relationship between biodegradation rate of BTEX and aquifer heterogeneity is complex and non-linear.

### 3.3.1.2. Anisotropic Hydraulic Conductivity Field

Table 3.5 shows the calculated biodegradation rates for BTEX contamination at anisotropic fields. The biodegradation rates are calculated only for the two anisotropic hydraulic conductivity fields. For the field having CV of 50 %,  $h_x$  of 20 m, and  $h_y$  of 4 m, the calculated biodegradation rate is higher than the calculated mass attenuation rate for the field having CV of 150 %,  $h_x$  of 10 m, and  $h_y$  of 2 m. A comparison of biodegradation rate constants for isotropic and anisotropic hydraulic conductivity fields shows that anisotropy reduces the effect of CV and  $h$  on the variability of rate constants. Relative to isotropy, anisotropy causes about a 1 % decrease in biodegradation rate constant when CV is low (CV = 50 %), but it causes about 50 % increase in the rate constant when CV is very high (CV = 150 %). On the other hand, when CV is low (CV = 50 %), anisotropy causes about a 2 % increase in overall attenuation rate, while it causes about 40 % increase in the overall attenuation rate constant when CV is high (CV = 150 %). As seen in both of the anisotropic fields, anisotropy causes an increase in the overall attenuation rate.

Table 3.5. Biodegradation and overall attenuation rates and  $\lambda / k$  ratios of BTEX at anisotropic fields calculated by Buscheck and Alcantar Method

		Biodegradation Rates, $\lambda$ (1/d)	Overall Attenuation Rate, $k$ (1/d)	$\lambda / k$ (%)
CV = 50 %	$h_x = 20$ m $h_y = 4$ m	$4.58 \times 10^{-2}$ ( $4.64 \times 10^{-2}$ )*	$2.47 \times 10^{-2}$ ( $2.42 \times 10^{-2}$ )*	185.7 % (191.7%)*
CV = 150 %	$h_x = 10$ m $h_y = 2$ m	$3.10 \times 10^{-2}$ ( $2.03 \times 10^{-2}$ )*	$1.72 \times 10^{-2}$ ( $1.24 \times 10^{-2}$ )*	180.2 % (163.2%)*

\*Numbers in () gives the isotropic biodegradation and overall attenuation rate constants and  $\lambda / k$  ratios.

### 3.3.2. CONSERVATIVE TRACER METHOD

To differentiate the effect of biodegradation from the overall mass attenuation processes, BTEX should be corrected using a conservative tracer. The details of this method are explained in Chapter 2.

Table 3.6. Corrected BTEX concentrations observed in monitoring wells.

Hydraulic Conductivity Fields		Corrected BTEX Concentrations in Monitoring Wells (mg/L)								
		OW1*	OW2	OW3	OW4	OW5	OW6	OW7	OW8	OW9
Uniform		36.92	34.65	24.55	15.10	6.87	1.65	0.21	0.03	$3 \times 10^{-3}$
CV = 50 %	h = 5 m	30.87	22.75	13.74	4.42	0.56	0.06	0.01	$4 \times 10^{-4}$	-
	h = 10 m	30.70	25.99	17.39	10.57	4.92	1.27	0.17	0.02	$2 \times 10^{-3}$
	h = 20 m	34.42	28.18	17.28	6.60	0.98	0.06	$4 \times 10^{-3}$	-	-
CV = 100 %	h = 5 m	28.41	24.46	15.05	5.26	0.61	0.03	$1 \times 10^{-3}$	-	-
	h = 10 m	31.62	46.53	15.97	6.56	2.74	0.37	0.05	0.01	-
	h = 20 m	30.79	26.83	12.62	1.08	0.03	-	-	-	-
CV = 150 %	h = 5 m	30.61	29.00	18.27	7.72	1.16	0.10	-	-	-
	h = 10 m	29.47	17.94	10.40	3.36	0.59	0.10	0.01	-	-
	h = 20 m	25.63	8.01	0.22	$2 \times 10^{-3}$	-	-	-	-	-
CV = 50 %	h <sub>x</sub> = 20 m h <sub>y</sub> = 4 m	34.17	25.10	14.69	5.36	0.92	0.08	0.01	-	-
CV = 150 %	h <sub>x</sub> = 10 m h <sub>y</sub> = 2 m	34.26	29.10	18.34	9.78	1.21	0.11	0.02	$2 \times 10^{-3}$	-

\* located at the center of mass of the plume

In this study, as a conservative tracer, TMB (trimethyl benzene) is used. For the purpose of correction of BTEX concentrations, a set of TMB simulations were performed in the same flow fields where BTEX simulations were performed. Then BTEX concentrations were corrected using equation (2.48). Table 3.6 shows the corrected concentrations of BTEX for different hydraulic conductivity fields. In

order to find the biodegradation rates, using corrected BTEX concentration values, a linear regression analysis, involving corrected concentration of BTEX versus time plots, were conducted for each data set to calculate slope (m) of the regression line. The slope of the regression line directly gives the biodegradation rate of BTEX. These calculations are performed for all fields. Regression plots for Conservative Tracer Method are presented in Appendix F.

### **3.3.2.1. Isotropic Hydraulic Conductivity Field**

Table 3.7 shows the calculated biodegradation rates for BTEX at all isotropic fields using conservative tracer method. As seen in Table 3.7, the highest biodegradation rate ( $2.33 \times 10^{-2} \text{ d}^{-1}$ ) is observed for the field having CV value of 150 %, correlation length of 20 m, while the smallest biodegradation rate ( $0.66 \times 10^{-2} \text{ d}^{-1}$ ) is observed for field the having CV value of 150 %, correlation length of 10 m. Figure 3.23 shows biodegradation rates versus correlation length graph for CV = 50 %, 100 %, and 150 % and Figure 3.24 illustrates biodegradation rate versus CV graph for h = 5 m, 10 m, and 20 m. As seen from these figures, when h = 13 - 15 m, the biodegradation rate has a relatively mild variability between  $0.012 - 0.015 \text{ d}^{-1}$ , regardless of CV. However, when h  $\approx$  20 m, biodegradation rate increases drastically with increasing CV, implying that the affect of heterogeneity is becoming much more apparent when CV > 100 % and h  $\approx$  20 m. Moreover, for h = 5 m and 10 m cases, biodegradation rate decreases when CV increases. However, for h = 20 m case, biodegradation rate increases as CV increases. The relationship between biodegradation rate of BTEX and aquifer heterogeneity is complex and non-linear.

Table 3.7. Biodegradation rates of BTEX calculated by Conservative Tracer Method

		Biodegradation Rates (1/d)
<b>Uniform</b>		$1.35 \times 10^{-2}$
<b>CV = 50 %</b>	<b>h = 5 m</b>	$1.53 \times 10^{-2}$
	<b>h = 10 m</b>	$1.27 \times 10^{-2}$
	<b>h = 20 m</b>	$1.64 \times 10^{-2}$
<b>CV = 100 %</b>	<b>h = 5 m</b>	$1.20 \times 10^{-2}$
	<b>h = 10 m</b>	$1.15 \times 10^{-2}$
	<b>h = 20 m</b>	$1.77 \times 10^{-2}$
<b>CV = 150 %</b>	<b>h = 5 m</b>	$0.66 \times 10^{-2}$
	<b>h = 10 m</b>	$0.89 \times 10^{-2}$
	<b>h = 20 m</b>	$2.33 \times 10^{-2}$

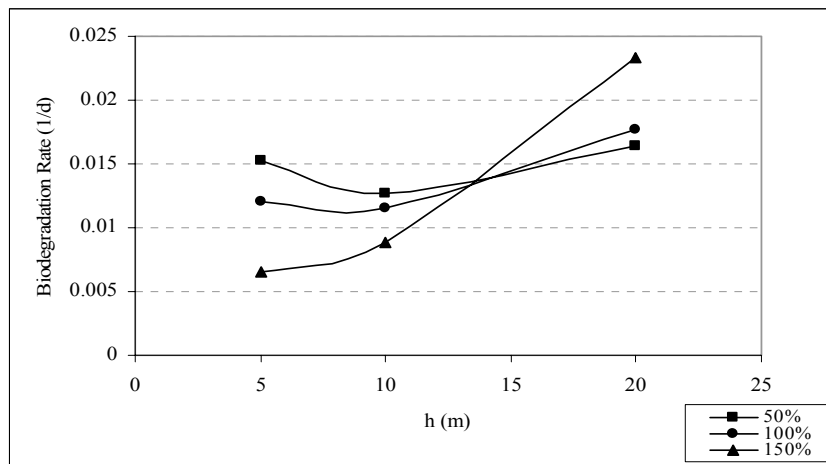


Figure 3.23. Biodegradation rate versus correlation length for CV = 50 %, CV = 100 %, and CV = 150 %.

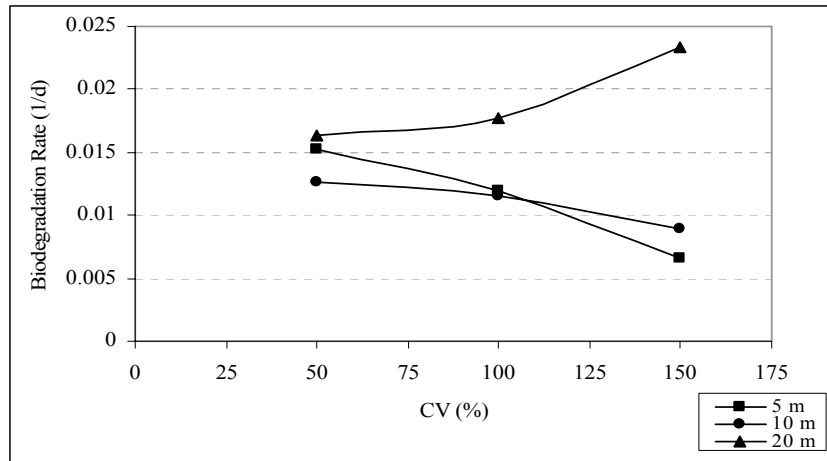


Figure 3.24 Biodegradation rate versus CV for  $h = 5$  m,  $h = 10$  m, and  $h = 20$  m.

### 3.3.2.2. Anisotropic Hydraulic Conductivity Field

Table 3.8 shows the calculated biodegradation rates for BTEX contamination at the anisotropic fields. The biodegradation rates are calculated only two anisotropic fields. For the field having CV of 50 %,  $h_x$  of 20 m, and  $h_y$  of 4 m the calculated biodegradation rate is higher than the calculated biodegradation rate for the field having CV of 150 %,  $h_x$  of 10 m, and  $h_y$  of 2 m. Table 3.8 illustrates that, as also seen in isotropic fields, higher degradation rate is obtained in the field having higher CV (CV = 150 %). When compared the biodegradation rate constants for isotropic and anisotropic hydraulic conductivity fields, relative to isotropy, anisotropy causes about a 1 % increase in biodegradation rate constant when CV is low (CV = 50 %), while it causes about nearly 35 % increase in the rate constant when CV is high (CV = 150 %). As seen in both of the anisotropic fields, anisotropy causes an increase in the biodegradation rate constants.

Table 3.8. Biodegradation rates of BTEX at anisotropic fields calculated by Conservative Tracer Method

		<b>Biodegradation Rates (1/d)</b>
<b>CV = 50 %</b>	<b>h<sub>x</sub> = 20 m h<sub>y</sub> = 4 m</b>	1.66 x 10 <sup>-2</sup> (1.64 x 10 <sup>-2</sup> )*
<b>CV = 150 %</b>	<b>h<sub>x</sub> = 10 m h<sub>y</sub> = 2 m</b>	1.19 x 10 <sup>-2</sup> (0.89 x 10 <sup>-2</sup> )*

\*Numbers in () gives the isotropic rate constants.

Table 3.9 tabulates biodegradation rates calculated by both Buscheck and Alcantar and Conservative Tracer Methods. As seen in Table 3.9, the biodegradation rate constants calculated by using Buscheck and Alcantar Method are greater than the rate constants calculated by using Conservative Tracer Method; in other words, Buscheck and Alcantar Method gives nearly three times greater biodegradation rate constants than Conservative Tracer Method. The biggest difference is seen for the field having CV of 150 % and h of 20 m, where highest degradation rates are calculated by using both methods. This difference can be because of the assumptions used for Buscheck and Alcantar and Conservative Tracer Method or can be due to some calculation or sampling errors.

The calculated degradation rates for uniform hydraulic conductivity field are also different from each other. In the fate and transport simulations of BTEX contamination, a set of hydrocarbon decay rates, according to electron acceptors, are input to the Visual MODFLOW program. The highest decay rate is given to the system for aerobic reactions (0.051 d<sup>-1</sup>), while smallest rate is given for methanogenesis (0.002 d<sup>-1</sup>). When the calculated degradation rates for uniform flow field are compared to the initial hydrocarbon decay rates, it can be said that the calculated rates by using both of the methods are in between 0.002 and 0.051 d<sup>-1</sup>.

Table 3.9. Biodegradation rates of BTEX calculated by two different methods.

		<b>Biodegradation Rates by Buscheck And Alcantar Method (1/d)</b>	<b>Biodegradation Rates by Conservative Tracer Method (1/d)</b>
<b>Uniform</b>		$3.08 \times 10^{-2}$	$1.35 \times 10^{-2}$
<b>CV = 50 %</b>	<b>h = 5 m</b>	$4.01 \times 10^{-2}$	$1.53 \times 10^{-2}$
	<b>h = 10 m</b>	$2.89 \times 10^{-2}$	$1.27 \times 10^{-2}$
	<b>h = 20 m</b>	$4.64 \times 10^{-2}$	$1.64 \times 10^{-2}$
<b>CV = 100 %</b>	<b>h = 5 m</b>	$3.34 \times 10^{-2}$	$1.20 \times 10^{-2}$
	<b>h = 10 m</b>	$2.51 \times 10^{-2}$	$1.15 \times 10^{-2}$
	<b>h = 20 m</b>	$6.54 \times 10^{-2}$	$1.77 \times 10^{-2}$
<b>CV = 150 %</b>	<b>h = 5 m</b>	$1.69 \times 10^{-2}$	$0.66 \times 10^{-2}$
	<b>h = 10 m</b>	$2.03 \times 10^{-2}$	$0.89 \times 10^{-2}$
	<b>h = 20 m</b>	$10.46 \times 10^{-2}$	$2.33 \times 10^{-2}$
<b>CV = 50 %</b>	<b>h<sub>x</sub> = 20 m h<sub>y</sub> = 4 m</b>	$4.58 \times 10^{-2}$	$1.66 \times 10^{-2}$
<b>CV = 150 %</b>	<b>h<sub>x</sub> = 10 m h<sub>y</sub> = 2 m</b>	$3.10 \times 10^{-2}$	$1.19 \times 10^{-2}$

### 3.3.3. FUNCTIONAL RELATIONSHIP BETWEEN RATE CONSTANTS AND HETEROGENEITY

After all biodegradation rates are calculated, a numerical relationship between rate constants and heterogeneity level is found. In order to achieve this goal another computer program, STATGRAPHICS is used. Two functional relationships are obtained for isotropic heterogeneous fields from the biodegradation rate constants calculated by two different methods, Buscheck and Alcantar and Conservative Tracer Methods.

Two sets of nine biodegradation rate constants, calculated for the isotropic fields, are drawn on 3-dimensional surface plot to see the relationship between the correlation length, CV and rate constants. Figure 3.25 and 3.26 demonstrate the 3-dimensional

surface plots of the biodegradation rates for Buscheck and Alcantar and Conservative Tracer Method, respectively.

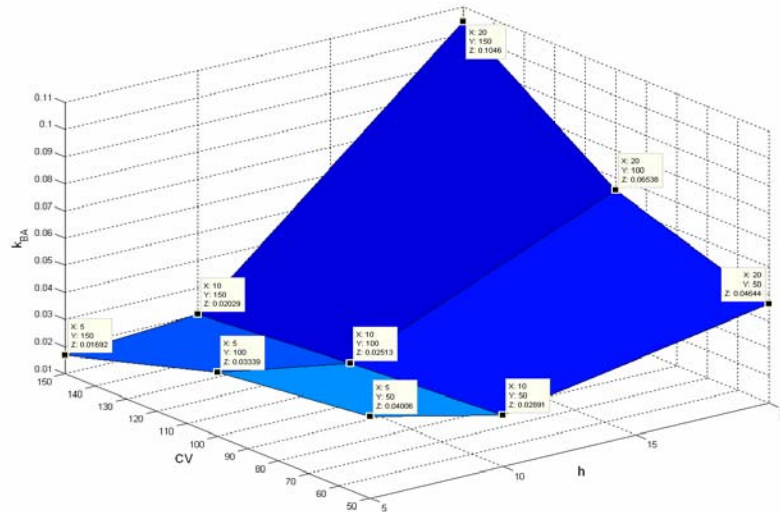


Figure 3.25 3-Dimensional surface plot of biodegradation rates for Buscheck and Alcantar Method.

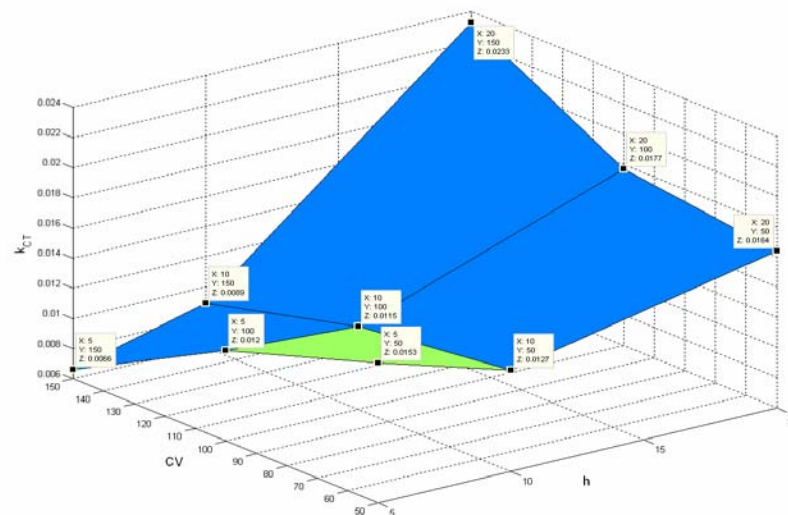


Figure 3.26 3-Dimensional surface plot of biodegradation rates for Conservative Tracer Method.

As seen from Figures 3.25 and 3.26, there is no linear relationship between the correlation lengths, CVs and biodegradation rates. According to these graphs, non-linear regression analyses are applied to find a relationship between biodegradation rates and the heterogeneity level. For the non-linear regression analysis, the following empirical model equation is selected;

$$\lambda = a + (b*(CV)^c) + (d*(h)^e) \quad (3.3)$$

where  $\lambda$  is the first order biodegradation rate ( $T^{-1}$ ), CV is the coefficient of variation, h is the correlation length (L), and a, b, c, d and e are constants.

The regression analysis fitting equation (3.3) to data given in Table 3.9 yielded the following empirical relationships for the Buscheck and Alcantar and Conservative Tracer Method, respectively as;

Buscheck and Alcantar Method:

$$k = 0.023 + (0.0035 * CV^{2.47727}) + \left( 0.00002 * \left( \frac{h}{10} \right)^{11.1421} \right) \quad R^2 = 67.26 \% \quad (3.4)$$

Conservative Tracer Method:

$$k = 0.005 + (0.0063 * CV^{-0.2527}) + \left( 0.00008 * \left( \frac{h}{10} \right)^{6.7349} \right) \quad R^2 = 66.02 \% \quad (3.5)$$

The quality of the multiple non-linear regression is given by correlation coefficient, namely R-squared. In this non-linear regression analyses, the R-squared values are obtained. For the Buscheck and Alcantar method, R-squared value is found as 67.26 % and for the Conservative Tracer Method, R-squared value is found as 66.02 %.

## CHAPTER 4

### SUMMARY AND CONCLUSION

Groundwater pollution by petroleum-derived hydrocarbons, especially BTEX, released from underground storage tanks and pipelines is a widespread environmental problem. Monitored Natural Attenuation (MNA) can be an inexpensive and effective cleanup option for remediation of BTEX contaminated sites. MNA relies on such natural processes as biodegradation, dispersion, dilution, and sorption, to reduce the concentration of pollutants at contaminated sites. The rate of contaminant mass attenuation through these natural processes to a large extent affected by the groundwater flow regime, which is primarily controlled by the aquifer heterogeneity, more specifically spatial variability of hydraulic conductivity.

Hydraulic conductivity, via its control over groundwater flux and velocity, affects the concentration distribution within the plume, which in turn, plays a determining role on the rate of mass attenuation, in specific, biodegradation rates of contaminants along the flow direction. The primary objective of this research was to quantitatively describe the relationship between the biodegradation rates of BTEX and aquifer heterogeneity. The different levels of aquifer heterogeneity can quantitatively be described by the mean, variance, and correlation length of hydraulic conductivity field.

The generation of a functional relationship between biodegradation rate constant, which is commonly assumed to follow first-order reaction kinetics, and the statistical parameters of the aquifer heterogeneity can be beneficial when assessing the effectiveness of the natural attenuation processes to achieve the pre-specified cleanup

goals at a given site during feasibility studies. In fact, initial screening studies conducted based on site specific data is the first and the most essential step in the feasibility studies to decide if MNA alone is to be the cleanup approach.

During the site characterization stage of the initial screening studies, a semi-quantitative information regarding the level of heterogeneity can easily be obtained by a number of drill-hole investigation data. For example, using the lithological data and the available databases for hydraulic conductivity, it is possible to estimate the statistical properties, such as CV and correlation scale, for the spatial variability of hydraulic conductivity. Therefore, given the knowledge of the functional relationship between biodegradation rate constant and the statistical parameters of aquifer heterogeneity, one can obtain a first approximation for the biodegradation rate constant, which in turn ultimately can be used at the initial screening stage to assess the effectiveness of MNA to achieve the cleanup goals without need for extensive site specific analytical concentration data. Towards this end, groundwater flow and BTEX fate and transport are simulated numerically within synthetically generated heterogeneous aquifers characterized by random but spatially correlated hydraulic conductivity fields. The major findings of this numerical study are summarized as follows:

- The hydraulic conductivity field generation results show that, for isotropic fields, when the correlation length is short, smaller size areas of high and low conductivity zones are spread across the entire flow field and this behavior becomes much more evident as CV increases. It is clear that the hydraulic conductivity data spread over a larger range, as CV increases, at a given correlation length.
- The hydraulic conductivity field generation results also show that, for anisotropic field, since the correlation length in y-direction is smaller than the value in x-direction, great changes in hydraulic conductivities are observed in short distances along y-direction. Thus, the high and low conductivity zones are seen as squeezed in y-direction and extended in x-direction. Furthermore,

in anisotropic fields, the areal extents of high and low conductivity zones are small and spread across the entire flow field when correlation length is short.

- At the isotropic and anisotropic heterogeneous conductivity fields, depending on the hydraulic conductivity distribution, head distribution and velocity fields change across the entire flow fields. The results also show that, because of the directional change in the velocity vectors, the head contours have irregular shape and the irregularity of these contours increase as CV increases, for a given correlation length. The most irregular head contours are observed in the field having CV of 150 %. Change in the correlation length does not affect the shape and spacing of head contours but affects the position of a given head contour within the flow domain.
- The shape of the plume is more affected by the CV. As CV increases, the irregularity and distortion of the plume shape increases. As both CV and h increases plume size shrinks; this shrinkage becomes much more apparent with time. CV affects the plume size more than h.
- It should be noticed that, while CV is constant, the plumes move faster at the fields having correlation length of 10 m than the plumes at the other fields. Because the plumes move slowly at correlation lengths of 5 m and 20 m, the plumes stay longer at the system and goes down the degradation processes for longer times, when CV is constant. Therefore, the plumes at fields having correlation lengths of 5 m and 20 m are smaller than the plumes at fields having correlation length of 10 m. On the other hand, when correlation length is constant, as CV increases, the plume slows down and stays longer at the model domain, so that areal extent of the plume decreases. Therefore, smaller plumes are observed at hydraulic conductivity fields having higher CV at a constant correlation length value. The smallest plume developed in the hydraulic conductivity field with CV = 150 % and h = 20 m, while the largest plume occurred in hydraulic conductivity field with CV = 50 % and h = 5 m.
- The fate and transport simulation results also show that the rate of the reduction in the peak concentration decreases both with time and distance from the source. This situation indicates that the efficiency of the attenuation

mechanisms, especially biodegradation, decreases with time. The biodegradation effectiveness generally depends on the electron acceptor concentration, so as time increases, the concentration of the electron acceptors decrease in all fields, regardless of CV and h.

- For isotropic hydraulic conductivity fields, there is one order of magnitude difference between the calculated biodegradation rate constants, calculated by Buscheck and Alcantar Method. However, there is no such difference between the overall attenuation rates. The highest biodegradation rate ( $1.05 \times 10^{-1} \text{ d}^{-1}$ ) and overall attenuation rate ( $3.47 \times 10^{-1} \text{ d}^{-1}$ ) are observed for the field having CV value of 150 %, correlation length of 20 m, while the smallest biodegradation rate ( $1.69 \times 10^{-2} \text{ d}^{-1}$ ) and overall attenuation rate ( $1.02 \times 10^{-1} \text{ d}^{-1}$ ) are observed for field having CV value of 150 %, correlation length of 5 m. For  $h = 5 \text{ m}$  and  $h = 10 \text{ m}$  cases biodegradation rate decreases when CV increases. However, for  $h = 20 \text{ m}$  case biodegradation rate increases as CV increases. The same behavior is also seen in degradation rates calculated by Conservative Tracer Method. However, the calculated degradation rates are smaller than that calculated by Buscheck and Alcantar Method. This difference can be because of the assumptions used for Buscheck and Alcantar and Conservative Tracer Method. The results of the degradation rate calculations shows that the relationship between biodegradation rate of BTEX and aquifer heterogeneity is complex and non-linear.
- In case of anisotropic hydraulic conductivity fields, for the field having CV of 50 %,  $h_x$  of 20 m, and  $h_y$  of 4 m the calculated biodegradation rate is higher than the calculated biodegradation rate for the field having CV of 150 %,  $h_x$  of 10 m, and  $h_y$  of 2 m. For CV = 50 %, biodegradation rates for isotropic and anisotropic fields are closed to each other; whereas for CV = 150 %, a difference is obtained between biodegradation rates for isotropic and anisotropic fields. Therefore, it can be stated that, in fields having low CV values, the anisotropy does not affect the degradation rates, while, in fields

having high CV values, the degradation rates of BTEX increase by the help of anisotropy effects.

- During MNA feasibility studies, for the aquifer heterogeneity level of  $CV < 100\%$  and  $h < 10\text{ m}$ , a minimum recommended biodegradation rate constant value of  $0.02\text{ d}^{-1}$  can be used, where as for the aquifer heterogeneity level of  $CV > 100\%$  and  $h > 10\text{ m}$ , using a minimum biodegradation rate constant value of  $0.06\text{ d}^{-1}$  can be recommended.
- Finally, two functional relationships are obtained for isotropic heterogeneous fields from the biodegradation rate constants calculated by two different methods, Buscheck and Alcantar and Conservative Tracer Methods. Non-linear regression analyses are applied and a non-linear relationship between biodegradation rates and the heterogeneity level is obtained. This numerical relationship can be beneficial in assessing the natural attenuation capacity of a contaminated site. Moreover, it can be used as an approximation to the degradation rates of BTEX in a field scale applications.

Since naturally occurring attenuation mechanisms are complex, the relationship between aquifer heterogeneity and biodegradation rates is important for assessing of the aquifer natural attenuation capacity. In order to find a better relationship between heterogeneity level and degradation rates, fate and transport of BTEX can be simulated at different sites having different heterogeneity levels. Since as CV increases at a given h, degradation rates are drastically increase, the effect of CV can be investigated by using higher CV values. Furthermore, in order to assess the anisotropy effect on fate and transport of BTEX, exactly, different anisotropy ratios can be applied, in future studies.

## REFERENCES

- [1]. Bear, J., *Hydraulics of Groundwater*, McGraw-Hill, New York, NY., 1979
  
- [2]. Buscheck, T.E., Alcantar, C.M, *Regression Techniques and Analytical Solutions to Demonstrate Intrinsic Bioremediation*, In: *Proceeding of the Battelle International Symposium on In Situ and On-Site Bioreclamation*, Columbus, OH, pp. 109-116, 1995.
  
- [3]. Carsel R.F., Parrish R.S., *Developing Joint Probability Distributions of Soil-water Retention Characteristics*, *Water Resources Research*, Vol. 24, pp. 755-769, 1988.
  
- [4]. Chen, Y.M., Abriola, L.M., Barcelona, M.J., *Simulation of Intrinsic Bioremediation Processes at Wurtsmith Air Force Base, Michigan*, In: *Alleman, B.C., Leeson, A. (Chairs), In Situ and On-Site Bioremediation*, Vol. 1, Battelle Press, Columbus, OH, pp. 55-60, 1997.
  
- [5]. Clement, T.P., *A Modular Computer Code for Simulating Reactive Multi-species Transport in 3-Dimensional Groundwater Systems*, prepared for The U.S. Department of Energy Under Contract DE-AC06-76RLO 1830, 1997.
  
- [6]. Dale, M., *Natural Attenuation Processes and Site Monitoring*, *Proceedings of the 2<sup>nd</sup> Australia and New Zealand Conference on Environmental Geotechnics*, Newcastle 28-30 November, pp. 295-307, 2001.
  
- [7]. Fetter, C.W., *Contaminant Hydrogeology*, Macmillan Publishing Company, New York, NY, 1993.
  
- [8]. Harbaugh, A.W., Banta, E.R., Hill, M.C., McDonald, M.C., *Modflow-2000 The U.S. Geological Survey Modular Ground-Water Model—User Guide To Modularization Concepts And The Ground-Water Flow Process*, U.S. Geological Survey, 2002.

- [9]. Kao, C.M., and Wang, C.C., Control of BTEX Migration by Intrinsic Bioremediation at a Gasoline Spill Site, *Water Resource*, No. 13, pp. 3413-3423, 2000.
- [10]. Kao, C.M., and Wang, Y.S., Field Investigation of the Natural Attenuation and Intrinsic Biodegradation Rates at an Underground Storage Tank Site, *Environmental Geology*, 40 (4-5), 2001.
- [11]. Kemblowski M. W., J. P. Salanitro, G. M. Deeley, and C.C. Stanley, the Fate and Transport of Residual Hydrocarbon in Groundwater-A Case Study, *Proceedings Petroleum Hydrocarbons and Organic Chemicals in Groundwater: Prevention, Detection, and Restoration*, National Water Well Association/API, Houston, TX, , pp. 207-231, 1987.
- [12]. Lee, M. K., Sounders, J. A., and Wolf, L. W., Stochastic Analysis of In-Situ Bioremediation Within Heterogeneous Porous Media: *Proceedings 4<sup>th</sup> International Symposium on In-situ and On-site Bioremediation*, New Orleans, LA., Battalle Press, Vol. 5, pp. 583-588, 1997.
- [13]. Lu, G., Clement, T.P., Zheng, C., and Wiedemeier, T.H., Natural Attenuation of BTEX Compounds: Model Development and Field-Scale Application, *Ground Water*, Sep/Oct 1999, 37, 5, pp. 707, 1999.
- [14]. MacQuarrie, K.B.T., Sudicky, E.A., and Frind, E.O., Simulation of Biodegradable Organic Contaminants in Groundwater: 1. Numerical Formulation and Model Calibration, *Water Resources Research*, Vol. 26, No.2, pp. 227-222, 1990.
- [15]. MacQuarrie, K.B.T. and Sudicky, E.A., Simulation of Biodegradable Organic Contaminants in Groundwater: 2. Plume Behavior in Uniform and Random Flow Fields, *Water Resources Research*, Vol. 26, No.2, pp. 223-239, 1990.
- [16]. Natural Attenuation of Chlorinated Solvents in Groundwater: Principles and Practices, prepared by The Interstate Technology and Regulatory Cooperation Work Group, In Situ Bioremediation Work Team, 1999.

- [17]. Newell, C.J., McLeod, R.K., Gonzales, J.R., and Wilson, J.T., BIOSCREEN Natural Attenuation Decision Support System, User's Manual-Version 1.3, National Risk Management Research Laboratory Office of Research and Development U.S. Environmental Protection Agency, Cincinnati, Ohio, EPA/600/R-96/087, 1996.
- [18]. Rifai, H.S., Bedient, P.B., Haasbeek, J.F., and Borden, R.C., BIOPLUME II: Computer Model of Two-Dimensional Contaminant Transport Under The Influence of Oxygen Limited Biodegradation in Groundwater, User's Manual-Version 1.0 Prepared for U.S. Environmental Protection Agency, Washington DC., EPA/600/S8-88/093, pp. 73, 1989.
- [19]. Sun, Y. and Clement T.P., A Decomposition Method for Solving Coupled Multispecies Reactive Transport Problems, *Transport in Porous Media Journal*, 1404, pp. 1-20, 1998.
- [20]. Sun, Y., Peterson, J.N., Clement, T.P., and Hooker, B.S., Effects of Reaction Kinetics on Predicted Concentration Profiles During Subsurface Bioremediation, *Journal of Contaminant Hydrology*, Vol. 31, pp. 359-372, 1998.
- [21]. Tompson, A.F.B., Ababou, R., and Gelhar, L.W., Application and Use of the Three-Dimensional Turning Bands Random Field Generator: Single Realization Problems, March 1987.
- [22]. Tompson, A.F.B., Ababou, R., Gelhar, L.W., Implementation of the 3-D Turning Bands Random Field Generator, *Water Resources Research*, Vol. 25, No. 10, pp. 2227-2243, 1989.
- [23]. Ünlü, K., Assessing Risk of Groundwater Pollution from Land-Disposed Wastes, *Journal of Environmental Engineering*, Vol. 120, No. 6, November/December 1994.
- [24]. Ünlü, K., Nielsen, D.R., Biggar, J.W., and Morkoc, F., Statistical Parameters Characterizing the Spatial Variability of Selected Soil Hydraulic Properties, *Soil Science Society of America Journal*, Vol. 54, No.6, 1990.

- [25]. Visual MODFLOW v.3.0 User's Manual, Waterloo Hydrogeologic Inc., 2002.
- [26]. Walt, W., McNab, Jr., and Doohar, B.P., A Critique of a Steady-State Analytical Method for Estimating Contaminant Degradation Rates, Ground Water, Vol. 36, No. 6, pp. 983-987, 1998.
- [27]. Weaver, J.W., Wilson, J.T., and Kampbell, D.H., Case Study of Natural Attenuation of Trichloroethene at St. Joseph, Michigan., Symposium on Natural Attenuation of Chlorinated Organics in Groundwater, Dallas, 1996
- [28]. Wiedemeier, T.H., Wilson, J.T., Kampbell, D.H., Miller, R.N., and Hansen, J.E., Technical Protocol for Implementing Intrinsic Remediation with Long-Term Monitoring for Natural Attenuation of Fuel Contamination Dissolved in Groundwater (Revision 0), Air Force Center for Environmental Excellence, Brooks AFB, TX, 1995.

## APPENDIX A. INPUT DATA OF RANDOM FIELD GENERATOR

Table A.1. Physical input data of the random field generator for CV = 50 %.

	<b>CV = 50%</b> <b>h= 5 m</b>	<b>CV = 50%</b> <b>h= 10 m</b>	<b>CV = 50%</b> <b>h= 20 m</b>
Line 1: IDATE, IRUN	-	-	-
Line 2: NX, NY, NZ *	301,201,1	301,201,1	301,201,1
Line 3: DX, DY, DZ	0.5, 0.5, 0	0.5, 0.5, 0	0.5, 0.5, 0
Line 4: XL1, XL2, XL3	5, 5, 0	10, 10, 0	20, 20, 0
Line 5: CONDG, SIG	$6.47 \times 10^{-5}$ , 0.47238	$6.47 \times 10^{-5}$ , 0.47238	$6.47 \times 10^{-5}$ , 0.47238

Table A.2. Physical input data of the random field generator for CV = 100 %.

	<b>CV =100%</b> <b>h= 5 m</b>	<b>CV = 100%</b> <b>h= 10 m</b>	<b>CV = 100%</b> <b>h= 20 m</b>
Line 1: IDATE, IRUN	-	-	-
Line 2: NX, NY, NZ *	301,201,1	301,201,1	301,201,1
Line 3: DX, DY, DZ	0.5, 0.5, 0	0.5, 0.5, 0	0.5, 0.5, 0
Line 4: XL1, XL2, XL3	5, 5, 0	10, 10, 0	20, 20, 0
Line 5: CONDG, SIG	$5.115 \times 10^{-5}$ , 0.83255	$5.115 \times 10^{-5}$ , 0.83255	$5.115 \times 10^{-5}$ , 0.83255

Table A.3. Physical input data of the random field generator for CV = 150 %.

	<b>CV = 150%</b> <b>h= 5 m</b>	<b>CV = 150%</b> <b>h= 10 m</b>	<b>CV = 150%</b> <b>h= 20 m</b>
Line 1: IDATE, IRUN	-	-	-
Line 2: NX, NY, NZ *	301,201,1	301,201,1	301,201,1
Line 3: DX, DY, DZ	0.5, 0.5, 0	0.5, 0.5, 0	0.5, 0.5, 0
Line 4: XL1, XL2, XL3	5, 5, 0	10, 10, 0	20, 20, 0
Line 5: CONDG, SIG	$4.013 \times 10^{-5}$ , 1.0857	$4.013 \times 10^{-5}$ , 1.0857	$4.013 \times 10^{-5}$ , 1.0857

The parametric input data is related to the simulation itself, but not the characteristics of generated field. Thus, the parametric data for the random field generation are same in all of the fields. Table A.4 shows the parametric input data of isotropic random field generator.

Table A.4. Parametric input data of the random field generator for isotropic fields.

	<b>CV = 50%</b> <b>h= 5m, 10m, 20m</b>	<b>CV = 100%</b> <b>h= 5m, 10m, 20 m</b>	<b>CV = 150%</b> <b>h= 5m, 10 m, 20m</b>
Line 1:NLINE,DELZET,NZTEST	100, 0.1, 2000	100, 0.1, 2000	100, 0.1, 2000
Line 2: BIGK, DK	100, 0.25	100, 0.25	100, 0.25
Line 3: NMONT, IU, NL	10, 210467, 11	10, 210467, 11	10, 210467, 11
Line 4: CMIN, CMAX, NDELTA	-3, 3, 20	-3, 3, 20	-3, 3, 20
Line 5: KS(J), J=1, 3	1, 1, 0	1, 1, 0	1, 1, 0
Line 6: ILOG	1	1	1
Line 7: NFILE, TFILE	NSCALEF.OUT TSCALEF.OUT	NSCALEF.OUT TSCALEF.OUT	NSCALEF.OUT TSCALEF.OUT

The physical and parametric input data for two different anisotropic fields are given in Table A.5. and Table A.6, respectively.

Table A.5. Physical input data of random field generator for two anisotropic hydraulic conductivity fields.

	<b>CV =50%</b> <b><math>h_x = 20 \text{ m}, h_y = 4 \text{ m}</math></b>	<b>CV = 150%</b> <b><math>h_x = 10 \text{ m}, h_y = 2 \text{ m}</math></b>
Line 1: IDATE, IRUN	-	-
Line 2: NX, NY, NZ *	301,201,1	301,201,1
Line 3: DX, DY, DZ	0.5, 0.5, 0	0.5, 0.5, 0
Line 4: XL1, XL2, XL3	20, 4, 0	10, 2, 0
Line 5: CONDG, SIG	$6.47 \times 10^{-5}$ , 0.47238	$4.013 \times 10^{-5}$ , 1.0857

Table A.6. Parametric input data of the random field generator for anisotropic fields.

	<b>CV =50%</b> <b><math>h_x = 20 \text{ m}, h_y = 4 \text{ m}</math></b>	<b>CV = 150%</b> <b><math>h_x = 10 \text{ m}, h_y = 2 \text{ m}</math></b>
Line 1:NLINE,DELZET,NZTEST	100, 0.1, 2000	100, 0.1, 2000
Line 2: BIGK, DK	100, 0.25	100, 0.25
Line 3: NMONT, IU, NL	10, 210467, 11	10, 210467, 11
Line 4: CMIN, CMAX, NDELTA	-3, 3, 20	-3, 3, 20
Line 5: KS(J), J=1, 3	1, 1, 0	1, 1, 0
Line 6: ILOG	1	1
Line 7: NFILE, TFILE	NSCALEF.OUT TSCALEF.OUT	NSCALEF.OUT TSCALEF.OUT

## APPENDIX B. STATISTICAL PARAMETER GRAPHS OF RANDOM FIELD GENERATOR

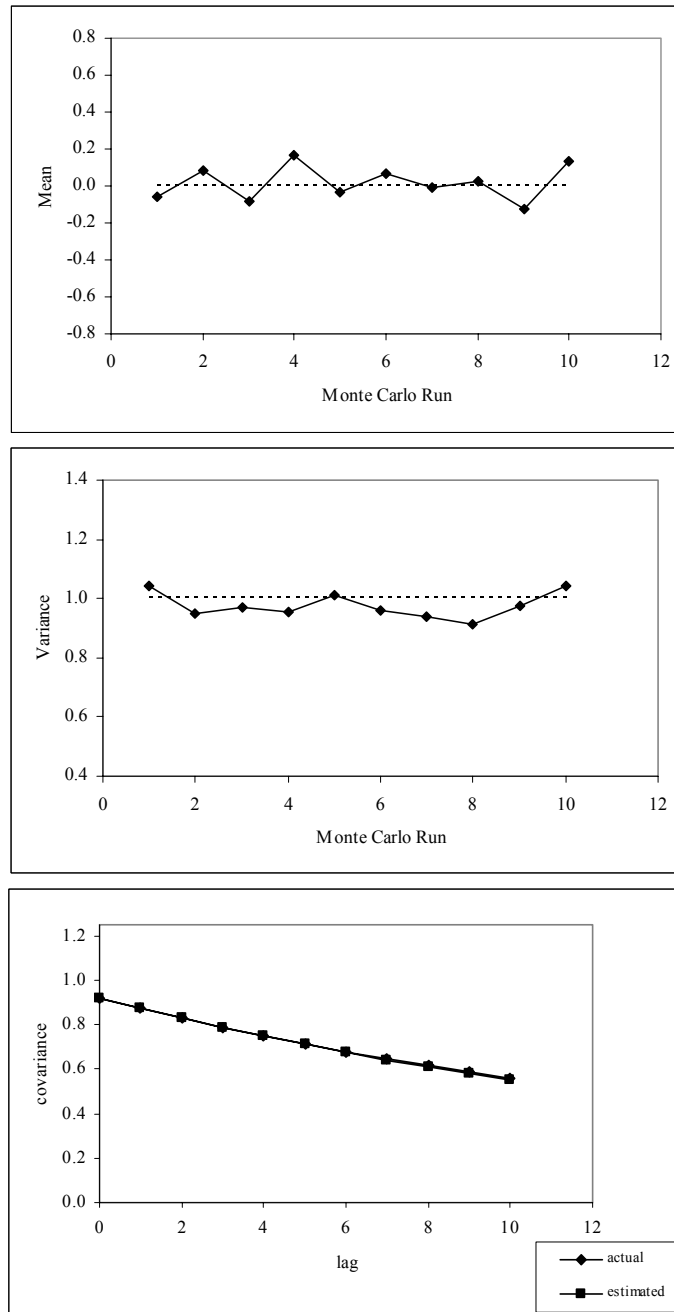


Figure B.1. Mean, Variance and Covariance estimate for isotropic hydraulic conductivity field having CV = 50 % and h = 10 m.

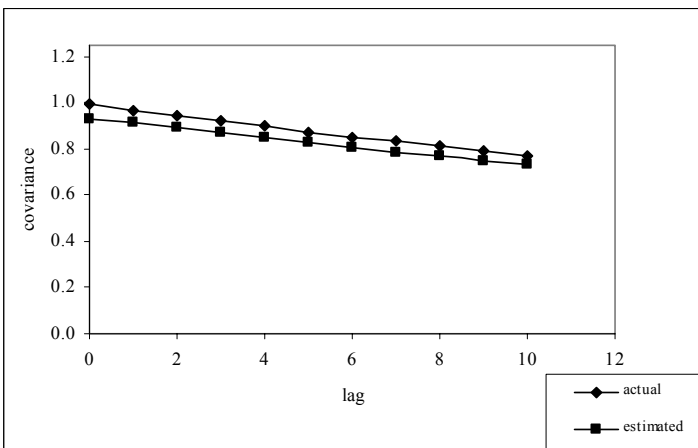
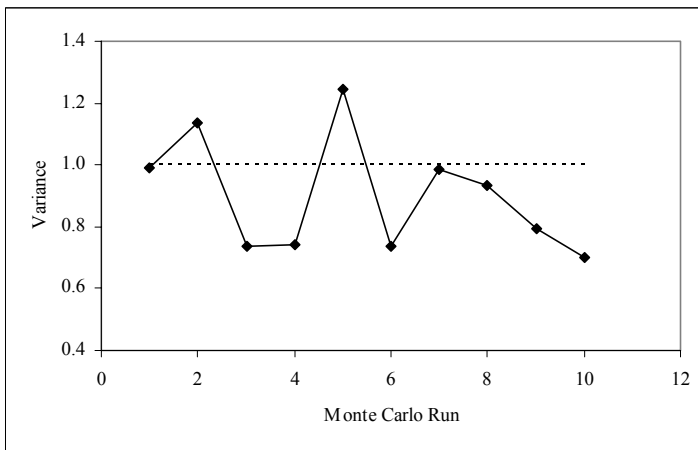
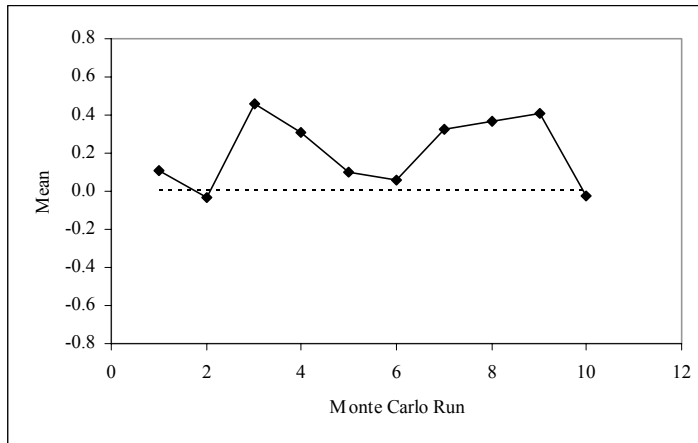


Figure B.2. Mean, Variance and Covariance estimate for isotropic hydraulic conductivity field having CV = 50 % and h = 20 m.

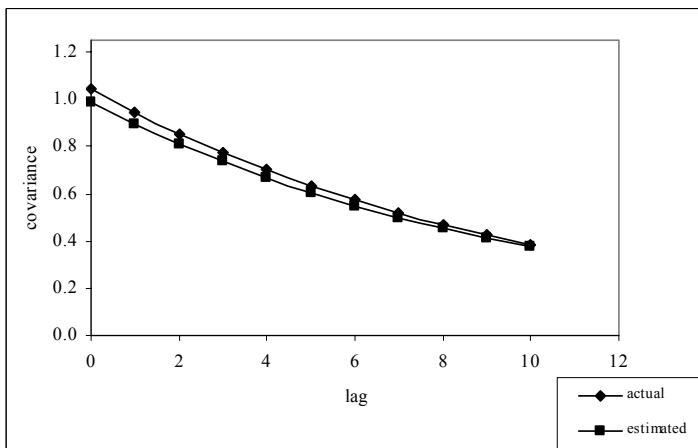
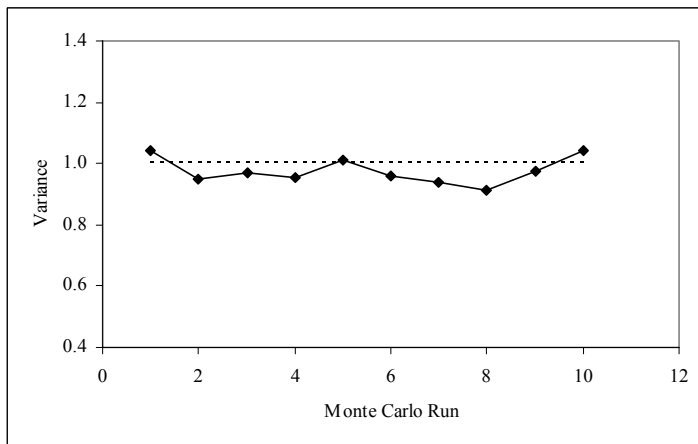
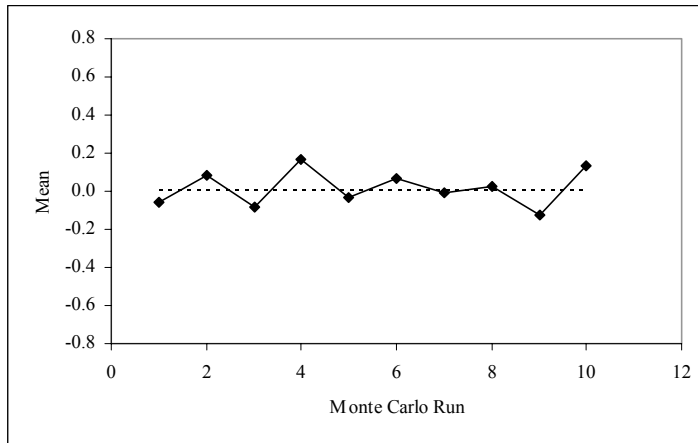


Figure B.3. Mean, Variance and Covariance estimate for isotropic hydraulic conductivity field having CV = 100 % and h = 5 m.

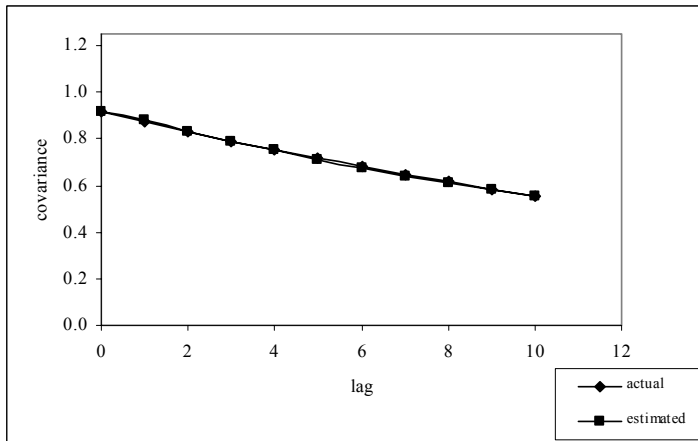
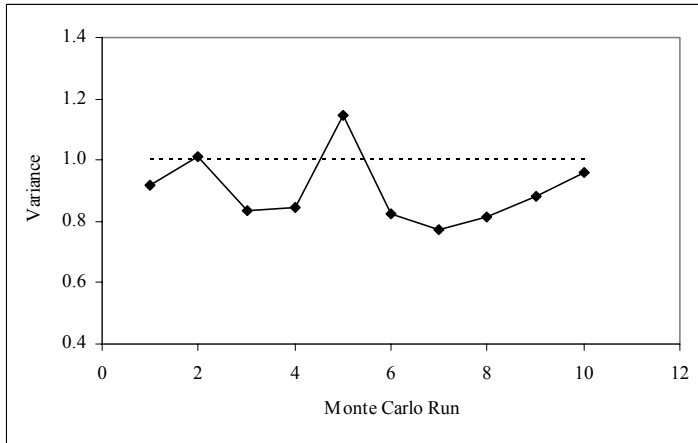
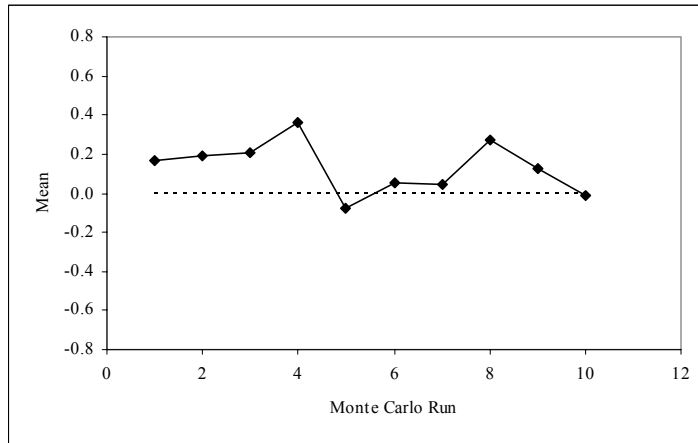
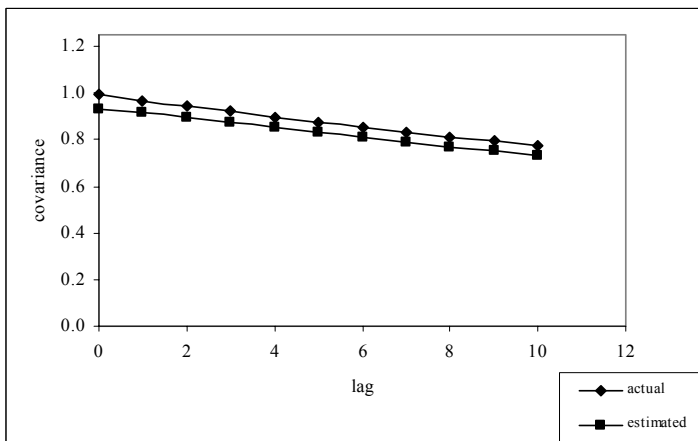
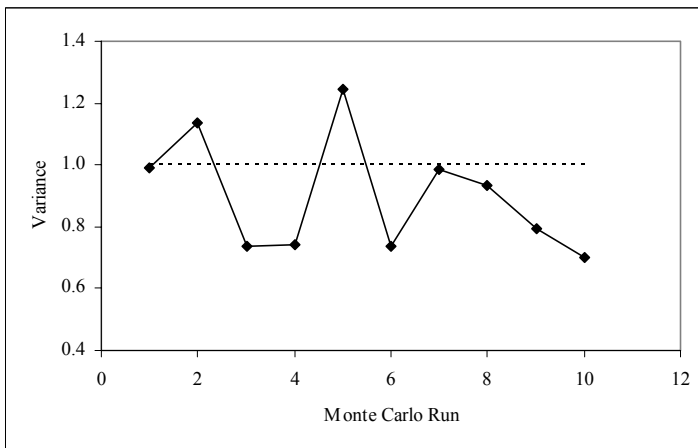
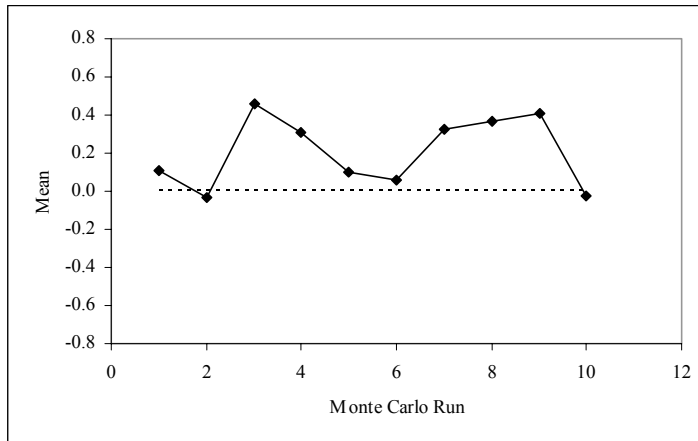


Figure B.4. Mean, Variance and Covariance estimate for isotropic hydraulic conductivity field having  $CV = 100\%$  and  $h = 10\text{ m}$



FigureB.5. Mean, Variance and Covariance estimate for isotropic hydraulic conductivity field having CV = 100 % and h = 20 m.

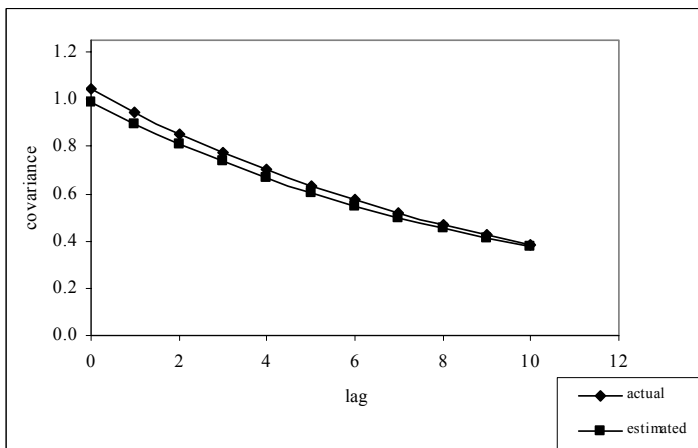
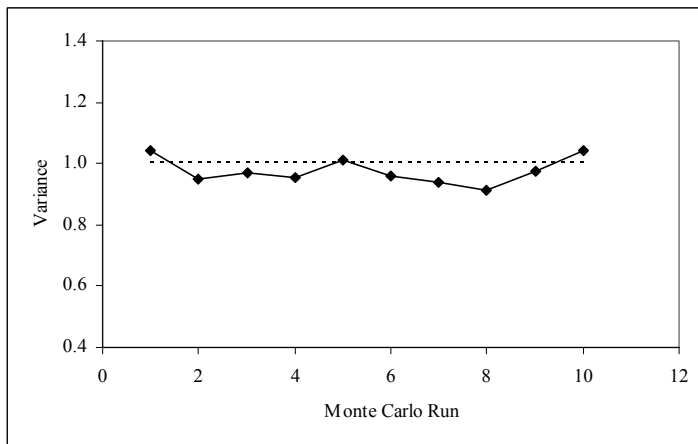
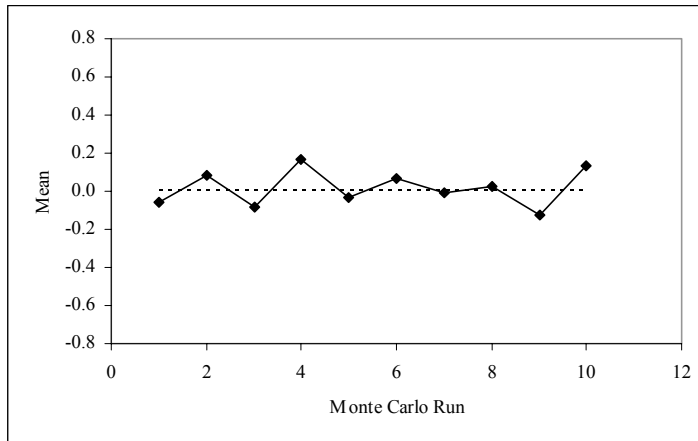


Figure B.6. Mean, Variance and Covariance estimate for isotropic hydraulic conductivity field having CV = 150 % and h = 5 m.

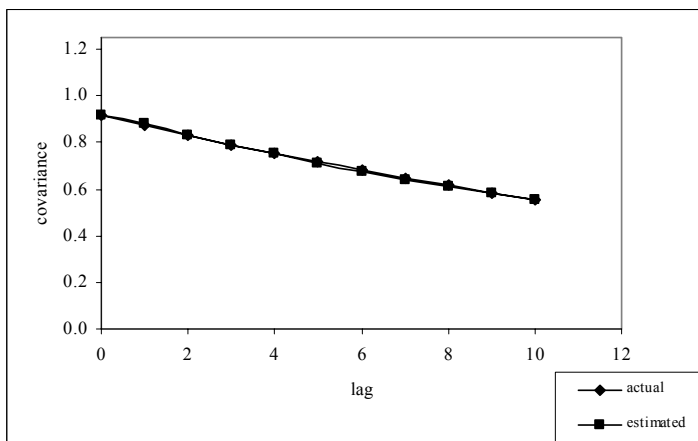
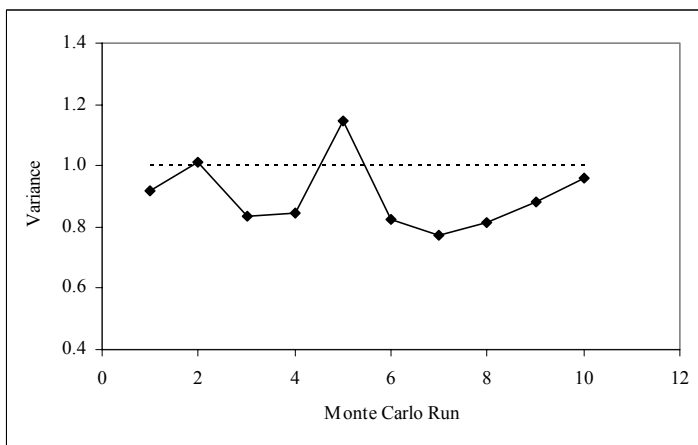
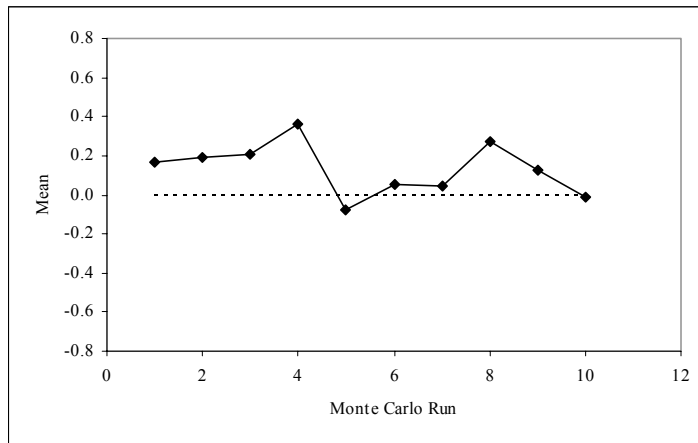


Figure B.7. Mean, Variance and Covariance estimate for isotropic hydraulic conductivity field having CV = 150 % and h = 10 m.

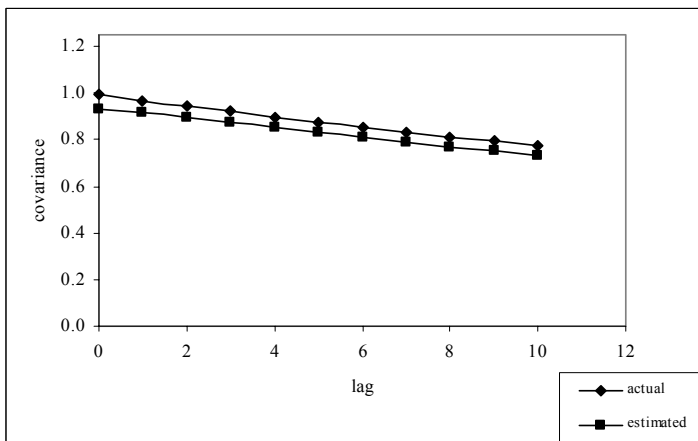
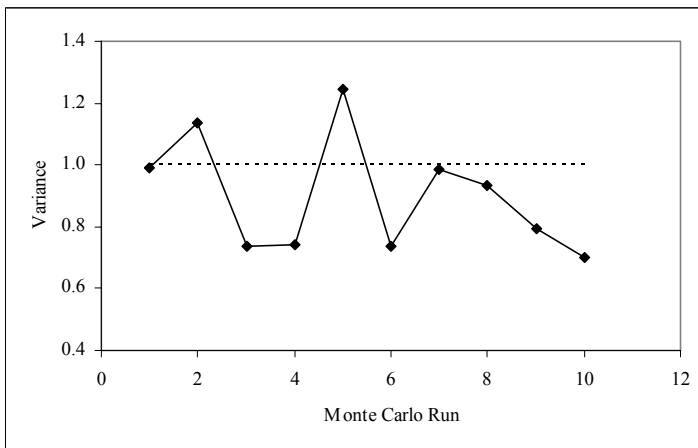
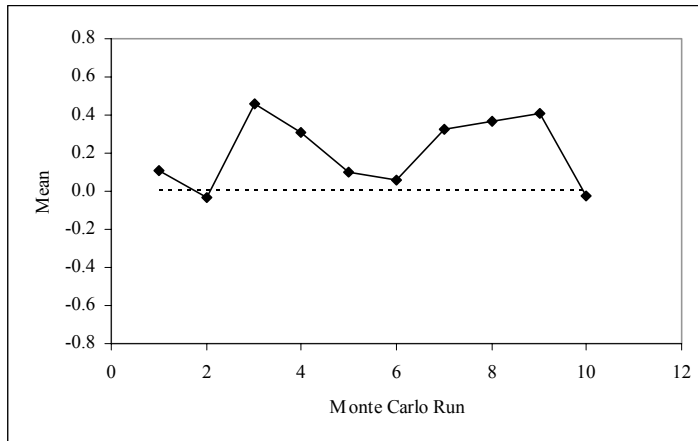


Figure B.8. Mean, Variance and Covariance estimate for isotropic hydraulic conductivity field having CV = 150 % and h = 20 m.

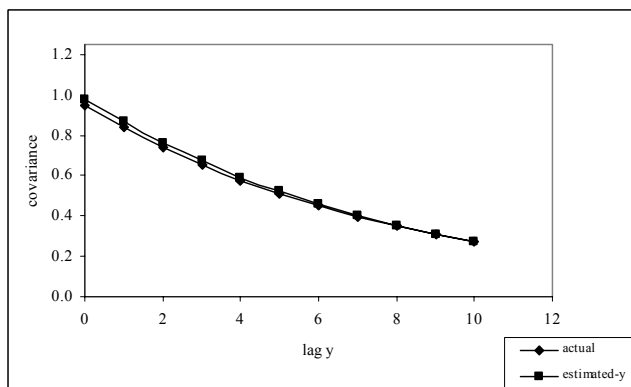
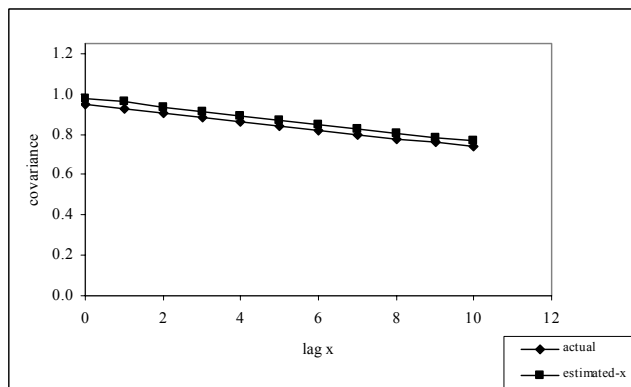
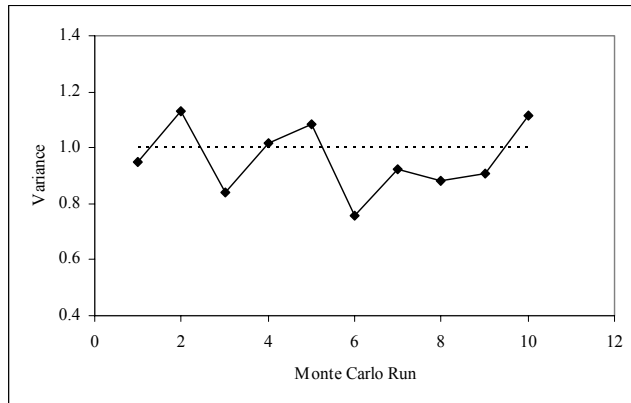
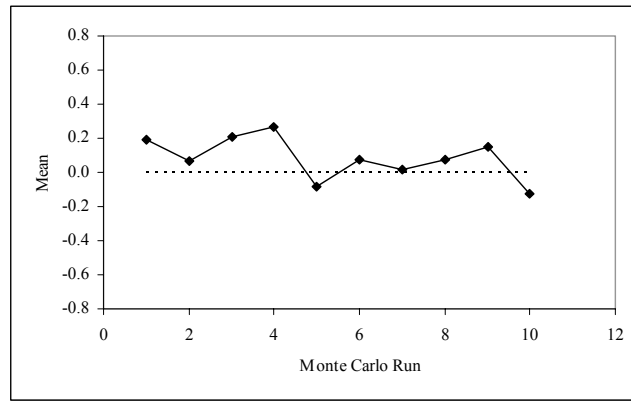


Figure B.9. Mean, Variance and Covariance estimates for anisotropic field having  $CV = 50\%$ ,  $h_x = 20$  m and  $h_y = 4$  m.

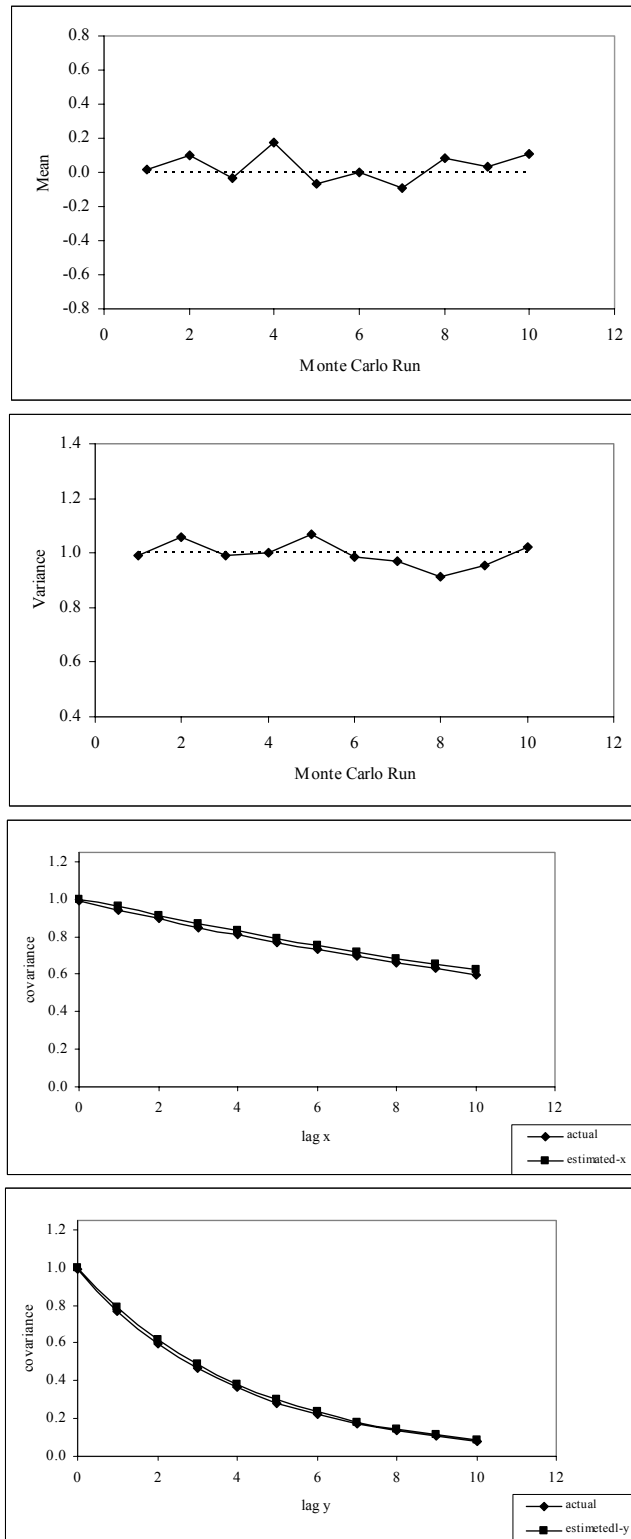


Figure B.10. Mean, Variance and Covariance estimates for anisotropic field having  $CV = 150\%$ ,  $h_x = 10$  m and  $h_y = 2$  m.

# APPENDIX C. HEAD DISTRIBUTIONS OF SIMULATED FIELDS

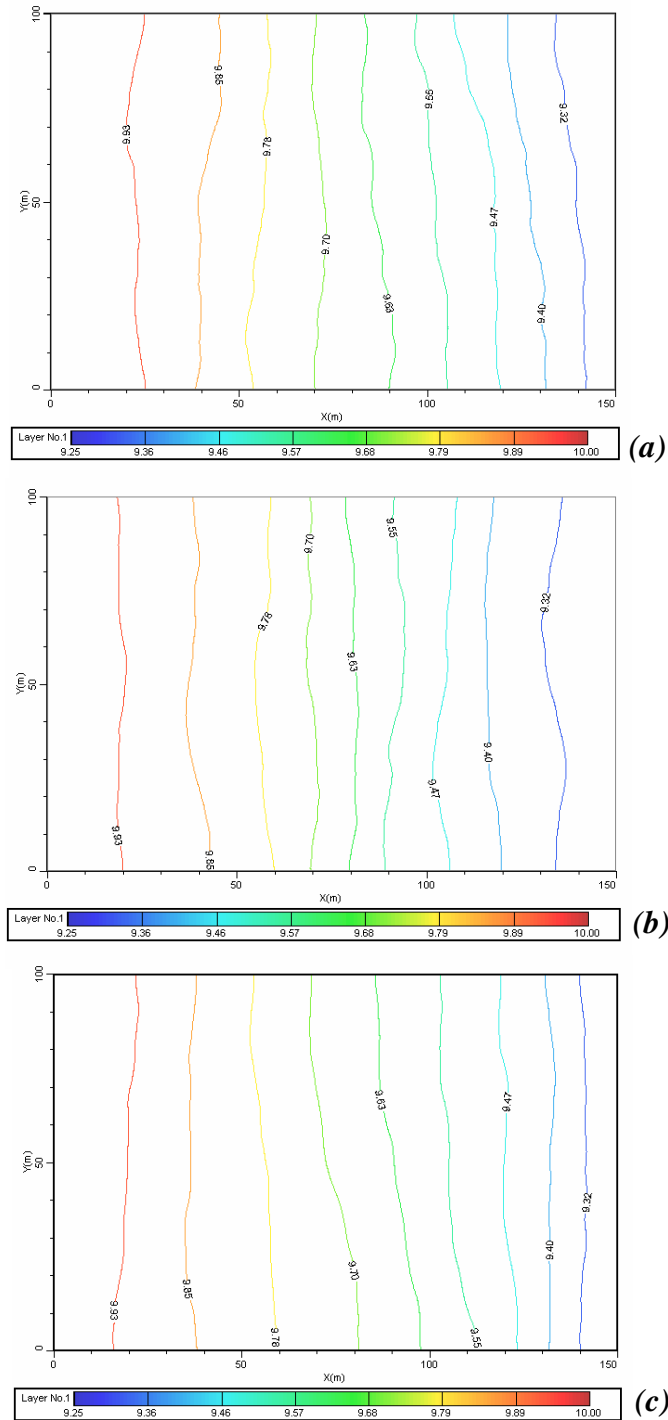


Figure C.1. Head distribution (a)  $h = 5\text{m}$ , (b)  $10\text{m}$ , (c)  $20\text{m}$ , when  $CV = 50\%$ .

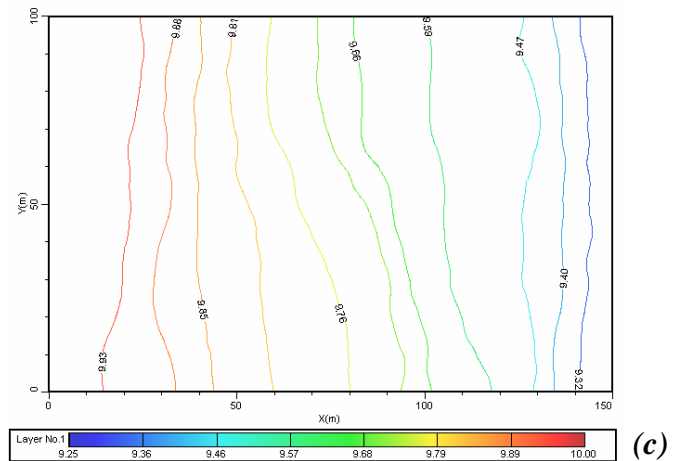
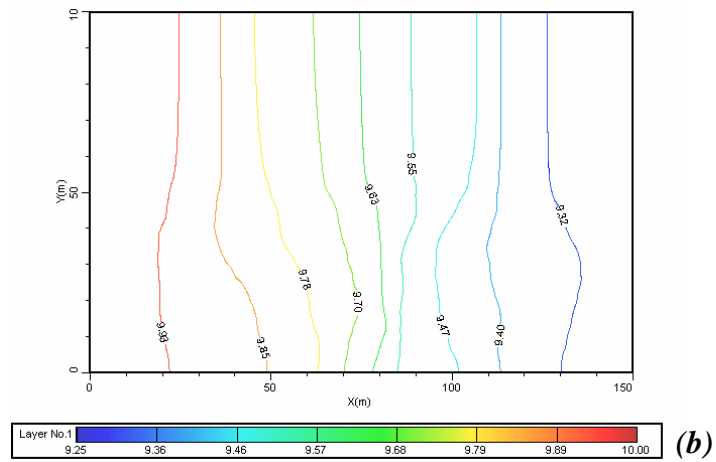
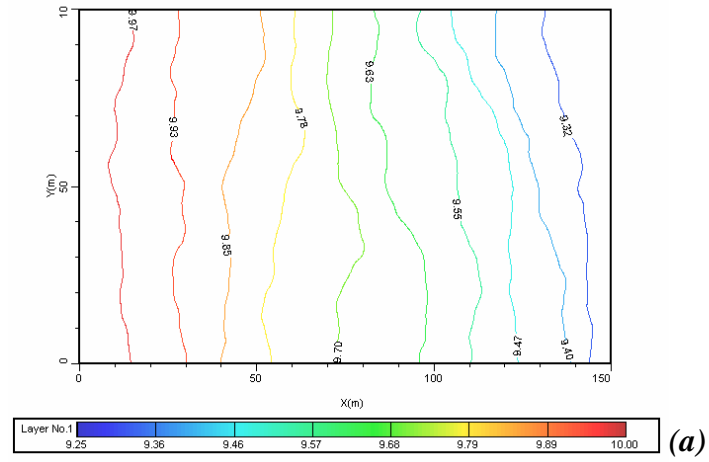


Figure C.2. Head distribution (a)  $h = 5\text{m}$ , (b)  $10\text{m}$ , (c)  $20\text{m}$ , when  $CV = 100\%$ .

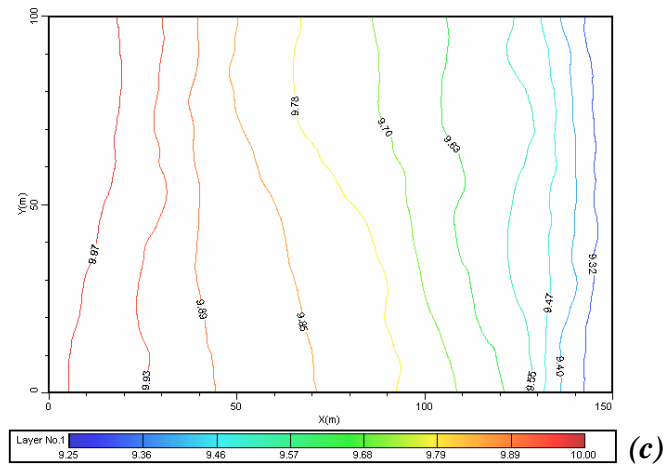
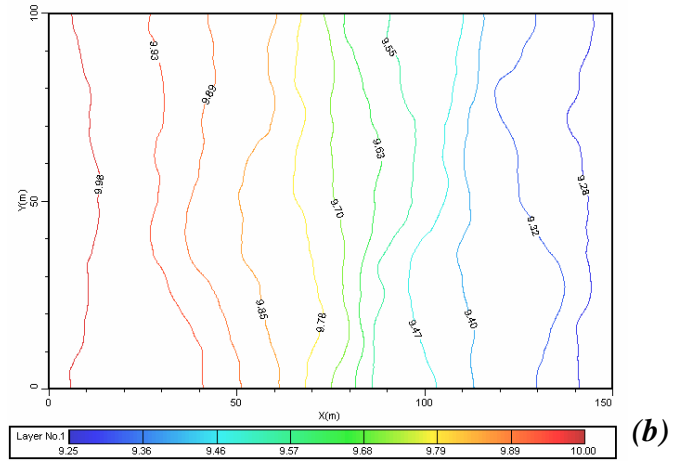
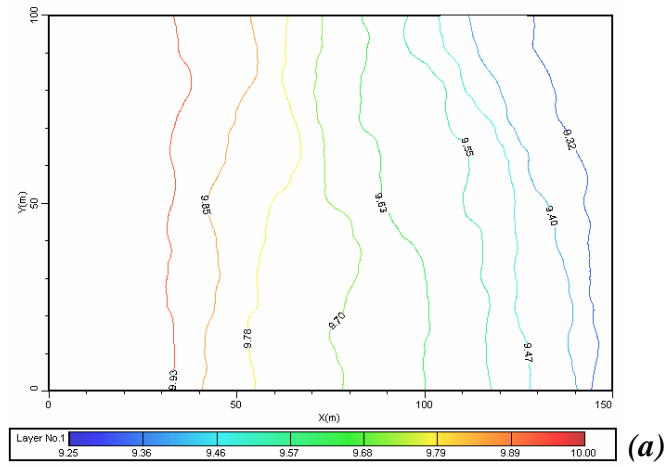


Figure C.3. Head distribution (a)  $h = 5\text{m}$ , (b)  $10\text{m}$ , (c)  $20\text{m}$ , when  $CV = 150\%$ .

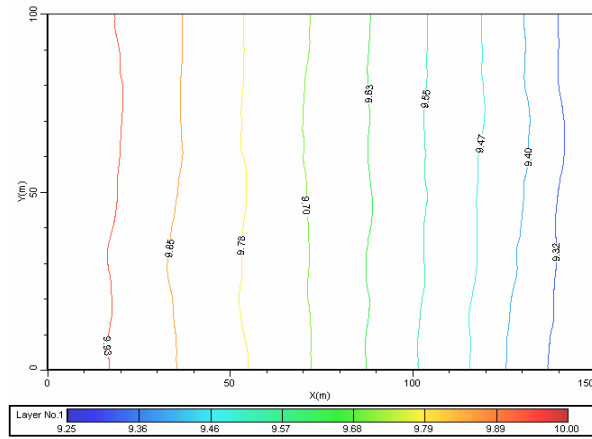


Figure C.4. Head distribution of Anisotropic Field CV = 50 %,  $h_x = 20$  m and  $h_x = 4$  m.

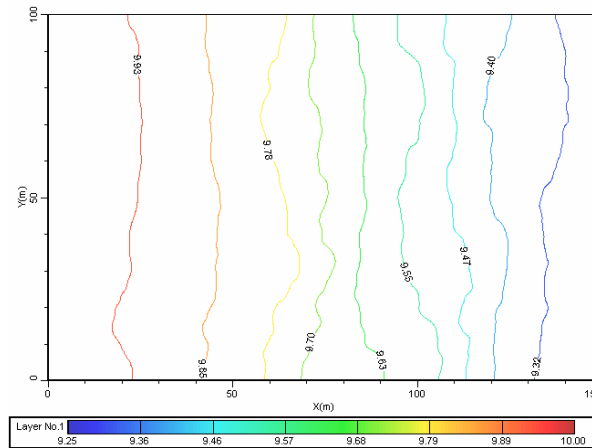


Figure C.5. Head distribution of Anisotropic Field CV = 150 %,  $h_x = 10$  m and  $h_x = 2$  m.

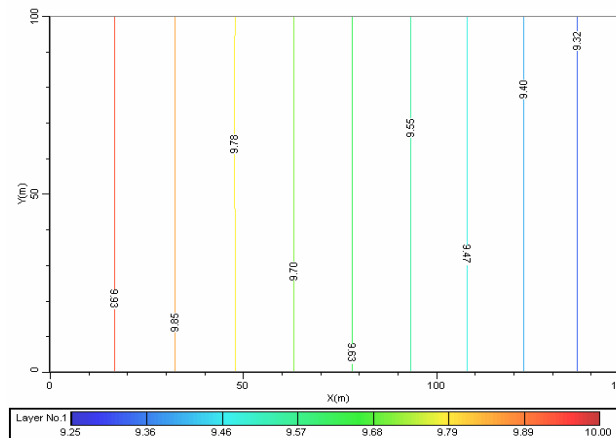


Figure C.6. Head distribution of Uniform Field.

## APPENDIX D. BTEX PLUMES AT THE END OF THE SIMULATION PERIOD

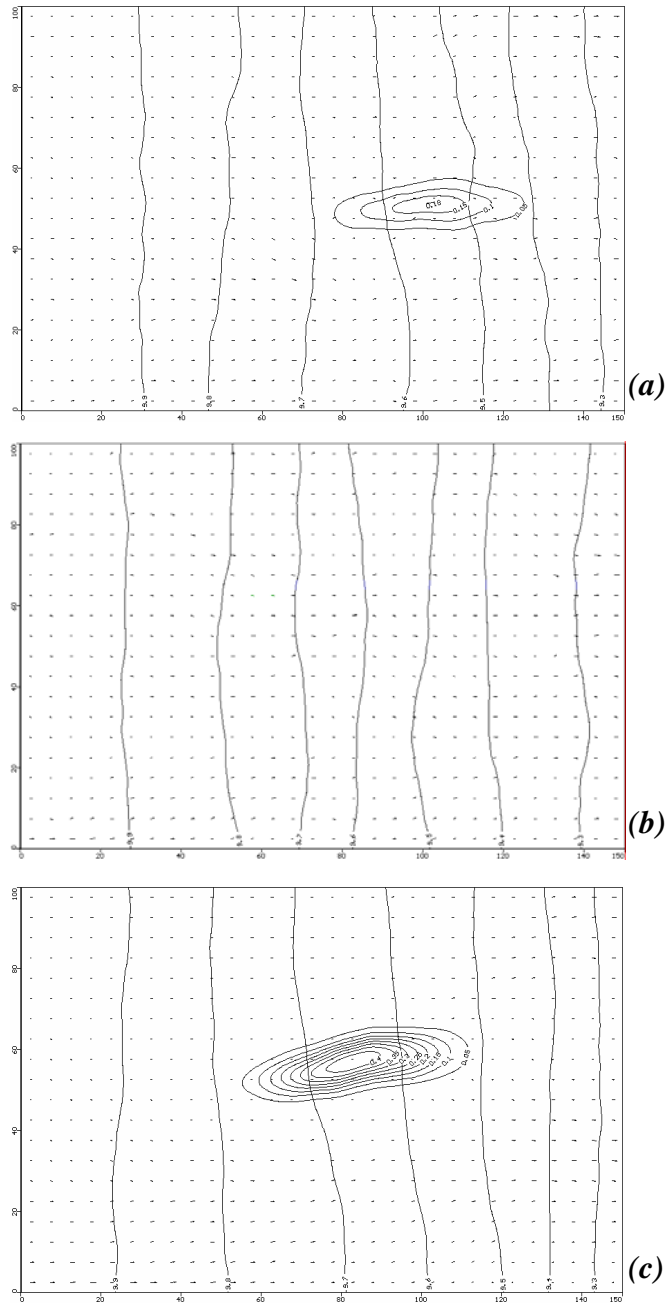


Figure D.1. BTEX plumes at 1000 days for isotropic fields having  
(a)  $h = 5$  m, (b)  $h = 10$  m, (c)  $h = 20$  m, when  $CV = 50\%$ .

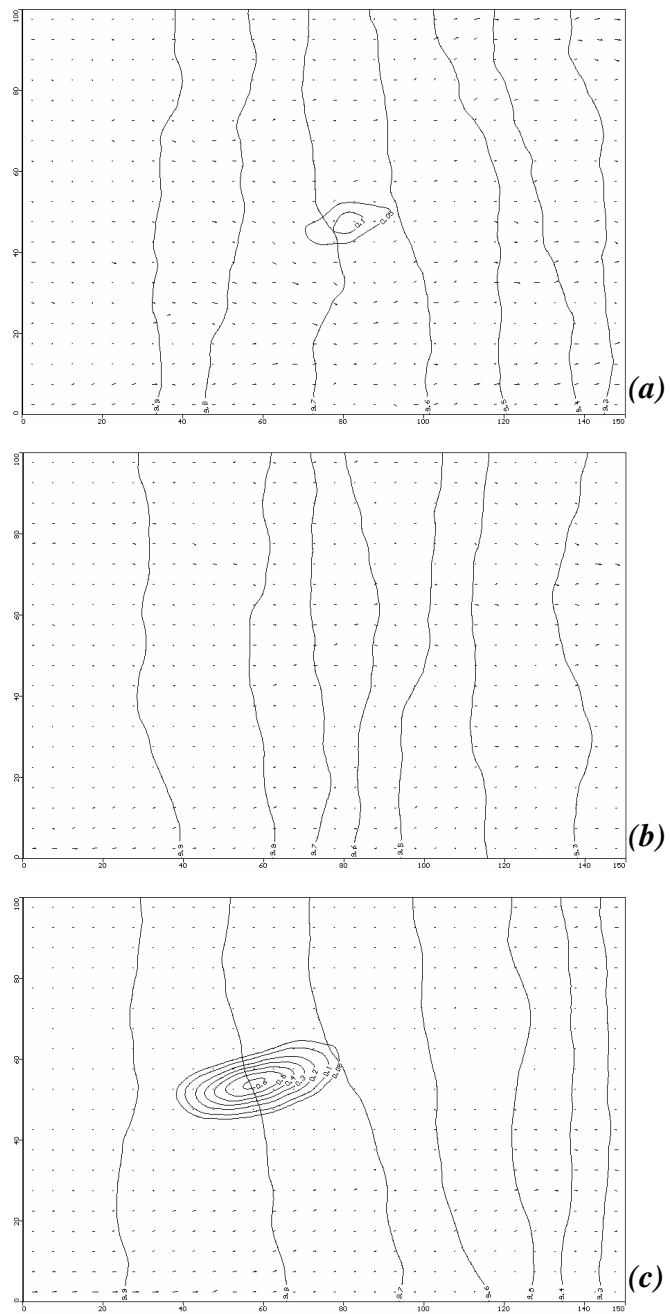


Figure D.2. BTEX plumes at 1000 days for isotropic fields having  
 (a)  $h = 5$  m, (b)  $h = 10$  m, (c)  $h = 20$  m, when  $CV = 100\%$ .

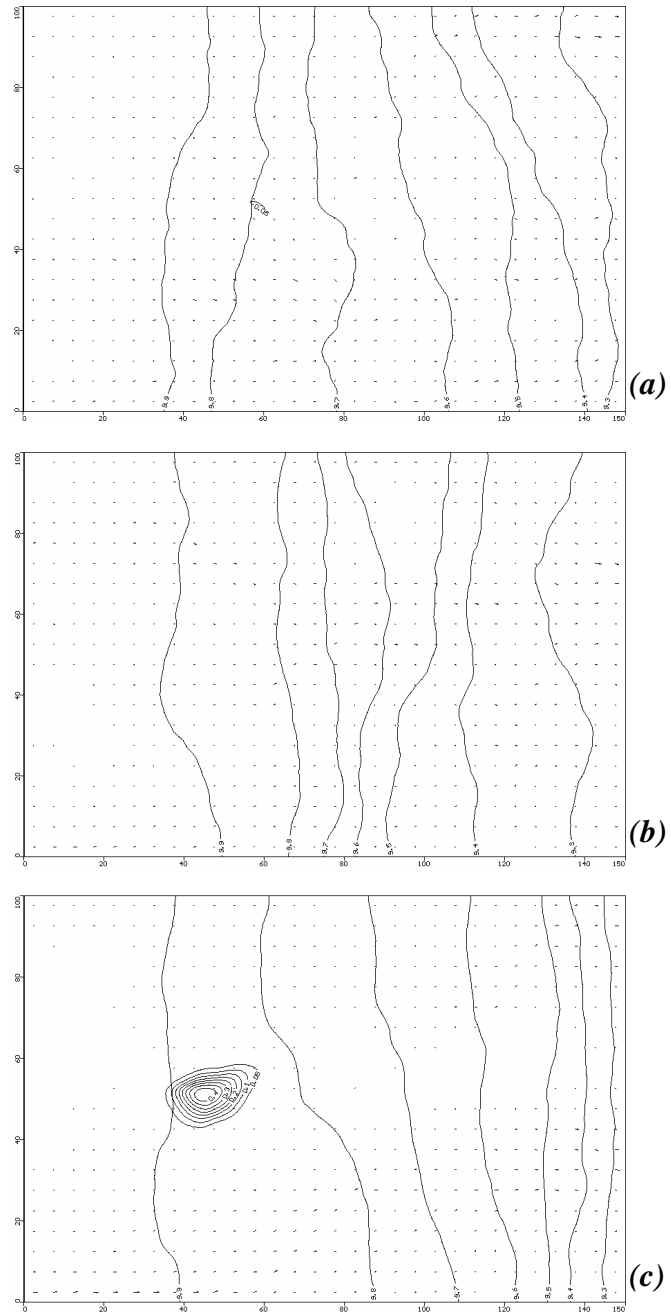


Figure D.3. BTEX plumes at 1000 days for isotropic fields having  
 (a)  $h = 5$  m, (b)  $h = 10$  m, (c)  $h = 20$  m, when  $CV = 150\%$ .

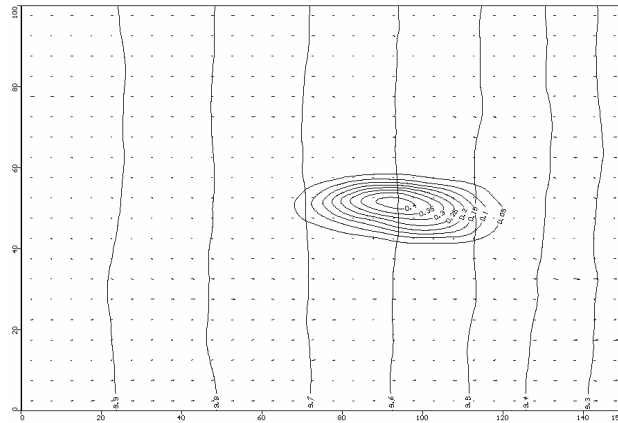


Figure D.4. BTEX plumes at 1000 days for anisotropic fields having  
h of 20 m and CV of 50 %.

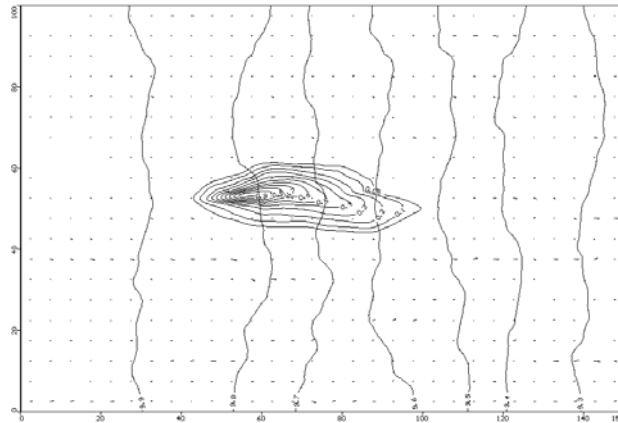


Figure D.5. BTEX plumes at 1000 days for anisotropic fields having  
h of 10 m and CV of 150 %.

## APPENDIX E. OBSERVATION WELL TRANSECTS

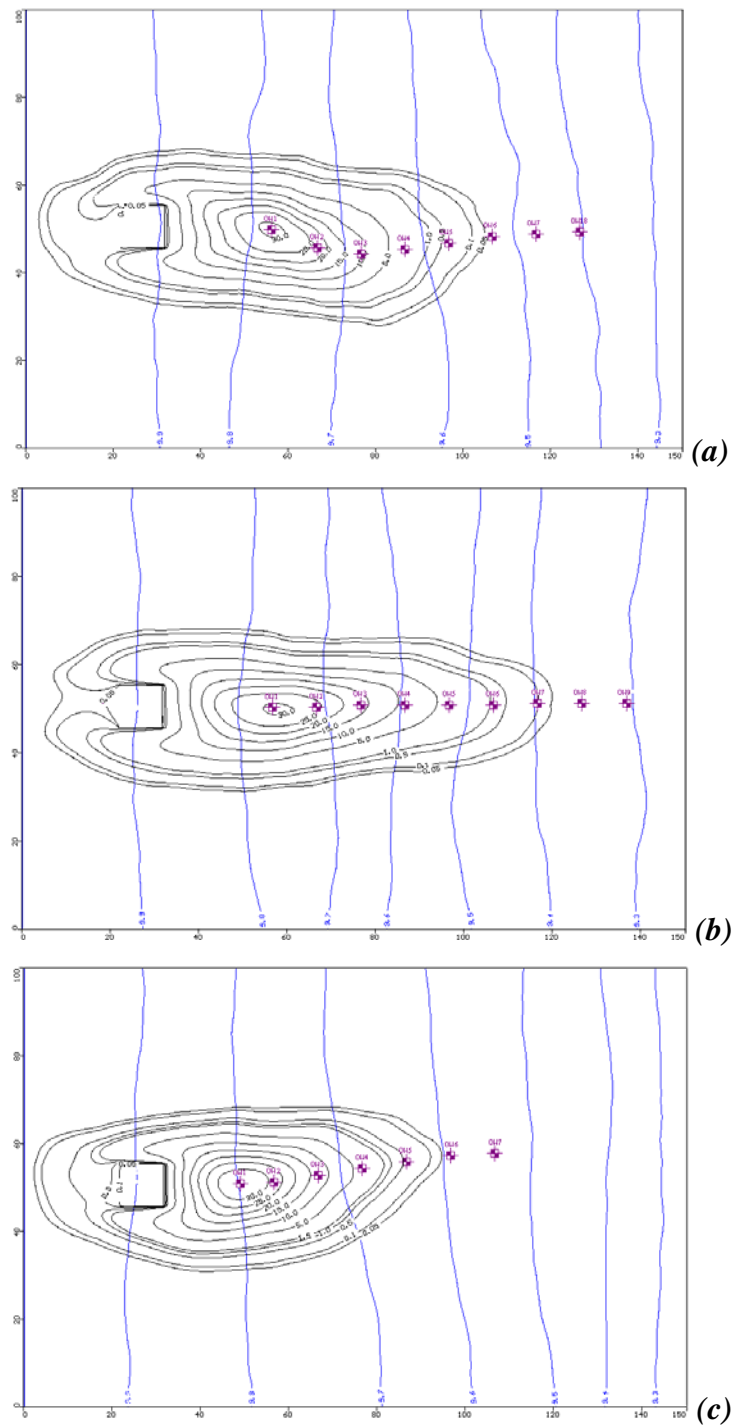


Figure E.1. Observation Well Locations, (a) 5 m, (b)  $h = 10\text{m}$ , (c)  $h = 20\text{m}$ , when  $CV = 50\%$ .

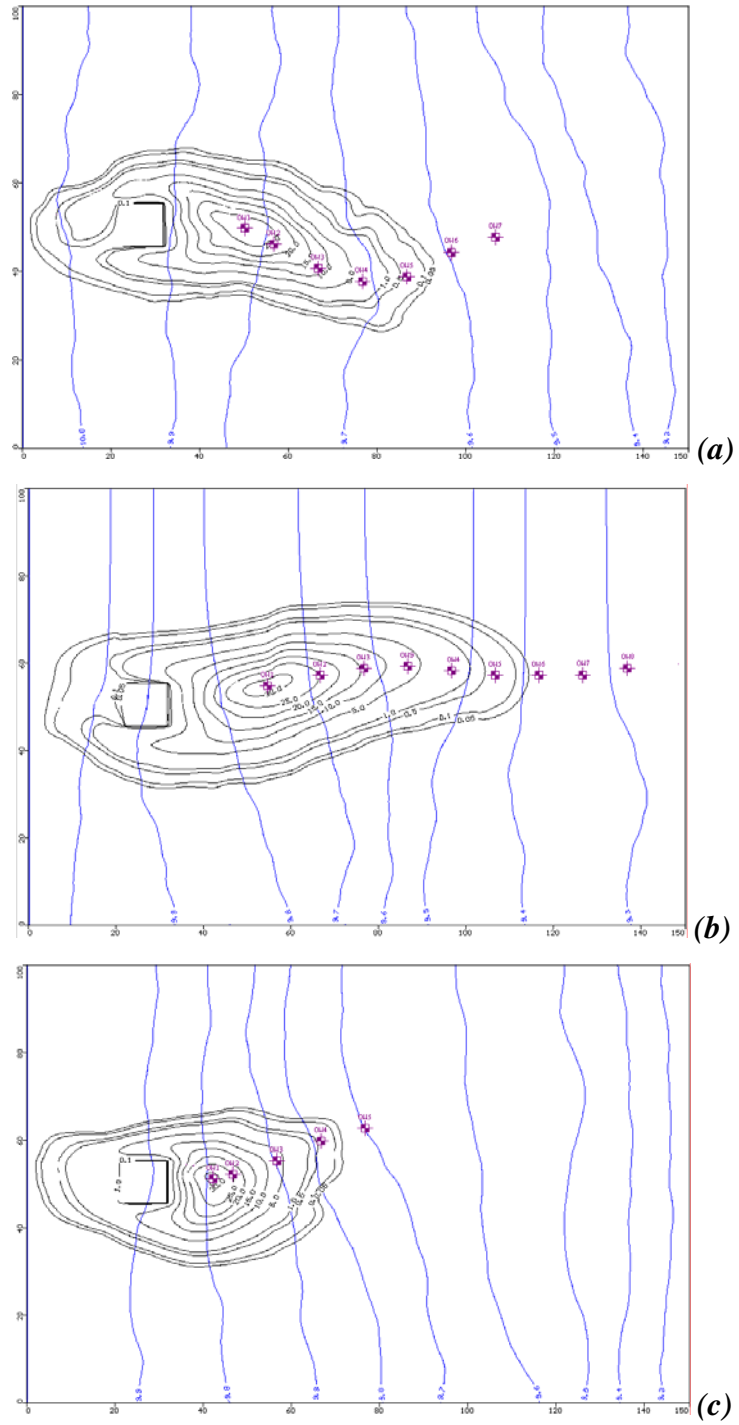


Figure E.2. Observation Well Locations, (a) 5 m, (b)  $h = 10$  m, (c)  $h = 20$  m, when  $CV = 100\%$ .

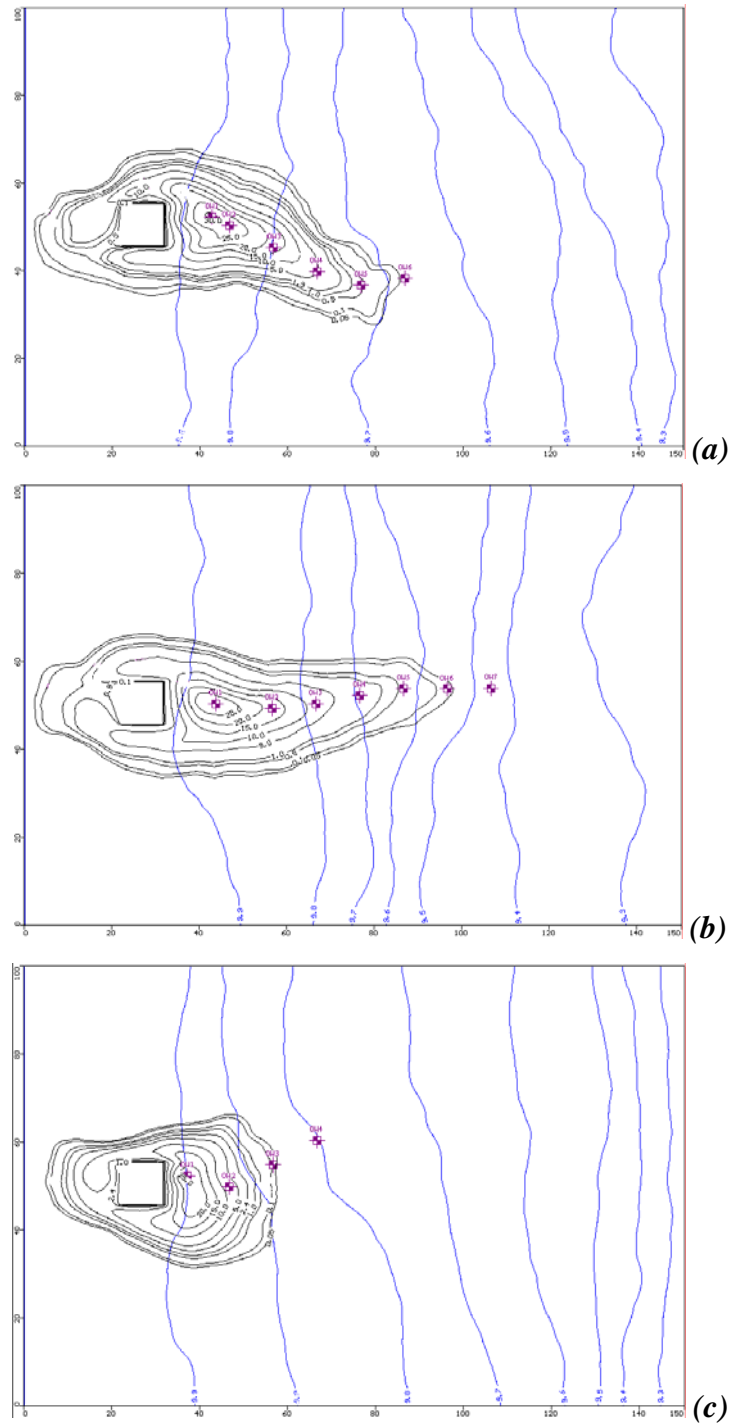


Figure E.3. Observation Well Locations, (a) 5 m, (b)  $h = 10$ m, (c)  $h = 20$ m, when  $CV = 150\%$ .

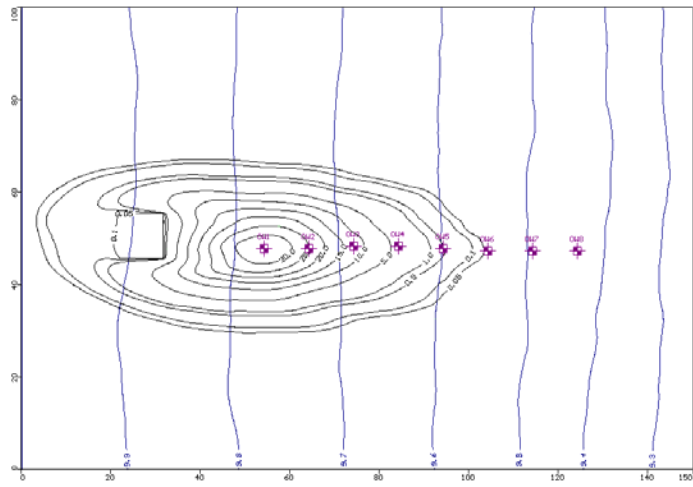


Figure E.4. Observation Well Locations, when  $CV = 50\%$ ,  
 $h_x = 20\text{m}$ , and  $h_y = 4\text{ m}$ .

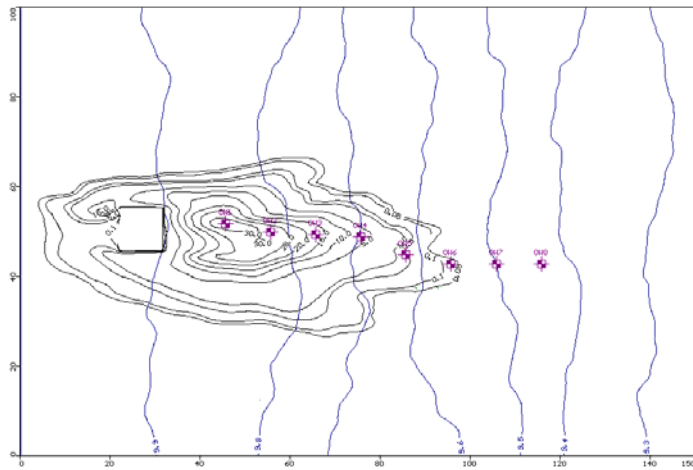


Figure E.4. Observation Well Locations, when  $CV = 150\%$ ,  
 $h_x = 10\text{m}$ , and  $h_y = 2\text{ m}$

# APPENDIX F. LINEAR REGRESSION ANALYSIS GRAPHS FOR BUSCHECK AND ALCANTAR METHOD

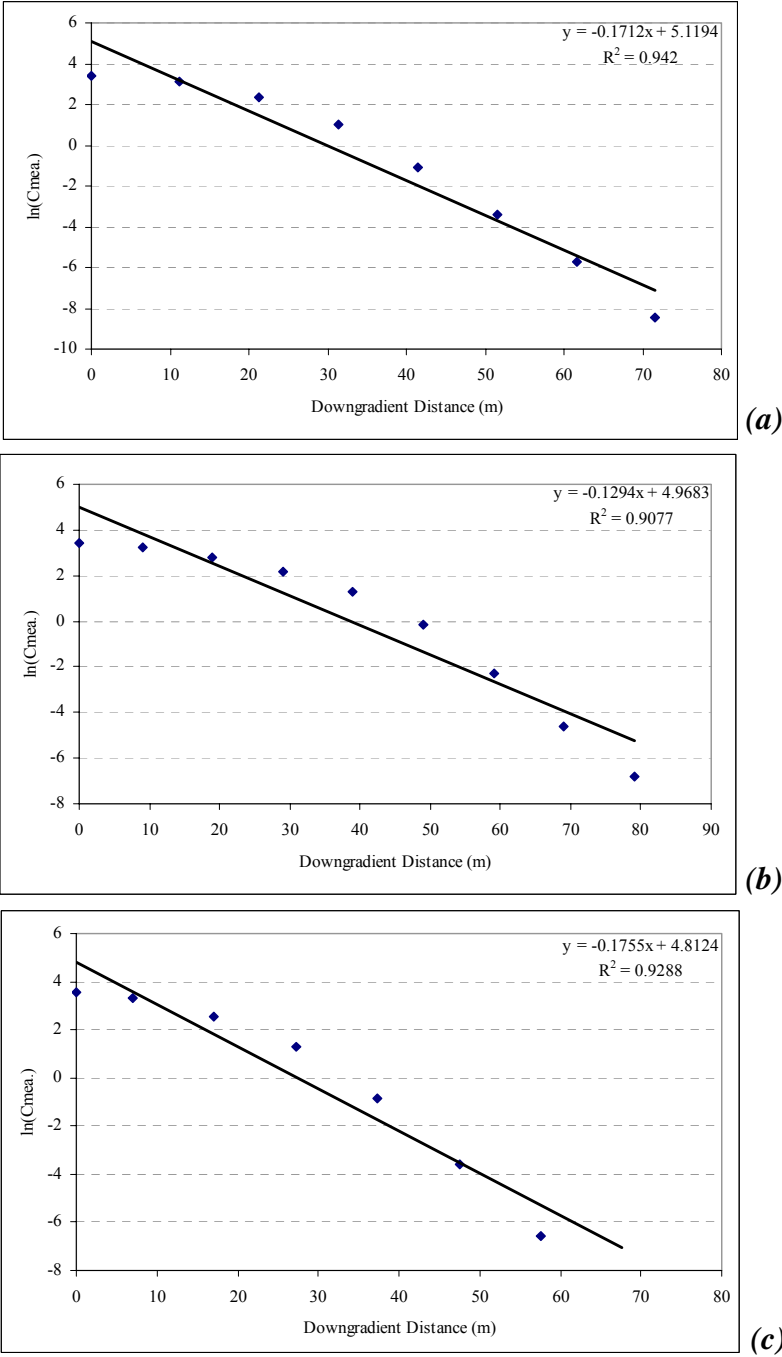


Figure E.1.  $\ln(C_{mea})$  versus downgradient distance graph, (a)  $h = 5$ , (b)  $h = 10$ , (c)  $h = 20$ , for  $CV = 50\%$ .

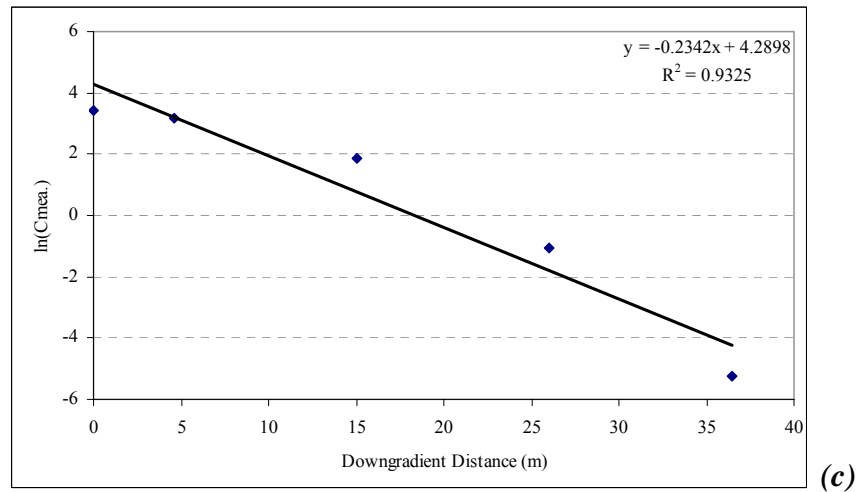
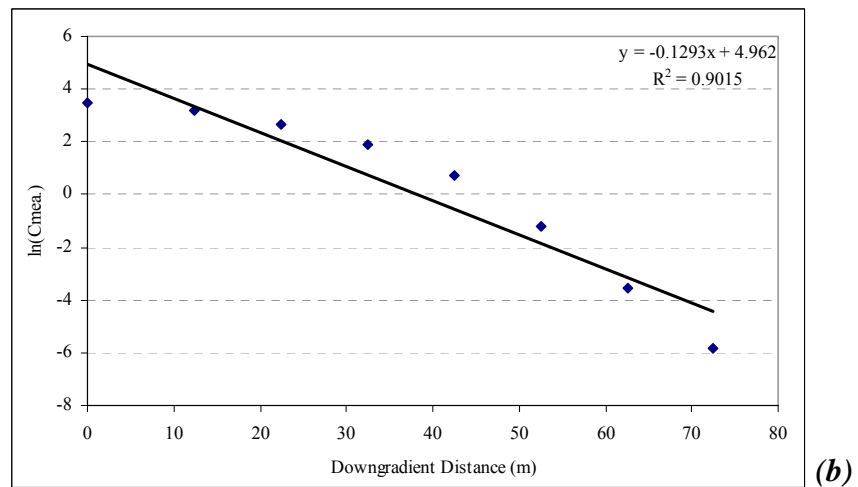
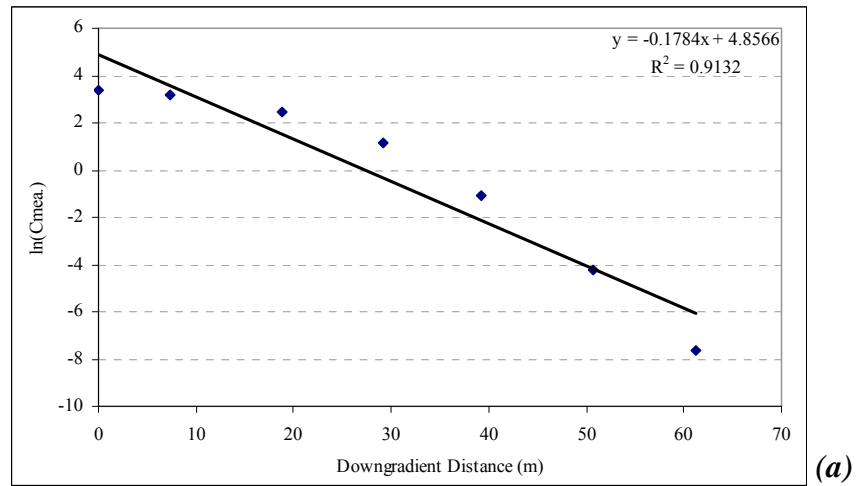


Figure E.2.  $\ln(C_{mea})$  versus downgradient distance graph, (a)  $h = 5$ , (b)  $h = 10$ , (c)  $h = 20$ , for  $CV = 100\%$ .

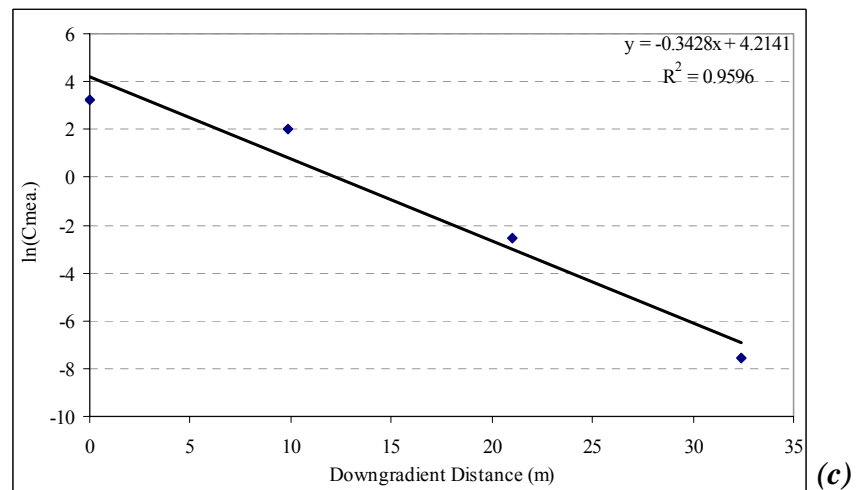
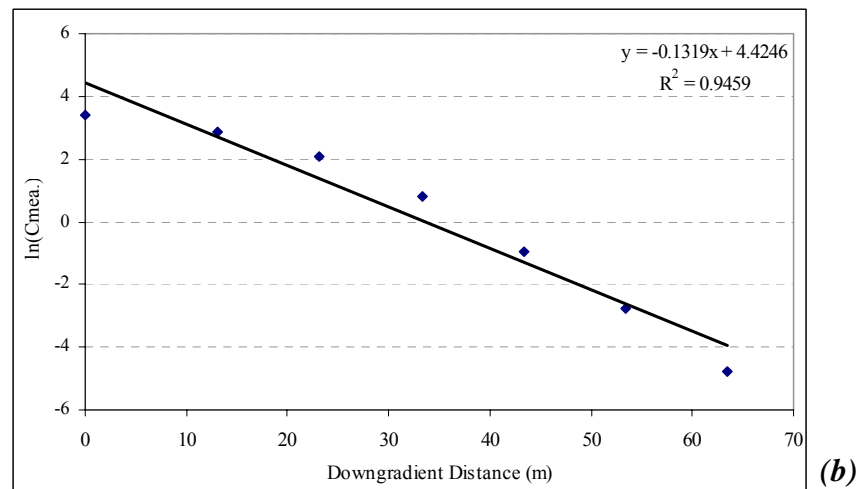
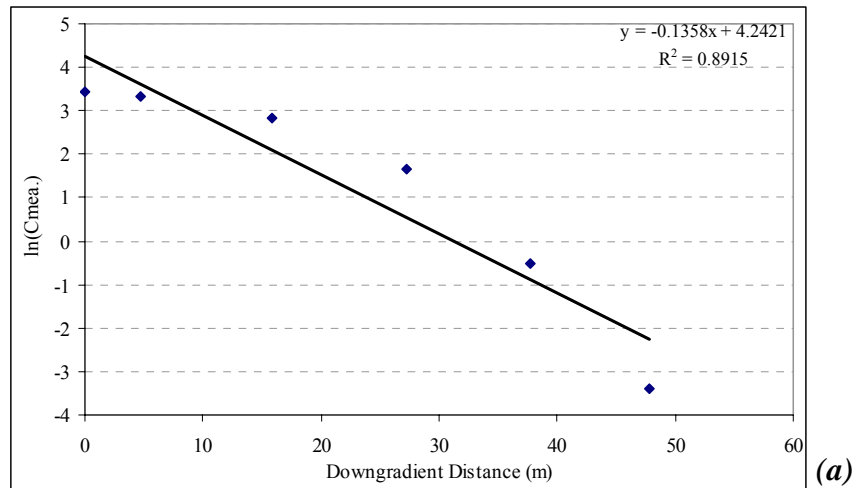


Figure E.3.  $\ln(C_{mea})$  versus downgradient distance graph, (a)  $h = 5$ , (b)  $h = 10$ , (c)  $h = 20$ , for  $CV = 150\%$ .

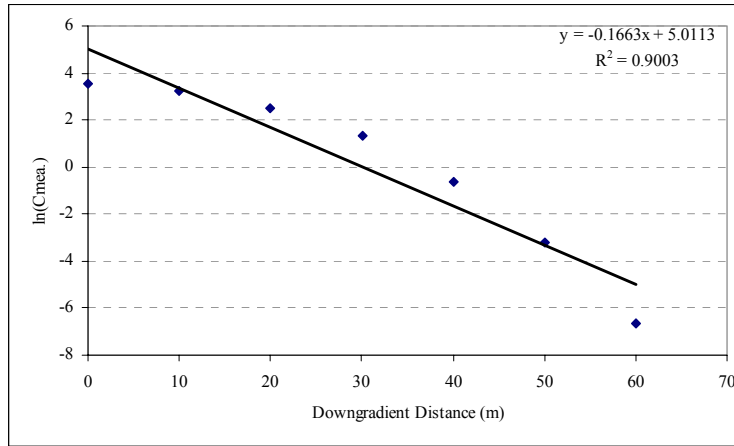


Figure E.4.  $\ln(C_{mea})$  versus downgradient distance for anisotropic field having  $CV = 50\%$ ,  $h_x = 20$  m, and  $h_y = 4$  m.

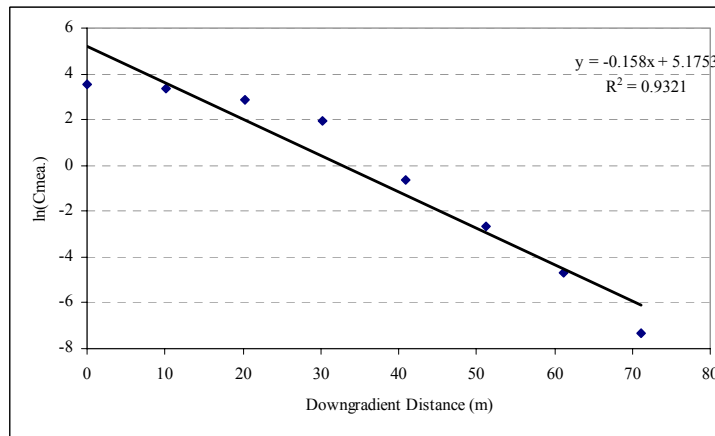


Figure E.5.  $\ln(C_{mea})$  versus downgradient distance for anisotropic field having  $CV = 150\%$ ,  $h_x = 10$  m, and  $h_y = 2$  m.

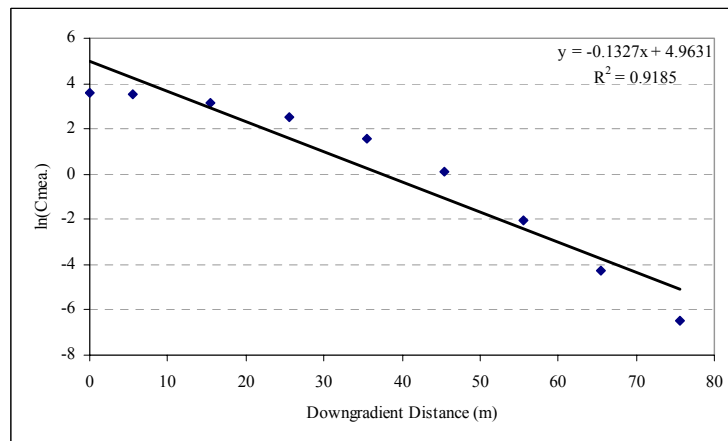


Figure E.6.  $\ln(C_{mea})$  versus downgradient distance for uniform field.

## APPENDIX F. LINEAR REGRESSION ANALYSIS GRAPHS FOR CONSERVATIVE TRACER METHOD

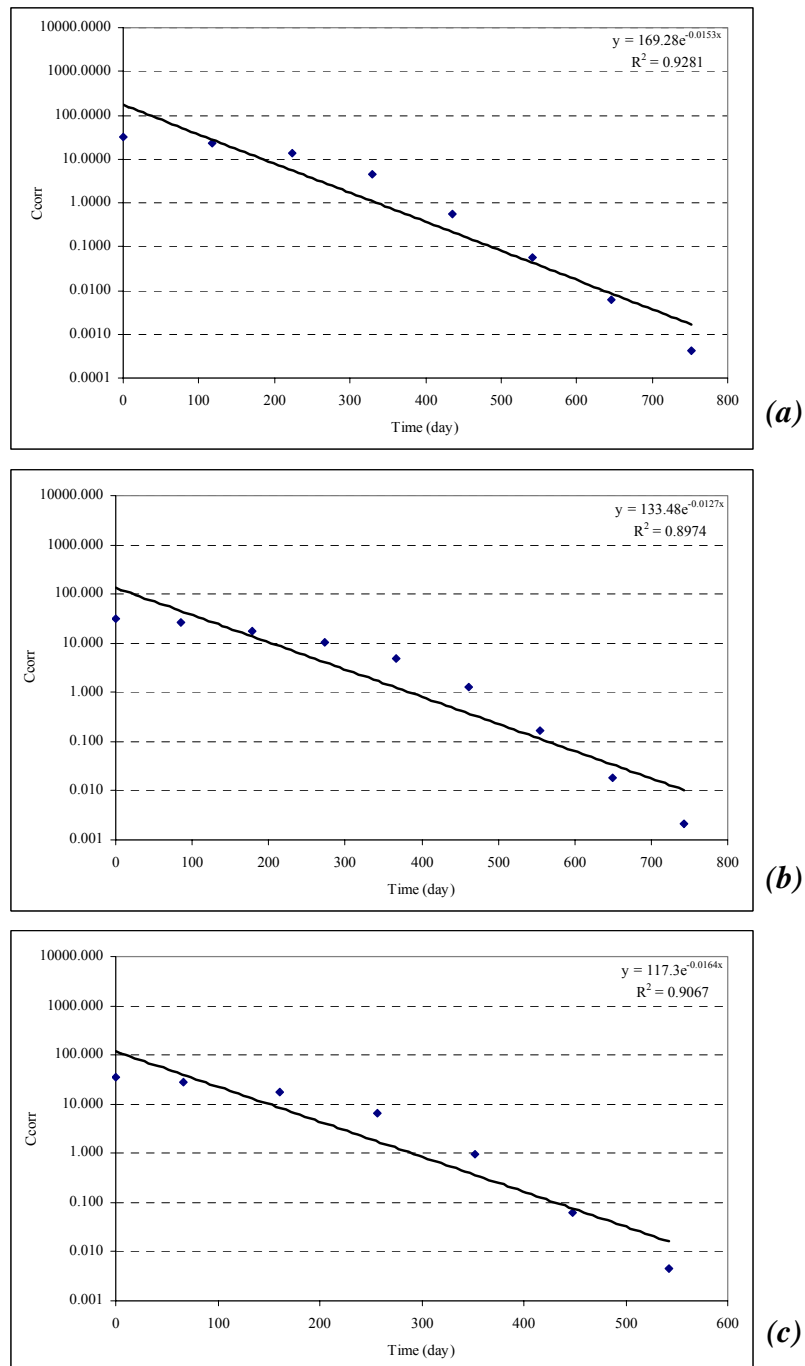
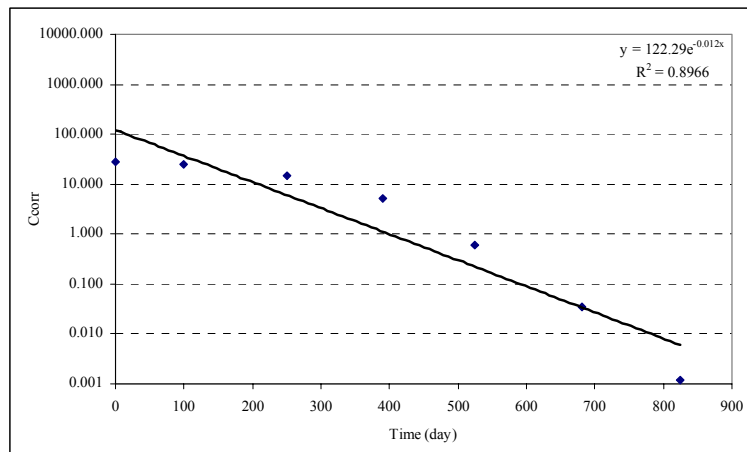
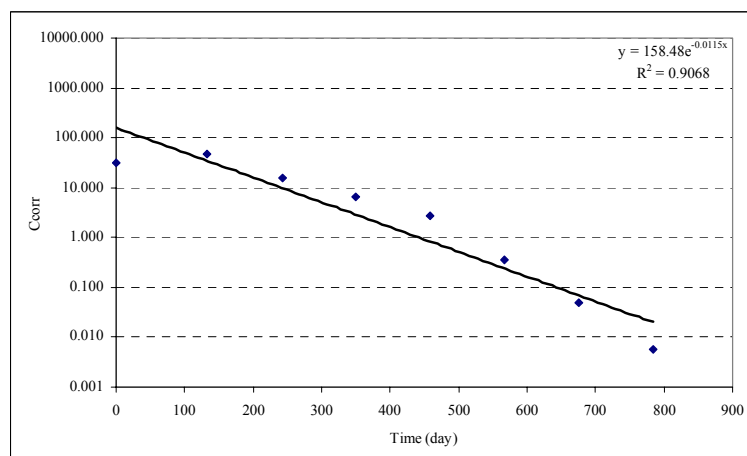


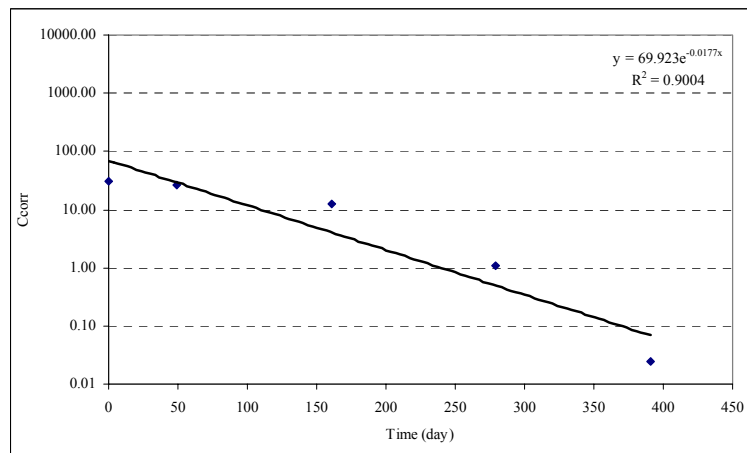
Figure F.1.  $C_{corr}$  on logarithmic scale versus time graph, (a)  $h = 5$ , (b)  $h = 10$ ,  
(c)  $h = 20$ , for  $CV = 50\%$ .



(a)

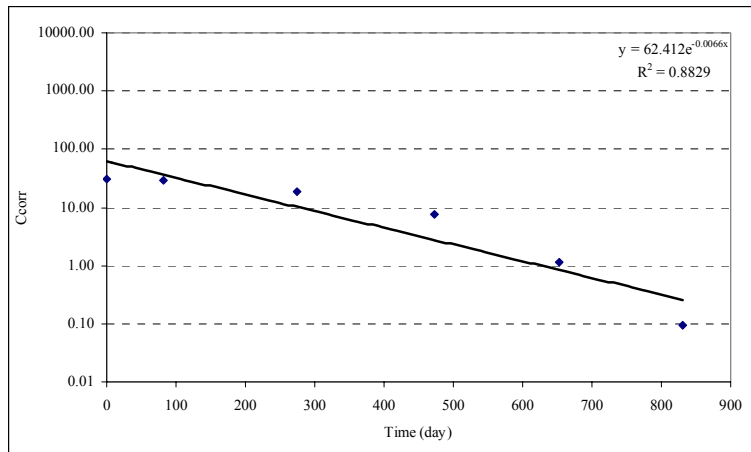


(b)

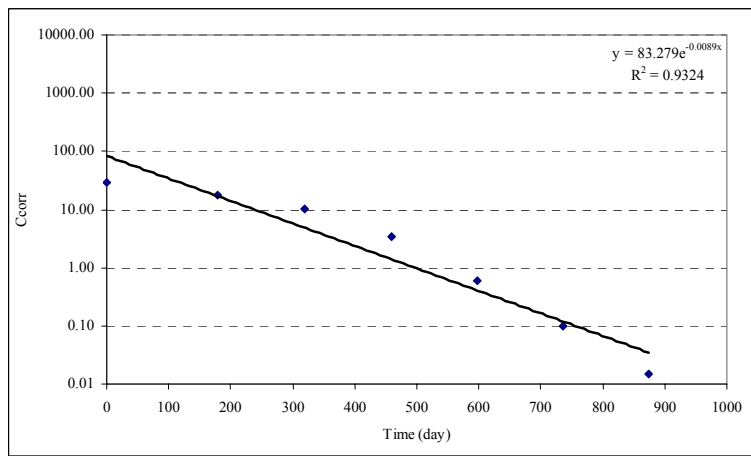


(c)

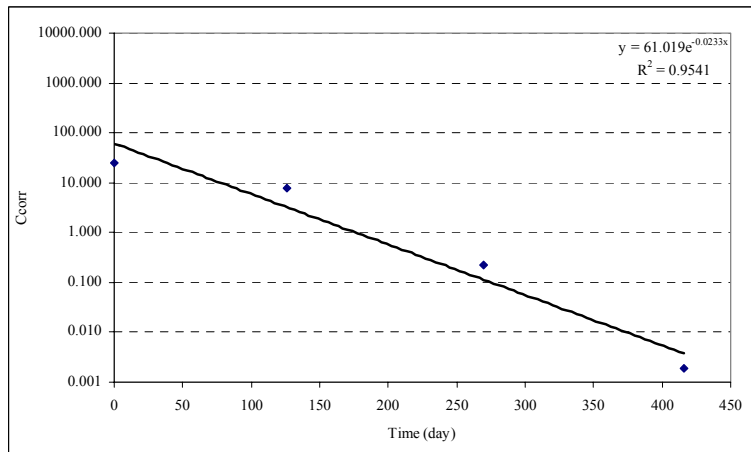
Figure F.2.  $C_{corr}$  on logarithmic scale versus time graph, (a)  $h = 5$ , (b)  $h = 10$ ,  
(c)  $h = 20$ , for  $CV = 100\%$ .



(a)



(b)



(c)

Figure F.3.  $C_{corr}$  on logarithmic scale versus time graph, (a)  $h = 5$ , (b)  $h = 10$ , (c)  $h = 20$ , for  $CV = 150\%$ .

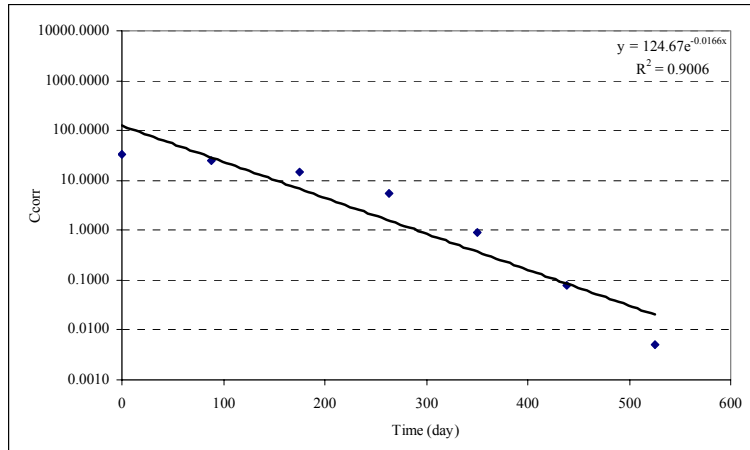


Figure F.4.  $C_{corr}$  on logarithmic scale versus time graph, for anisotropic field having CV of 50 % and  $h = 20$ .

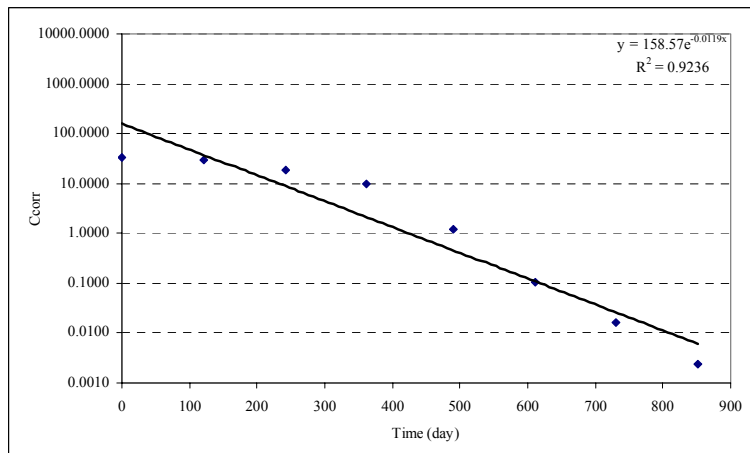


Figure F.5.  $C_{corr}$  on logarithmic scale versus time graph, for anisotropic field having CV of 150 % and  $h = 10$ .

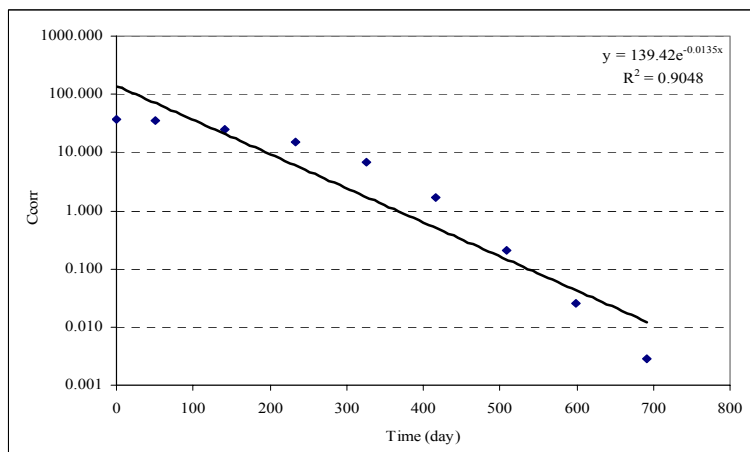


Figure F.5.  $C_{corr}$  on logarithmic scale versus time graph, for Uniform Field.